Proton-Antiproton Annihilation and Meson Spectroscopy with the Crystal Barrel^{*}

Claude Amsler Physik-Institut der Universität Zürich, Winterthurerstrasse 190, CH-8057 Zürich, Switzerland

November 26, 2024

Abstract

This report reviews the achievements of the Crystal Barrel experiment at the Low Energy Antiproton Ring (LEAR) at CERN. During seven years of operation Crystal Barrel has collected very large statistical samples in $\overline{p}p$ annihilation, especially at rest and with emphasis on final states with high neutral multiplicity. The measured rates for annihilation into various two-body channels and for electromagnetic processes have been used to test simple models for the annihilation mechanism based on the quark internal structure of hadrons. From three-body annihilations three scalar mesons, $a_0(1450)$, $f_0(1370)$ and $f_0(1500)$ have been established in various decay modes. One of them, $f_0(1500)$, may be identified with the expected ground state scalar glueball.

Contents

1	Introduction	2		
2	Proton-Antiproton Annihilation at Rest			
	2.1 S- and P-wave annihilation at rest	4		
3	The Crystal Barrel Experiment	6		
	3.1 Detector	6		
	3.2 Photon reconstruction			
	3.3 Available data	8		
4	Annihilation into Two Mesons	8		
	4.1 Annihilation into two neutral mesons	9		
	4.2 The annihilation mechanism	10		

*Submitted to Reviews of Modern Physics

5	Electromagnetic Processes 13			
	5.1	Radiative annihilation	13	
	5.2	Search for light gauge bosons in pseudoscalar meson decays	14	
	5.3	$\eta \to 3\pi$	15	
	5.4	$\eta' \to \pi^+ \pi^- \gamma \dots $	16	
	5.5	Radiative ω decays	16	
6	Pro		18	
	6.1	Annihilation into $\pi^0 \phi$, $\eta \phi$ and $\gamma \phi$	19	
	6.2	ϕ/ω ratio	20	
7	Me	son Spectroscopy 2	22	
	7.1	Introduction	22	
	7.2	Spin-parity analysis	23	
	7.3	K -matrix analysis $\ldots \ldots \ldots$	26	
8	An		29	
	8.1		30	
	8.2		31	
	8.3		32	
	8.4	1 0	33	
	8.5		34	
	8.6		34	
	8.7		35	
	8.8	$\overline{p}p \to \pi^{\pm}K^{\mp}K_L \dots \dots$	36	
9	Anı	$ \begin{array}{llllllllllllllllllllllllllllllllllll$	87	
10			88	
	10.1	$a_0(1450)$	39	
		$J_0(-0,0)$ and $J_0(-0,00)$ is the set of	41	
	10.3	$f_2(1565)$	43	
11	E/ι	Decay to $\eta\pi\pi$ 4	14	
12	Sun	nmary and Outlook 4	1 6	
13	13 Acknowledgements			

1 Introduction

Low energy antiproton-proton annihilation at rest is a valuable tool to investigate phenomena in the low energy regime of Quantum Chromodynamics (QCD). Due to the absence of Pauli blocking, the antiproton and proton overlap and one expects the interactions between constituent quarks and antiquarks (annihilation, pair creation or rearrangement) to play an important role in the annihilation process. From bubble chamber experiments performed in the sixties (Armenteros and French, 1969) one knows that annihilation proceeds through $q\bar{q}$ intermediate meson resonances. The $\omega(782)$, $f_1(1285)$, $E/\eta(1440)$ and $K_1(1270)$ mesons were discovered and numerous properties of other mesons ($a_0(980)$, $K^*(892)$, $\phi(1020)$, $a_2(1320)$) were studied in low energy $\bar{p}p$ annihilation. With the advent of QCD one now also predicts states made exclusively of gluons (glueballs), of a mixture of quarks and gluons (hybrids) and multiquark states, all of which can be produced in $\overline{p}p$ annihilation.

With the invention of stochastic cooling and the operation of the Low Energy Antiproton Ring (LEAR) from 1983 to 1996, intense and pure accelerator beams of low momentum antiprotons between 60 and 1940 MeV/s were available at CERN. It is impressive to compare the high flux of today's antiproton beams (> $10^6 \ \overline{p}/s$) with the rate of about 1 \overline{p} every 15 minutes in the early work when the antiproton was discovered, back in 1955 (Chamberlain, 1955).

This survey covers the results obtained with the Crystal Barrel, designed to study low energy $\overline{p}p$ annihilation with very high statistics, in particular annihilation into n charged particles (*n*-prong) and m neutrals (π^0, η, η' or ω) with $m \ge 2$, leading to final states with several photons. These annihilation channels occur with a probability of about 50% and have not been investigated previously. They are often simpler to analyze due to C-parity conservation which limits the range of possible quantum numbers for the intermediate resonances and the $\overline{p}p$ initial states.

The experiment started data taking in late 1989 and was completed in autumn 1996 with the closure of LEAR. Most of the data analyzed so far were taken with stopping antiprotons in liquid hydrogen on which I shall therefore concentrate. This article is organized as follows: After a brief reminder of the physical processes involved when antiprotons are stopped in liquid hydrogen (section 2), I shall describe in section 3 the Crystal Barrel apparatus and its performances. The review then covers results relevant to the annihilation mechanism and the roles of quarks in the annihilation process (section 4). Electromagnetic processes are covered in section 5. The observation of a strangeness enhancement may possibly be related to the presence of strange quarks in the nucleon (section 6). After describing the mathematical tools for extracting masses and spins of intermediate resonances (section 7) I shall review in sections 8 to 10 what is considered to be the main achievement, the discovery of several new mesons, in particular a scalar $(J^P = 0^+)$ state around 1500 MeV, which is generally interpreted as the ground state glueball. Section 11 finally describes the status of pseudoscalars in the 1400 MeV region.

In this review I shall concentrate on results published by the Crystal Barrel Collaboration or submitted for publication before summer 1997¹. Alternative analyses have been performed by other groups using more flexible parametrizations and also data from previous experiments (e.g. Bugg (1994, 1996), Abele (1996a)). I shall only refer to them without describing them in detail since they basically lead to the same results. Results on \overline{pd} annihilation will not be reviewed here. They include the observation of the channels $\overline{pd} \to \pi^0 n, \eta n, \omega n$ (Amsler, 1995a), $\overline{pd} \to \Delta(1232)\pi^0$ (Amsler, 1995b) which involve both nucleons in the reaction process.

2 Proton-Antiproton Annihilation at Rest

Earlier investigations of low energy $\overline{p}p$ annihilation have dealt mainly with final states involving charged mesons (π^{\pm}, K^{\pm}) or $K_S \to \pi^+\pi^-$, with at most one missing (undetected) π^0 , due to the lack of a good γ detection facility (for reviews, see Armenteros and French (1969), Sedlák and Šimák (1988) and Amsler and Myhrer (1991)).

The average charged pion multiplicity is 3.0 ± 0.2 for annihilation at rest and the average π^0 multiplicity is 2.0 ± 0.2 . The fraction of purely neutral annihilations (mainly from channels like $3\pi^0$, $5\pi^0$, $2\pi^0\eta$ and $4\pi^0\eta$ decaying to photons only) is (3.9 ± 0.3) % (Amsler, 1993a). This number is in good agreement with an earlier estimate from

¹All Crystal Barrel publications are listed with their full titles in the reference section.

bubble chambers, $(4.1 \ ^{+0.2}_{-0.6})$ % (Ghesquière, 1974). In addition to pions, η mesons are produced with a rate of about 7 % (Chiba, 1987) and kaons with a rate of about 6% of all annihilations (Sedlák and Šimák, 1988).

In fireball models the pion multiplicity $N = N_+ + N_- + N_0$ follows a Gaussian distribution (Orfanidis and Rittenberg, 1973). The pion multiplicity distribution at rest in liquid hydrogen is shown in Fig. 1. Following the model of Pais (1960) one expects on statistical grounds the branching ratios to be distributed according to $1/(N_+!N_-!N_0!)$ for a given multiplicity N. The open squares show the predictions normalized to the measured branching ratios from channels with charged pions and $N_0 \leq 1$ (Armenteros and French, 1969). The full circles show the data from bubble chambers, together with Crystal Barrel results for $N_0 > 1$. The fit to the data (curve) leads to $\sigma = 1$ for a Gauss distribution assuming $\langle N \rangle = 5$. The open circles show an estimate from bubble chamber experiments which appears to overestimate the contribution from N = 5 (Ghesquière, 1974).

2.1 S- and P-wave annihilation at rest

Stopping antiprotons in hydrogen are captured to form antiprotonic hydrogen atoms (protonium). The probability of forming a $\overline{p}p$ atom is highest for states with principal quantum number $n \sim 30$ corresponding to the binding energy (13.6 eV) of the K-shell electron ejected during the capture process. Two competing de-excitation mechanisms occur: (i) the cascade to lower levels by X-ray or external Auger emission of electrons from neighbouring H₂-molecules and (ii) Stark mixing between the various angular momentum states due to collisions with neighbouring H₂ molecules. Details on the cascade process can be found in Batty (1989). In liquid hydrogen, Stark mixing dominates (Day, 1960) and the $\overline{p}p$ system annihilates with the angular momentum $\ell = 0$ from high S levels (S-wave annihilation) due to the absence of angular momentum barrier. The initial states are the spin singlet (s = 0) ${}^{1}S_{0}$ and the spin triplet (s = 1) ${}^{3}S_{1}$ levels with parity $P = (-1)^{\ell+1}$ and C-parity $C = (-1)^{\ell+s}$, hence with quantum numbers

$$J^{PC}({}^{1}S_{0}) = 0^{-+} \text{ and } J^{PC}({}^{3}S_{1}) = 1^{--}.$$
 (1)

The cascade, important in low density hydrogen (e.g. in gas), populates mainly the n = 2 level (2P) from which the $\overline{p}p$ atom annihilates due its small size: The K_{α} transition from 2P to 1S has been observed at LEAR in gaseous hydrogen (Ahmad, 1985; Baker, 1988). Compared to annihilation, it is suppressed with a probability of (98 ± 1) % at atmospheric pressure. Annihilation with relative angular momentum $\ell = 1$ (P-wave annihilation) can therefore be selected by detecting the L X-rays to the 2P levels, in coincidence with the annihilation products. This procedure permits the spectroscopy of intermediate meson resonances produced from the P-states

$$J^{PC}({}^{1}P_{1}) = 1^{+-}, \quad J^{PC}({}^{3}P_{0}) = 0^{++}, J^{PC}({}^{3}P_{1}) = 1^{++} \text{ and } J^{PC}({}^{3}P_{2}) = 2^{++}.$$
(2)

Annihilation from P-states has led to the discovery of the $f_2(1565)$ meson (May, 1989).

The much reduced Stark mixing in low density hydrogen also allows annihilation from higher P levels. At 1 bar, S- and P-waves each contribute about 50% to annihilation (Doser, 1988). Annihilation from D-waves is negligible due to the very small overlap of the p and \overline{p} wave functions.

The assumption of S-wave dominance in liquid hydrogen is often a crucial ingredient to the amplitude analyses when determining the spin and parity of an intermediate resonance in the annihilation process, since the quantum numbers of the initial state must be known. The precise fraction of P-wave annihilation in liquid has been the subject of a longstanding controversy. The reaction $\overline{p}p \to \pi^0 \pi^0$ can only proceed through the P-states 0^{++} or 2^{++} (see section 4.1) while $\pi^+\pi^-$ also proceeds from S-states (1^{--}) . The annihilation rate $B(\pi^0\pi^0)$ for this channel in liquid has been measured earlier by several groups but with inconsistent results (Devons, 1971; Adiels, 1987; Chiba, 1988).

Crystal Barrel has determined the branching ratio for $\overline{p}p \to \pi^0 \pi^0$ in liquid by measuring the angles and energies of the four decay photons (Amsler, 1992a). The main difficulties in selecting this channel are annihilation into $3\pi^0$ which occurs with a much higher rate and, most importantly, P-wave annihilation in flight. The former background source can be reduced with the good γ detection efficiency and large solid angle of Crystal Barrel, while the latter can be eliminated thanks to the very narrow stop distribution from cooled low-energy antiprotons from LEAR (0.5 mm at 200 MeV/c). The small contamination from annihilation in flight can easily be subtracted from the stopping distribution by measuring the annihilation vertex. The latter was determined by performing a 5 constraints (5C) fit to $\overline{p}p \to \pi^0 \pi^0$, assuming energy conservation, two invariant 2γ -masses consistent with $2\pi^0$ and momentum conservation perpendicular to the beam axis. The branching ratio for $\pi^0 \pi^0$ is

$$B(\pi^0 \pi^0) = (6.93 \pm 0.43) \times 10^{-4}, \tag{3}$$

in agreement with Devons (1971) but much larger than Adiels (1987) and Chiba (1988). From the annihilation rate $B(\pi^+\pi^-)_{2P}$ into $\pi^+\pi^-$ from atomic 2P-states (Doser, 1988) one can, in principle, extract the fraction f_p of *P*-wave annihilation in liquid²:

$$f_p = 2 \frac{B(\pi^0 \pi^0)}{B(\pi^+ \pi^-)_{2P}} = (28.8 \pm 3.5)\%.$$
(4)

This is a surprisingly large contribution. However, Eq. (4) assumes that the population of the fine and hyperfine structure states is the same for the 2P as for the higher P levels which is in general not true. In liquid, strong Stark mixing constantly repopulates the levels. A P-state with large hadronic width, for instance ${}^{3}P_{0}$ (Carbonell, 1989), will therefore contribute more to annihilation than expected from a pure statistical population. On the other hand, in low pressure gas or for states with low principal quantum numbers the levels are populated according to their statistical weights. The branching ratio for annihilation into a given final state is given in terms of the branching ratios B_{i}^{S} and B_{i}^{P} from the two S-, respectively the four P-states (Batty, 1996):

$$B = [1 - f_P(\rho)] \sum_{i=1}^{2} w_i^S E_i^S(\rho) B_i^S + f_P(\rho) \sum_{i=1}^{4} w_i^P E_i^P(\rho) B_i^P,$$
(5)

where ρ is the target density. The purely statistical weights are

$$w_i^S = \frac{2J_i + 1}{4}, \ w_i^P = \frac{2J_i + 1}{12}.$$
 (6)

The enhancement factors E_i describe the departure from pure statistical population $(E_i=1)$. For $\pi^0\pi^0$ in liquid one obtains

$$B(\pi^0 \pi^0) = f_P(\text{liq})[\frac{1}{12} E_{{}^3P_0}(\text{liq}) B_{{}^3P_0}(\pi^0 \pi^0)]$$

²In Doser (1988) f_p was found to be (8.6 ± 1.1) %, when using the most precise measurement for $\pi^0 \pi^0$ available at that time (Adiels, 1987).

$$+\frac{5}{12}E_{^{3}P_{2}}(\text{liq})B_{^{3}P_{2}}(\pi^{0}\pi^{0})],$$
(7)

and for $\pi^+\pi^-$ from 2P states

$$B(\pi^{+}\pi^{-})_{2P} = 2\left[\frac{1}{12}B_{^{3}P_{0}}(\pi^{0}\pi^{0}) + \frac{5}{12}B_{^{3}P_{2}}(\pi^{0}\pi^{0})\right].$$
(8)

It is obviously not possible to determine $f_P(\text{liq})$ unless the enhancement factors are unity (and hence Eq. (4) follows). The enhancement factors have been calculated with an X-ray cascade calculation (Batty, 1996) using the observed yields of K and L X-rays in antiprotonic atoms and the predicted hadronic widths from optical potential models of the $\overline{p}p$ interaction (Carbonell, 1989). For example, Batty (1996) finds typically $E_{3P_0}(\text{liq}) \sim$ 2.3 and $E_{3P_2}(\text{liq}) \sim 1.0$. The branching ratios B_i and $f_P(\rho)$ were then fitted to the measured two-body branching ratios for $\overline{p}p \to \pi^0 \pi^0, \pi^+ \pi^-, K^+ K^-, K_S K_S$ and $K_S K_L$ at various target densities, with and without L X-ray coincidence. The fraction of P-wave annihilation is shown in Fig. 2 as a function of density. In liquid hydrogen one obtains

$$f_P(\text{liq}) = (13 \pm 4)\%,$$
 (9)

a more realistic value when compared to Eq. (4).

3 The Crystal Barrel Experiment

3.1 Detector

Figure 3 shows a sketch of the Crystal Barrel detector (Aker, 1992). The incoming antiprotons entered a 1.5 T solenoidal magnet along its axis and interacted in a liquid hydrogen target, 44 mm long and 17 mm in diameter. A segmented silicon counter in front of the target defined the incoming beam. The final state charge multiplicity was determined online with two cylindrical proportional wire chambers (PWC). The charged particle momentum was measured by a jet drift chamber (JDC) which also provided π/K separation below 500 MeV/c by ionization sampling.

Photons were detected in a barrel-shaped assembly of 1,380 CsI(Tl) crystals, 16.1 radiation lengths long (30 cm), with photodiode readout. The crystals were oriented towards the interaction point and covered a solid angle of $0.97 \times 4\pi$. Each crystal, wrapped in teflon and aluminized mylar, was enclosed in a 100 μ m thick titanium container. The light (peaking at 550 nm) was collected at the rear end by a wavelength shifter and the re-emitted light was detected by a photodiode glued on the edge of the wavelength shifter. With the low electronic noise of typically 220 keV the energy resolution was

$$\frac{\sigma}{E} = \frac{0.025}{E[\text{GeV}]^{\frac{1}{4}}}\tag{10}$$

and photons could be detected efficiently down to 4 MeV. The angular resolution was typically $\sigma = 20$ mrad for both polar and azimuthal angles. The mass resolution was $\sigma = 10$ MeV for π^0 and 17 MeV for $\eta \to 2\gamma$.

A rough calibration of the electromagnetic calorimeter was first obtained with traversing minimum ionizing pions which deposit 170 MeV in the crystals. The final calibration was achieved with 0-prong events using 2γ invariant masses from π^0 decays. An energy dependent correction was applied to take shower leakage at the rear end of the crystals into account. The stability of the calibration was monitored with a light pulser system. The JDC had 30 sectors, each with 23 sense wires at radial distances between 63 mm and 239 mm) read out on both ends by 100 MHz flash ADC's. The position resolution in the plane transverse to the beam axis ($r\phi$ coordinates) was $\sigma = 125 \ \mu m$ using slow gas, a 90:10 % CO₂/isobutane mixture. The coordinate z along the wire was determined by charge division with a resolution of $\sigma = 8$ mm. This led to a momentum resolution for pions of $\sigma/p \simeq 2$ % at 200 MeV/c, rising to $\simeq 7\%$ at 1 GeV/c for those tracks that traversed all JDC layers.

The z coordinates were calibrated by fitting straight tracks from 4-prong events without magnetic field. The momentum calibration was performed with monoenergetic pions and kaons from the two-body final states $\pi^+\pi^-$ and K^+K^- . Pressure and temperature dependent drift time tables were generated and fitted to the measured momentum distribution.

In 1994 the JDC was replaced by a new jet drift chamber with only 15 sectors for the 6 innermost layers. In 1995 the PWC's were also replaced by a microstrip vertex detector (SVX) consisting of 15 single-sided silicon detectors arranged in a windmill configuration at a radial distance of 13 mm around the target (Fig. 4). Each detector had 128 strips with a pitch of 50 μ m running parallel to the beam axis. The increase of charge multiplicity between the SVX and the inner layers of the JDC permitted to trigger on $K_S \to \pi^+\pi^-$. The SVX also provided an improved vertex resolution in $r\phi$ and a better momentum resolution.

For annihilation at rest in liquid hydrogen the \overline{p} incident momentum was 200 MeV/c with typically 10⁴ incident \overline{p} /s to minimize pile-up in the crystals. For annihilation in gaseous hydrogen the liquid target was replaced by a hydrogen flask at 13 bar. The incident momentum was 105 MeV/c. Since the annihilation rate was higher than the maximum possible data acquisition speed, a multilevel trigger could be used. The two PWC's and the inner layers (2 - 5) of the JDC determined the charged multiplicity of the final state. Events with long tracks could be selected for optimum momentum resolution by counting the charged multiplicity in the outer layers (20 and 21) of the JDC. A hardwired processor determined the cluster multiplicity in the barrel. A processor then fetched the digitized energy deposits in the barrel, computed all two-photon invariant masses thus providing a trigger on the π^0 or η multiplicity (Urner, 1995).

3.2 Photon reconstruction

We now briefly describe the photon reconstruction which is particularly relevant to the results reviewed in this article. Photon induced electromagnetic showers spread out over several crystals. The size of a cluster depends on the photon energy and varies from 1 to about 20 crystals. The reconstruction of photons is done by searching for clusters of neighbouring crystals with energy deposits of at least 1 MeV. The threshold for cluster identification (typically between 4 and 20 MeV) depends on the annihilation channel being studied. Local maxima with a predefined threshold (typically between 10 and 20 MeV) are then searched for within clusters. When only one local maximum is found, the photon energy is defined as the cluster energy and the direction is given by the center of gravity of the crystals, weighted by their energies. When n local maxima are found within a cluster, the latter is assumed to contain showers from n photons. In this case the cluster energy E_C is shared between the n subclusters of nine crystals with energies E_i around the local maxima. Hence the photon energies are given by

$$E_{\gamma,i} = \frac{E_i}{\sum_{j=1}^n E_j} E_C.$$
(11)

Additional clusters mocking photons are due to shower fluctuations which may develop small but well separated satellites in the vicinity of the main shower. These "split-offs" can be removed by requiring a minimum separation between the showers. However, this cut may reduce the detection efficiency for high energy π^0 's since photons from π^0 decay cluster around the minimum opening angle. The opening angle between two photons with energies $E_1 \leq E_2$ from π^0 decay is given by

$$\cos \phi = 1 - \frac{(1+R)^2}{2\gamma^2 R}$$
 with $R = \frac{E_1}{E_2}$, (12)

where $\gamma = E_{\pi^0}/m_{\pi^0}$. Hence for all pairs of neighbouring clusters one calculates R and removes the low energy clusters whenever $\cos\phi$ is larger than given by Eq. (12), assuming the maximum possible value of γ in the annihilation channel under consideration (Pietra, 1996).

Clusters generated by ionizing particles can be removed by matching the impact points extrapolated from the reconstructed tracks in the JDC. However, split-offs from charged particles are more cumbersome to eliminate. They are initiated, for example, from neutrons which travel long distances before being absorbed. These split-offs can be suppressed by requiring momentum and energy conservation in the annihilation process (kinematic fits).

3.3 Available data

The bulk of the Crystal Barrel data consists in $\overline{p}p$ annihilation at rest and in flight in liquid hydrogen. As discussed above, annihilation from initial P-states is enhanced when using a gaseous target. Annihilation in deuterium at rest allows the formation of $\overline{N}N$ bound states below $2m_N$, the spectator neutron (or proton) removing the excess energy (for a review on baryonium states, see Amsler (1987)). With a spectator proton one gains access to $\overline{p}n$ annihilation, a pure isospin I = 1 initial state.

The data collected by Crystal Barrel are shown in Table 1. Data were taken in liquid hydrogen, gaseous hydrogen (13 bar) and in liquid deuterium with a minimum bias trigger (requiring only an incident antiproton) or with the multiplicity trigger requiring 0-prong or *n*-prong with long tracks in the JDC. In addition, data were collected with specialized triggers enhancing specific final states. As a comparison, the largest earlier sample of annihilations at rest in liquid was obtained by the CERN-Collège de France collaboration with about 100,000 pionic events and 80,000 events containing at least one $K_S \to \pi^+\pi^-$ (Armenteros and French, 1969). The Asterix collaboration collected some 10⁷ pionic events in gaseous hydrogen at 1 bar (for a review and references see Amsler and Myhrer (1991)). The total number of annihilations at rest in liquid hydrogen collected by Crystal Barrel is 10⁸. The triggered 0-prong sample alone corresponds to 6.3×10^8 annihilations.

4 Annihilation into Two Mesons

Consider a pair $M\overline{M}$ of charge conjugated mesons in the eigenstate of isospin *I*. The *P*-, *C*- and *G*-parities are:

$$P(M\overline{M}) = (-1)^L, \tag{13}$$

$$C(M\overline{M}) = (-1)^{L+S}, \tag{14}$$

$$G(M\overline{M}) = (-1)^{L+S+I}, (15)$$

where L is the relative angular momentum and S the total spin. For the $\overline{p}p$ system with angular momentum ℓ and spin s one has

$$P(\overline{p}p) = (-1)^{\ell+1}, \tag{16}$$

$$C(\overline{p}p) = (-1)^{\ell+s}, \tag{17}$$

$$G(\overline{p}p) = (-1)^{\ell+s+I}.$$
(18)

For annihilation into two mesons the two sets of equations relate the quantum numbers of the initial state to those of the final state since P, C, G and I are conserved. In addition, L, S, ℓ and s must be chosen so that the total angular momentum J is conserved:

$$|L - S| \le J \le L + S, \quad |\ell - s| \le J \le \ell + s.$$

$$\tag{19}$$

Since P, C and G are multiplicative quantum numbers these relations are especially restrictive for mesons that are eigenstates of C and G, e.g. for neutral non-strange mesons. For example, for two identical neutral non-strange pseudoscalars (e.g. $\pi^0\pi^0$) with S = 0, C = +1, Eq. (14) implies that L is even and then Eq. (16) requires ℓ to be odd (annihilation from P-states only). Equation (15) further requires with G = +1 that I = 0and hence with Eq. (18) annihilation from the $(I = 0) \ 0^{++}$ or 2^{++} atomic states.

For a pair of non-identical neutral pseudoscalars (e.g. $\pi^0 \eta$) L may be odd and hence the possible quantum numbers are 0^{++} , 1^{-+} , 2^{++} , 3^{-+} , etc. However, 1^{-+} and 3^{-+} do not couple to $\overline{p}p$ since Eqs. (16) and (17) require ℓ even and s = 0 and hence J even. In fact these "exotic" quantum numbers do not couple to any fermion-antifermion pair and are, in particular, excluded for $q\overline{q}$ mesons.

4.1 Annihilation into two neutral mesons

Crystal Barrel has measured the branching ratios for $\overline{p}p$ annihilation into two neutral light mesons from about 10⁷ annihilations into 0-prong (Amsler, 1993b). These data have been collected by vetoing charged particles with the PWC's and the internal layers of the JDC. The lowest γ -multiplicity was four (e.g. $\pi^0\pi^0, \pi^0\eta$) and the highest nine (e.g. $\eta\omega$, with $\eta \to 3\pi^0$ and $\omega \to \pi^0\gamma$). To control systematic errors in the detection efficiency, some of these branching ratios have been determined from different final state multiplicities. For example, η decays to 2γ and $3\pi^0$ and hence $\eta\eta$ is accessible from 4γ and 8γ events.

Figure 5 shows a scatterplot of 2γ -invariant masses for events with 4γ . Events have been selected by requiring four clusters in the barrel and applying momentum and energy conservation (4C fit). Signals from $\pi^0\pi^0$, $\pi^0\eta$, $\eta\eta$ and even $\pi^0\eta'$ are clearly visible. The dark diagonal band at the edge is due to wrong combinations. The detection and reconstruction efficiency was typically 40% for 4γ events, obtained by Monte Carlo simulation with GEANT. As discussed above, two neutral pseudoscalars couple only to atomic Pstates and are therefore suppressed in liquid hydrogen. On the other hand, the channels $\pi^0\omega$ and $\eta\omega$ couple to 3S_1 and hence have a larger branching ratio. In spite of the good detection efficiency of the detector one therefore observes the background signals from $\pi^0\omega$ and $\eta\omega$, where ω decays to $\pi^0\gamma$ with a missing (undetected) photon.

Figure 6 shows the $\pi^0 \gamma$ momentum distribution for $\overline{p}p \to 4\pi^0 \gamma$ events (8C fit requiring $4\pi^0$). The peak at 657 MeV/c is due to the channel $\overline{p}p \to \eta\omega$. For these 9γ events the detection efficiency was 10%.

The branching ratios are given in Table 2. They are always corrected for the unobserved (but known) decay modes of the final state mesons (Barnett, 1996). For Crystal Barrel data the absolute normalization was provided by comparison with $\pi^0 \pi^0$ which has been measured with minimum bias data (Eq. (3)). Signals for $\omega \pi^0$ and $\omega \eta$ have also been observed for ω decaying to $\pi^+\pi^-\pi^0$, leading to $\pi^+\pi^-4\gamma$ (Schmid, 1991). Figure 7 shows the $\pi^+\pi^-\pi^0$ invariant mass spectrum for $\pi^+\pi^-\pi^0\eta$ events. The branching ratio for $\omega\pi^0$ and $\omega\eta$ are in excellent agreement with the ones from 0-prong (Table 2).

The angular distribution in the ω rest frame contains information on the initial atomic state. The distribution of the angle between the normal to the plane spanned by the three pions and the direction of the recoiling η is plotted in the inset of Fig. 7. Using the method described in section 7.2 one predicts the distribution $\sin^2\theta$ for annihilation from ${}^{3}S_{1}$ while the distribution should be isotropic for annihilation from ${}^{1}P_{1}$. The fit (curve) allows (12 $\pm 4)\%$ P-wave. Figure 8 shows the angular distribution of the γ in the ω rest frame for $\omega\eta(\omega \to \pi^{0}\gamma)$. The predicted distribution is $(1 + \cos^{2}\theta)$ from ${}^{3}S_{1}$ and is again isotropic for ${}^{1}P_{1}$. The fit (curve) allows $(9 \pm 3)\%$ P-wave. However, these results assume that the relative angular momentum between η and ω is L = 0 from ${}^{1}P_{1}$, thus neglecting L = 2. Without this assumption, the fraction of P-wave cannot be determined from the angular distributions due to the unknown interference between the L = 0 and L = 2 amplitudes.

Some of the branching ratios for two-neutral mesons have been measured earlier (Adiels, 1989; Chiba, 1988) by detecting and reconstructing π^0 's or η 's with small solid angle detectors and observing peaks in the π^0 or η inclusive momentum spectra. Since the branching ratios are small, these early data are often statistically weak or subject to uncertainties in the baseline subtraction from the inclusive spectra. In fact most of the Crystal Barrel results disagree with these measurements which should not be used anymore. Table 2 therefore updates Table 1 in Amsler and Myhrer (1991).

4.2 The annihilation mechanism

There is currently no model which completely and satisfactorily describes the measured two-body branching ratios listed in Table 2 (for a review of annihilation models and references, see Amsler and Myhrer (1991). Since the proton and the antiproton wavefunctions overlap one expects quarks to play an important role in the annihilation dynamics. For instance, $\bar{p}p$ annihilation into two mesons can be described by the annihilation of two $q\bar{q}$ pairs and the creation of a new pair (annihilation graph A) or by the annihilation of one $q\bar{q}$ pair and the rearrangement of the other two pairs (rearrangement graph R), see Fig. 9. At low energies there is, however, no consensus as to which operator should be used to describe the emission and absorption of gluons. In a first approach one assumes that only the flavor flow between initial and final states is important (Genz, 1983; Hartmann, 1988). The Quark Line Rule (QLR) states that annihilation into $u\bar{u}$ and $d\bar{d}$ is excluded if the A graph dominates, while annihilation into two $d\bar{d}$ mesons is forbidden if R dominates (see Fig. 9). The OZI-rule (Okubo, 1963) is a special case of the QLR: Annihilation into one or more $s\bar{s}$ mesons is forbidden. We shall confront these simple rules below with Crystal Barrel data.

Another approach, which we shall use, is the nearest threshold dominance model which describes reasonably well the observed final state multiplicity as a function of \overline{p} momentum (Vandermeulen, 1988). The branching ratio for annihilation into two mesons with masses m_a und m_b is given by

$$W = pC_0 C_{ab} \exp(-A\sqrt{s - (m_a + m_b)^2}),$$
(20)

where p is the meson momentum in the $\overline{p}p$ center of mass system with total energy \sqrt{s} , C_0 a normalization constant and C_{ab} a multiplicity factor depending on spin and isospin. The constant $A = 1.2 \text{ GeV}^{-1}$ has been fitted to the cross section for $\overline{p}p$ annihilation into $\pi^+\pi^-$ as a function of \overline{p} momentum. For annihilation into kaons the fit to kaonic channels requires the additional normalization factor $C_1/C_0 = 0.15$. Thus annihilation into the heaviest possible meson pair is enhanced with respect to phase space p by the exponential form factor in Eq. (20). This is natural in the framework of baryon exchange models which prefer small momentum transfers at the baryon-meson vertices.

In more refined models the branching ratios for annihilation at rest depend on the atomic wave function distorted by strong interaction at short distances (Carbonell, 1989). Predictions for the branching ratios therefore depend on models for the meson exchange potential which are uncertain below 1 fm. Also, the quark description has to be complemented by baryon and meson exchanges to take the finite size of the emitted mesons into account.

In the absence of strong interaction the $\overline{p}p$ atomic state is an equal superposition of isospin I = 0 and 1 states. Naively one would therefore expect half the protonium states to annihilate into a final state of given isospin. However, $\overline{p}p$ to $\overline{n}n$ transitions occuring at short distances may modify the population of I = 0 and I = 1 states and therefore enhance or reduce the annihilation rate to a final state of given isospin (Klempt, 1990; Jaenicke, 1991). Nonetheless, one expects that predictions for ratios of branching ratios for channels with the same isospin and proceeding from the same atomic states are less sensitive to model dependence. We shall therefore compare predictions from the QLR with ratios of branching ratios from Table 2.

The flavor content of the η and η' mesons is given by

$$|\eta\rangle = \frac{1}{\sqrt{2}} (|u\overline{u}\rangle + |d\overline{d}\rangle) \sin(\theta_i - \theta_p) - |s\overline{s}\rangle \cos(\theta_i - \theta_p), |\eta'\rangle = \frac{1}{\sqrt{2}} (|u\overline{u}\rangle + |d\overline{d}\rangle) \cos(\theta_i - \theta_p) + |s\overline{s}\rangle \sin(\theta_i - \theta_p),$$
 (21)

where $\theta_i = 35.3^\circ$ is the ideal mixing angle. The flavor wave functions of the π^0 and ρ^0 are

$$|\pi^{0}\rangle, |\rho^{0}\rangle = \frac{1}{\sqrt{2}}(|d\overline{d}\rangle - |u\overline{u}\rangle), \qquad (22)$$

and those of ω and ϕ , assuming ideal mixing in the vector nonet,

$$|\omega\rangle = \frac{1}{\sqrt{2}} (|u\overline{u}\rangle + |d\overline{d}\rangle), \quad |\phi\rangle = -|s\overline{s}\rangle.$$
(23)

The branching ratio for annihilation into two neutral mesons is then given by $B = \tilde{B} \cdot W$ with

$$\tilde{B} = |\langle \overline{p}p | T | M_1 M_2 \rangle|^2 = |\sum_{i,j} T([q_i \overline{q_i}]_1, [q_j \overline{q_j}]_2) \langle q_i \overline{q_i} | M_1 \rangle \langle q_j \overline{q_j} | M_2 \rangle|^2,$$
(24)

and ³ $q_i = u$ or d (Genz, 1985). In the absence of $s\overline{s}$ pairs in the nucleon, the QLR forbids the production of $s\overline{s}$ mesons and therefore the $s\overline{s}$ components in M_1 and M_2 can be ignored in Eq. (24). The predicted ratios of branching ratios are given by the first four rows in Table 3 for various channels from the same atomic states. They depend only on the pseudoscalar mixing angle θ_p . To extract θ_p the measured branching ratios from Table 2 must be first divided by W (Eq. (20)), ignoring C_0 and C_{ab} which cancel in the ratio.

The pseudoscalar mixing angle has been measured in various meson decays (e.g. η and η' radiative decays, J/ψ radiative decays to η and η') and is known to be close to -20°

³The theoretical prediction \tilde{B} has to be multiplied by two for a pair of non-identical mesons.

(Gilman and Kauffmann, 1987). The agreement with our simple model of annihilation is amazing (third column of Table 3). We emphasize that the predictions in the upper four rows of Table 3 are valid independently of the relative contributions from the A and R graphs.

Conversely, one can assume the validity of the model and extract from the first four rows in Table 3 the average

$$\theta_p = (-19.4 \pm 0.9)^{\circ}. \tag{25}$$

Leaving the constant A in Eq. (20) as a free fit parameter one obtains $\theta_p = (-17.3 \pm 1.8)^{\circ}$ from early Crystal Barrel data (Amsler, 1992b). Assuming now dominance of the planar graph A, the amplitudes $T([u\overline{u}]_1, [d\overline{d}]_2)$ and $T([d\overline{d}]_1, [u\overline{u}]_2)$ vanish and one obtains the predictions in the lower part of Table 3. The measurements lead in general to incorrect values for θ_p , presumably due to the contribution of the R graph. Also, for $\rho^0 \rho^0$ and $\omega \omega$ one expects from A dominance

$$\ddot{B}(\rho^0 \rho^0) = \ddot{B}(\omega \omega), \tag{26}$$

in violent disagreement with data (Table 2). On the other hand, if R dominates the amplitude $T([d\bar{d}]_1, [d\bar{d}]_2)$ vanishes and one predicts from Eq. (24) with $a^2 \equiv \sin^2(\theta_i - \theta_p)$ the inequality (Genz, 1990)

$$|a^{2}\sqrt{2\tilde{B}(\pi^{0}\pi^{0})} - \sqrt{2\tilde{B}(\eta\eta)}|^{2} \le 4a^{2}\tilde{B}(\pi^{0}\eta) \le |a^{2}\sqrt{2\tilde{B}(\pi^{0}\pi^{0})} + \sqrt{2\tilde{B}(\eta\eta)}|^{2},$$
(27)

which is fulfilled by data.

There is, however, a caveat: the predictions (24) have been compared to the measured branching ratios corrected by W. As pointed out earlier, Eq. (20) provides a good fit to the mutiplicity distribution in low energy $\overline{p}p$ annihilation as a function of \overline{p} momentum. Other correcting factors can, however, be found in the literature. In section 7 we shall use the phase space factor

$$W = pF_L^2(p) \tag{28}$$

where $F_L(p)$ is the Blatt-Weisskopf damping factor which suppresses high angular momenta L for small p. This factor is determined by the range of the interaction, usually chosen as 1 fm ($p_R = 197 \text{ MeV/c}$). Convenient expressions for $F_L(p)$ are given in Table 4. For p much larger than p_R , $F_L(p) \simeq 1$ and for p much smaller than p_R

$$F_L(p) \simeq p^L. \tag{29}$$

This last prescription provides a reasonable agreement when comparing the measured decay branching ratios of mesons, especially tensors, with predictions from SU(3), as we shall discuss in section 10.1. These alternative phase space factors may also be used to determine the pseudoscalar mixing angle. However, they do not lead to consistent values for θ_p (Amsler, 1992b). Agreement is achieved with prescription (20), which we shall also employ in the next section.

In conclusion, the naive quark model assuming only the QLR and two-body threshold dominance reproduces the correct pseudoscalar mixing angle from the measured twomeson final states. This is a clear indication for quark dynamics in the annihilation process. The relative contribution from R and A cannot be extracted but the non-planar graph R must contribute substantially to the annihilation process.

5 Electromagnetic Processes

5.1 Radiative annihilation

For annihilations leading to direct photons the isospin I = 0 and 1 amplitudes from the same $\overline{p}p$ atomic state interfere since isospin is not conserved in electromagnetic processes. Radiative annihilation $\overline{p}p \rightarrow \gamma X$, where X stands for any neutral meson, involves the annihilation of a $q\overline{q}$ pair into a photon. The branching ratios can be calculated from the Vector Dominance Model (VDM) which relates γ emission to the emission of ρ , ω and ϕ mesons (Delcourt, 1984). Assuming ideal mixing in the vector nonet one may actually neglect ϕ production which is forbidden by the QLR. The amplitude for $\overline{p}p \rightarrow \gamma X$ is then given by the coherent sum of the two I = 0 and I = 1 amplitudes with unknown relative phase β (fig. 10). According to VDM, the $\gamma \rho$ coupling $g_{\rho\gamma}$ is a factor of three stronger than the $\gamma \omega$ coupling. The branching ratio is then⁴

$$\tilde{B}(\gamma X) = A^2 [\tilde{B}(\rho X) + \frac{1}{9}\tilde{B}(\omega X) + \frac{2}{3}\sqrt{\tilde{B}(\rho X)\tilde{B}(\omega X)}\cos\beta],$$
(30)

with

$$A = \frac{eg_{\rho\gamma}}{m_{\rho}^2} = 0.055.$$
 (31)

Equation (30) provides lower and upper limits $(\cos\beta = \pm 1)$ for branching ratios.

Radiative annihilation has not been observed so far with the exception of $\pi^0 \gamma$ (Adiels, 1987). Crystal Barrel has measured the rates for $\pi^0 \gamma$, $\eta \gamma$, $\omega \gamma$ and has obtained upper limits for $\eta' \gamma$ and $\gamma \gamma$ (Amsler, 1993c). Annihilation into $\phi \gamma$ (Amsler, 1995c) is treated in section 6.1.

The starting data sample consisted of 4.5×10^6 0-prong events. Figure 11 shows a typical $\pi^0 \gamma$ event leading to three detected photons. The main background to $\pi^0 \gamma$ stems from annihilations into $\pi^0 \pi^0$ for which one of the photons from π^0 decay has not been detected, mainly because its energy lies below detection threshold (10 MeV). The π^0 momentum for $\pi^0 \gamma$ is slightly higher (5 MeV/c) than for $\pi^0 \pi^0$. The small downward shift of the π^0 momentum peak due to the $\pi^0 \pi^0$ contamination could be observed thanks to the good energy resolution of the detector and could be used to estimate the feedthrough from $\pi^0 \pi^0$: (29 ± 8) %, in agreement with Monte Carlo simulations. The result for the $\pi^0 \gamma$ branching ratio is given in Table 5. It disagrees with the one obtained earlier from the π^0 inclusive momentum spectrum: (1.74 ±0.22) × 10⁻⁵ (Adiels, 1987).

Results for $\eta\gamma, \omega\gamma$ and $\eta'\gamma$ are also given in Table 5. The ω was detected in its $\pi^0\gamma$ and the η' searched for in its 2γ decay mode. The main contaminants were $\eta\pi^0, \omega\pi^0$ and $\eta'\pi^0$, respectively, with one photon escaping detection. For $\overline{p}p \to \gamma\gamma$, 98 ± 10 events were observed of which 70 ± 8 were expected feedthrough from $\pi^0\gamma$ and $\pi^0\pi^0$. This corresponds to a branching ratio of $(3.3 \pm 1.5) \times 10^{-7}$ which the collaboration prefers to quote as an upper limit (Table 5).

The branching ratios, divided by W (Eq. (20)), are compared in Table 5 with the range allowed by Eq. (30). Apart from $\phi\gamma$ to which we shall return later, the results agree with predictions from VDM. For $\pi^0\gamma$ and $\eta\gamma$ (from 3S_1) the isospin amplitudes interfere destructively ($\cos\beta \sim -0.3$) while for $\omega\gamma$ (from 1S_0) they interfere constructively ($\cos\beta \sim 0.13$). We emphasize that these conclusions depend on the prescription for the phase space correction. With a phase space factor of the form p^3 one finds strongly destructive amplitudes (Amsler, 1993c), see also Locher (1994) and Markushin (1997).

⁴For two identical particles, e.g. $\rho^0 \rho^0$ or $\omega \omega$, the measured branching ratios divided by phase space, \tilde{B} , have to be multiplied by two.

No prediction can be made from VDM for $\gamma\gamma$ due to the contribution of three amplitudes with unknown relative phases: $\rho^0\omega$ from I = 1, $\rho^0\rho^0$ and $\omega\omega$ from I = 0. Also, the branching ratio for $\rho^0\rho^0$ is poorly known (Table 2).

5.2 Search for light gauge bosons in pseudoscalar meson decays

Extensions of the standard model allow additional gauge bosons, some of which could be light enough to be produced in the decay of pseudoscalar mesons (Dobroliubov and Ignatiev, 1988). Radiative decays $\pi^0, \eta, \eta' \to \gamma X$ are particularly suitable since they are only sensitive to gauge bosons X with quantum numbers $J^P = 1^-$. Branching ratios are predicted to lie in the range 10^{-7} to 10^{-3} (Dobroliubov, 1990). Experimental upper limits for $\pi^0 \to \gamma X$ are of the order 5×10^{-4} for long lived gauge bosons with lifetime $\tau > 10^{-7}$ s (Atiya, 1992). Short lived gauge bosons decaying subsequently to e^+e^- are not observed with an upper limit of 4×10^{-6} (Meijer Drees, 1992).

Crystal Barrel has searched for radiative decays where X is a long lived weakly interacting gauge boson escaping from the detector without interaction, or decaying to $\nu\overline{\nu}$. The search was performed using the reactions $\overline{p}p \to 3\pi^0$, $\pi^0\pi^0\eta$ and $\pi^0\pi^0\eta'$ at rest (Amsler, 1994a, 1996a) which occur with a sufficiently high probability (see Table 9 below) and are kinematically well constrained. Events with five photons were selected from a sample of 15 million annihilations into neutral final states (18 million for η' decays). Since the branching ratio for 0-prong annihilation is about 4%, the data sample corresponds to some 400 million $\overline{p}p$ annihilations in liquid hydrogen.

Events consistent with $\pi^0\pi^0$ decays and a single (unpaired) γ were then selected by requiring energy and momentum conservation for $\overline{p}p$ annihilation into $\pi^0\pi^0\pi^0$, $\pi^0\pi^0\eta$ or $\pi^0\pi^0\eta'$ with a missing π^0 , η or η' . Thus 3C kinematic fits were applied, ignoring the remaining fifth photon. The measured energy of the latter was then transformed into the rest frame of the missing pseudoscalar. In this frame a missing state X with mass m_X would produce a peak in the γ -energy distribution at

$$E_{\gamma}^* = \frac{m}{2} \left(1 - \frac{m_X^2}{m^2} \right),\tag{32}$$

with width determined by the experimental resolution, where m is the mass of the missing pseudoscalar. Thus, if X is simply a missing (undetected) γ from π^0, η or η' decay, one finds with $m_X = 0$ that $E_{\gamma}^* = m/2$, as expected.

The main source of background is annihilation into three pseudoscalars for which one of the photons escaped detection. This occurs for (i) photons with energies below detection threshold (E < 20 MeV) or (ii) for photons emitted into insensitive areas of the detector. The latter background can be reduced by rejecting events for which the missing γ could have been emitted e.g. in the holes along the beam pipe. The high efficiency and large angular coverage of the Crystal Barrel are therefore crucial in this analysis. For the $3\pi^0$ channel an important background also arose from $\overline{p}p \to \pi^0 \omega$ with $\omega \to \pi^0 \gamma$, leading to 5γ . This background could be reduced by rejecting events which satisfy the $\pi^0 \omega (\to \pi^0 \gamma)$ kinematics. For $\pi^0 \pi^0 \eta$, the background channel $K_S(\to 2\pi^0)K_L$ with an interacting K_L faking a missing η could be eliminated with appropriate kinematic cuts.

The E_{γ}^* -energy distribution for π^0 decay is shown in Fig. 12. The broad peak around 70 MeV is due to π^0 decays into 2γ where one γ has escaped detection, or from residual $\pi^0 \omega$ events. The fit to the distribution (full line) agrees with the simulated rate of background from $3\pi^0$ and $\pi^0 \omega$. The dotted line shows the expected signal for a state with mass $m_X = 120$ MeV, produced in π^0 decay with a branching ratio of 5×10^{-4} . The corresponding distributions for η and η' decays can be found in Amsler (1996a).

Upper limits for radiative decays are given in Fig. 13 as a function of m_X . The upper limit for π^0 decay is an order of magnitude lower than from previous experiments (Atiya, 1992). For η and η' decays no limits were available previously. Light gauge bosons are therefore not observed in radiative pseudoscalar decays at a level of 10^{-4} to 10^{-5} .

5.3 $\eta \rightarrow 3\pi$

The 3π decay of the η plays an important role in testing low energy QCD predictions. This isospin breaking decay is mainly due to the mass difference between u and d quarks. Crystal Barrel has measured the relative branching ratios for $\eta \to \pi^+\pi^-\pi^0$, $\eta \to 3\pi^0$ and $\eta \to 2\gamma$ from samples of annihilations into $2\pi^+2\pi^-\pi^0$, $\pi^+\pi^-3\pi^0$ and $\pi^+\pi^-2\gamma$, respectively (Amsler, 1995d). The ratios of partial widths are

$$r_{1} \equiv \frac{\Gamma(\eta \to 3\pi^{0})}{\Gamma(\eta \to \pi^{+}\pi^{-}\pi^{0})} = 1.44 \pm 0.13,$$

$$r_{2} \equiv \frac{\Gamma(\eta \to 2\gamma)}{\Gamma(\eta \to \pi^{+}\pi^{-}\pi^{0})} = 1.78 \pm 0.16.$$
(33)

The result for r_1 is in good agreement with chiral perturbation theory: 1.43 ± 0.03 (Gasser and Leutwyler, 1985) and 1.40 ± 0.03 when taking unitarity corrections into account (Kambor, 1996). With the known 2γ partial width (Barnett, 1996) one can calculate from r_2 the partial width $\Gamma(\pi^+\pi^-\pi^0) = 258 \pm 32$ eV, in accord with chiral perturbation theory ($\Gamma = 230$ eV), taking into account corrections to the u - d mass difference (Donoghue, 1992). In good approximation, the $\eta \to \pi^+\pi^-\pi^0$ Dalitz plot may be described by the matrix element squared

$$|M(x,y)|^2 \propto 1 + ay + by^2$$
(34)

with

$$y \equiv \frac{3T_0}{m(\eta) - m(\pi^0) - 2m(\pi^{\pm})} - 1,$$
(35)

where T_0 is the kinetic energy of the neutral pion. The parameters a and b were determined in Amsler (1995d), but more accurate values are now available from the annihilation channel $\overline{p}p \to \pi^0 \pi^0 \eta$. Abele (1997b) finds

$$a = -1.19 \pm 0.07, \quad b = 0.19 \pm 0.11,$$
(36)

in reasonable agreement with chiral perturbation calculations which predict a = -1.3 and b = 0.38 (Gasser and Leutwyler, 1985).

The matrix element for η decay to $3\pi^0$ is directly connected to the matrix element for the charged mode because $3\pi^0$ is an I = 1 state. The matrix element squared for η decay to $3\pi^0$ is given by

$$|M(z)|^2 = 1 + 2\alpha z, (37)$$

where z is the distance from the center of the $\eta \to 3\pi^0$ Dalitz plot,

$$z = \frac{2}{3} \sum_{i=1}^{3} \left[\frac{3E_i - m(\eta)}{m(\eta) - 3m(\pi^0)} \right]^2,$$
(38)

and where E_i are the total energies of the pions. Chiral perturbation theory up to nextto-leading order predict α to be zero (Gasser and Leutwyler, 1985) leading to a homogeneously populated Dalitz plot. Taking unitarity corrections into account, Kambor (1996) predicts $\alpha \sim -0.01$. Experiments have so far reported values for α compatible with zero, e.g. Alde (1984) finds -0.022 ± 0.023 .

Crystal Barrel has analyzed the $3\pi^0$ Dalitz plot with 98,000 η decays from the annihilation channel $\pi^0\pi^0\eta$, leading to 10 detected photons (Abele, 1997c). The background and acceptance corrected matrix element is shown in Fig. 14 as a function of z. The slope is clearly negative:

$$\alpha = -0.052 \pm 0.020. \tag{39}$$

5.4 $\eta' \rightarrow \pi^+ \pi^- \gamma$

The $\pi^+\pi^-\gamma$ decay mode of the η' is generally believed to proceed through the $\rho(770)\gamma$ intermediate state (Barnett, 1996). However, the ρ mass extracted from a fit to the $\pi^+\pi^-$ mass spectrum appears to lie some 20 MeV higher than for ρ production in $e^+e^$ annihilations. This effect is due to the contribution of the direct decay into $\pi^+\pi^-\gamma$ (Bityukov, 1991) through the so- called box anomaly (Benayoun, 1993). Crystal Barrel has studied the $\eta' \to \pi^+\pi^-\gamma$ channel where the η' is produced from the annihilation channels $\pi^0\pi^0\eta'$, $\pi^+\pi^-\eta'$ and $\omega\eta'$ (Abele, 1997i). Evidence for the direct decay was confirmed at the 4σ level by fitting the $\pi^+\pi^-$ mass spectrum from a sample of 7,392 η' decays. Including contributions from the box anomaly, the ρ mass turns out to be consistent with the standard value from e^+e^- annihilation. Using the known two-photon decay widths of η and η' and the $\eta \to \pi^+\pi^-\gamma$ decay spectrum from Layter (1973) the collaboration derived the pseudoscalar nonet parameters $f_{\pi}/f_1=0.91 \pm 0.02$, $f_8/f_{\pi}=0.90$ ± 0.05 and the pseudoscalar mixing angle $\theta_p = (-16.44 \pm 1.20)^{\circ}$.

5.5 Radiative ω decays

The rates for radiative meson decays can be calculated from the naive quark model using SU(3) and the OZI rule (O'Donnell, 1981). Assuming ideal mixing in the vector nonet one finds, neglecting the small difference between u and d quark masses:

$$\frac{B(\omega \to \eta\gamma)}{B(\omega \to \pi^0 \gamma)} = \frac{1}{9} \frac{p_\eta^3}{p_{\pi^0}^3} \cos^2(54.7^\circ + \theta_p) = 0.010, \tag{40}$$

where $p_{\pi} = 379$ MeV/c and $p_{\eta} = 199$ MeV/c are the decay momenta in the ω rest frame and θ_p is the pseudoscalar mixing angle (Amsler, 1992b). However, the production and decay of the ω and ρ mesons are coupled by the isospin breaking ω to ρ transition since these mesons overlap (for references on $\rho - \omega$ mixing, see O'Connell (1995)). Since the width of ρ is much larger than the width of ω , the effect of $\rho - \omega$ mixing is essential in processes where ρ production is larger than ω production, for example in e^+e^- annihilation where ω and ρ are produced with a relative rate of 1/9. The determination of the branching ratio for $\omega \to \eta \gamma$ varies by a factor of five depending on whether the interference between $\omega \to \eta \gamma$ and $\rho^0 \to \eta \gamma$ is constructive or destructive (Dolinsky, 1989). A similar effect is observed in photoproduction (Andrews, 1977). The GAMS collaboration has determined the $\omega \to \eta \gamma$ decay branching ratio, $(8.3 \pm 2.1) \times 10^{-4}$, using the reaction $\pi^-p \to \omega n$ at large momentum transfers, thus suppressing ρ production (Alde, 1994).

In $\overline{p}p$ annihilation at rest the branching ratio for $\omega \pi^0$ is much smaller than the branching ratio for $\rho^0 \pi^0$ while the converse is true for $\eta \omega$ and $\eta \rho^0$ (Table 2). We therefore expect that a determination of the $\omega \to \eta \gamma$ branching ratio from $\pi^0 \omega$, neglecting $\rho - \omega$ mixing, will lead to a larger value than from $\eta \omega$. However, a simultaneous analysis of both branching ratios, including $\rho - \omega$ mixing, should lead to consistent results and allow a determination of the relative phase between the two amplitudes. In Abele (1997d) the channels $\pi^0 \omega$ and $\eta \omega \ (\omega \to \eta \gamma)$ were reconstructed from 15.5 million 0-prong events with five detected γ 's. The events were submitted to a 6C kinematic fit assuming total energy and total momentum conservation, at least one $\pi^0 \to 2\gamma$ (or one $\eta \to 2\gamma$) and $\omega \to 3\gamma$. The $\omega \to 3\gamma$ Dalitz plots for $\pi^0 \omega$ and $\eta \omega$ are shown in Fig. 15, using the variables

$$x = \frac{T_2 - T_1}{\sqrt{3}Q}, \ y = \frac{T_3}{Q} - \frac{1}{3},\tag{41}$$

where T_1, T_2 and T_3 are the kinetic energies of the γ 's in the ω rest frame and $Q = T_1 + T_2 + T_3$. The prominent bands along the boundaries are due to $\omega \to \pi^0 \gamma$ and the weaker bands around the center to $\omega \to \eta \gamma$.

The main background contributions arose from 6γ events ($\overline{p}p \rightarrow 3\pi^0, 2\pi^0\eta, 2\eta\pi^0$) with a missing photon. This background (10% in the $\pi^0\omega$ and 5% in the $\eta\omega$ Dalitz plots) was simulated using the 3-pseudoscalar distributions discussed in section 8 and could be reduced with appropriate cuts (Pietra, 1996). After removal of the π^0 bands 147 ± 25 $\omega \rightarrow \eta\gamma$ events were found in the η bands of Fig. 15(a) and 123 ± 19 events in the η bands of Fig. 15(b).

The branching ratio for $\omega \to \eta \gamma$ was derived by normalizing on the known branching ratio for $\omega \to \pi^0 \gamma$, (8.5 ± 0.5) % (Barnett, 1996). Correcting for the reconstruction efficiency Abele (1997d) finds a branching ratio of $(13.1 \pm 2.4) \times 10^{-4}$ from $\pi^0 \omega$ and $(6.5 \pm 1.1) \times 10^{-4}$ from $\eta \omega$, hence a much larger signal from $\pi^0 \omega$.

Consider now the isospin breaking electromagnetic $\rho - \omega$ transition. The amplitude S for the reaction $\overline{p}p \to X(\rho - \omega) \to X\eta\gamma$ is, up to an arbitrary phase factor (Goldhaber, 1969):

$$S = \frac{|A_{\rho}||T_{\rho}|}{P_{\rho}} \left(1 - \frac{|A_{\omega}|}{|A_{\rho}|} \frac{e^{i\alpha}\delta}{P_{\omega}}\right) + e^{i(\alpha+\phi)} \frac{|A_{\omega}||T_{\omega}|}{P_{\omega}} \left(1 - \frac{|A_{\rho}|}{|A_{\omega}|} \frac{e^{-i\alpha}\delta}{P_{\rho}}\right), \qquad (42)$$

where A is the production and T the decay amplitude of the two mesons and $P_{\rho} \equiv m - m_{\rho} + i\Gamma_{\rho}/2$, $P_{\omega} \equiv m - m_{\omega} + i\Gamma_{\omega}/2$. The parameter δ was determined from $\omega, \rho \to \pi^+ \pi^-$: $\delta = (2.48 \pm 0.17)$ MeV (Weidenauer, 1993). The relative phase between the production amplitudes A_{ρ} and A_{ω} is α while the relative phase between the decay amplitudes T_{ρ} and T_{ω} is ϕ . In the absence of $\rho - \omega$ interference ($\delta = 0$) Eq. (42) reduces to a sum of two Breit-Wigner functions with relative phase $\alpha + \phi$. The magnitudes of the amplitudes A and T are proportional to the production branching ratios and the partial decay widths, respectively.

The production phase α can be determined from $\rho, \omega \to \pi^+\pi^-$ since the isospin violating decay amplitude $T(\omega \to \pi^+\pi^-)$ may be neglected, leaving only the first term in Eq. (42). A value for α consistent with zero, $(-5.4\pm4.3)^\circ$, was measured by Crystal Barrel, using the channel $\overline{p}p \to \eta\pi^+\pi^-$ where $\rho - \omega$ interference is observed directly (Abele, 1997a). This phase is indeed predicted to be zero in e^+e^- annihilation, in photoproduction and also in $\overline{p}p$ annihilation (Achasov and Shestakov, 1978).

With the branching ratios for $\omega \pi^0$, $\omega \eta$, $\pi^0 \rho^0$ and $\eta \rho^0$ given in Table 2 the intensity $|S|^2$ was fitted to the number of observed $\omega \to \eta \gamma$ events in $\omega \pi^0$ and $\omega \eta$, using Monte Carlo simulation. Both channels lead to consistent results for

$$B(\omega \to \eta \gamma) = (6.6 \pm 1.7) \times 10^{-4}, \tag{43}$$

in agreement with the branching ratio from $\eta\omega$, obtained by neglecting $\rho - \omega$ interference. The phase $\phi = (-20^{+70}_{-50})^{\circ}$ leads to constructive interference. The result Eq. (43) is in excellent agreement with Alde (1994) and with the constructive interference solution in e^+e^- , $(7.3 \pm 2.9) \times 10^{-4}$ (Dolinsky, 1989). This then solves the longstanding ambiguity in e^+e^- annihilation between the constructive ($\phi = 0$) and destructive ($\phi = \pi$) interference solutions. The branching ratio for $\rho^0 \to \eta\gamma$, $(12.2 \pm 10.6) \times 10^{-4}$, is not competitive but agrees with results from e^+e^- , $(3.8 \pm 0.7) \times 10^{-4}$ for constructive interference (Dolinsky, 1989; Andrews, 1977). Using Eq. (40) one then finds

$$\frac{B(\omega \to \eta \gamma)}{B(\omega \to \pi^0 \gamma)} = (7.8 \pm 2.1) \times 10^{-3}, \tag{44}$$

in agreement with SU(3).

The $\omega \to 3\gamma$ Dalitz plot is also useful to search for the direct process $\omega \to 3\gamma$ which is similar to the decay of $({}^{3}S_{1})$ orthopositronium into 3γ and has not been observed so far. By analogy, the population in the $\omega \to 3\gamma$ Dalitz plot is expected to be almost homogeneous except for a slight increase close to its boundaries (Ore and Powell, 1949). Using the central region in Fig. 15(a) which contains only one event (6 entries) one obtains the upper limit $B(\omega \to \pi^{0}\gamma) = 1.9 \times 10^{-4}$ at 95% confidence level. This is somewhat more precise that the previous upper limit, 2×10^{-4} at 90% confidence level (Prokoshkin and Samoilenko, 1995).

6 Production of ϕ Mesons

It has been known for some time that ϕ production is enhanced beyond expectation from the OZI rule in various hadronic reactions (Cooper, 1978). Let us return to Eq. (21) and replace η by ϕ and η' by ω . The mixing angle becomes the mixing angle θ_v in the vector nonet. According to the OZI rule, ϕ and ω can only be produced through their $u\overline{u} + d\overline{d}$ components. Hence ϕ production should vanish for an ideally mixed vector nonet $(\theta_v = \theta_i)$ in which ϕ is purely $s\overline{s}$. Since ϕ also decays to 3π this is not quite the case and we find for the ratio of branching ratios with a recoiling meson X and apart from phase space corrections,

$$\tilde{R}_X = \frac{B(X\phi)}{\tilde{B}(X\omega)} = \tan^2(\theta_i - \theta_v) = 4.2 \times 10^{-3} \text{ or } 1.5 \times 10^{-4},$$
(45)

for the quadratic ($\theta_v = 39^\circ$) or linear ($\theta_v = 36^\circ$) Gell-Mann-Okubo mass formula (Barnett, 1996).

The branching ratios for $\overline{p}n$ annihilation into $\pi^-\phi$ and $\pi^-\omega$ have been measured in deuterium bubble chambers. The ratio \tilde{R}_{π^-} lies in the range 0.07 to 0.22 indicating a strong violation of the OZI rule (for a review, see Dover and Fishbane (1989)). The Asterix experiment at LEAR has measured ϕ production in $\overline{p}p$ annihilation into $\pi^0\phi$, $\eta\phi$, $\rho^0\phi$ and $\omega\phi$ in gaseous hydrogen at NTP (50% P-wave annihilation) and in coincidence with atomic L X-rays (P-wave annihilation). The branching ratios for pure S-wave were then obtained indirectly by linear extrapolation (Reifenröther, 1991). With the corresponding ω branching ratios, then available from literature, the authors reported a strong violation of the OZI rule, especially for $\pi^0\phi$. Some of the branching ratios from Crystal Barrel are, however, in disagreement with previous results. We shall therefore review the direct measurement of ϕ production in liquid from Crystal Barrel and then reexamine the evidence for OZI violation with the two-body branching ratios listed in Table 2.

6.1 Annihilation into $\pi^0 \phi$, $\eta \phi$ and $\gamma \phi$

Crystal Barrel has studied the channels

$$\overline{p}p \to K_S K_L \pi^0 \text{ and } K_S K_L \eta,$$
(46)

where K_S decays to $\pi^0 \pi^0$ and η to $\gamma\gamma$, leading to six photons and a missing (undetected) K_L (Amsler, 1993d). The starting data sample consisted of 4.5×10^6 0-prong annihilations. By imposing energy and momentum conservation, the masses of the three reconstructed pseudoscalars and the K_S mass, a (5C) kinematic fit was applied leading to 2,834 $K_S K_L \pi^0$ and 72 $K_S K_L \eta$ events with an estimated background of 4%, respectively 36%.

The $K_S K_L \pi^0$ Dalitz plot is shown in Fig. 16. One observes the production of $K^*(892)$ $(\rightarrow K\pi)$ and $\phi(\rightarrow K_S K_L)$. A Dalitz plot analysis was performed with the method described in section 7.2. Since the *C*-parity of $K_S K_L$ is negative⁵ the contributing initial atomic S-state is 3S_1 . One obtains a good fit to the Dalitz plot with only two amplitudes, one for $K^*\overline{K}$ (and its charge conjugated $K\overline{K}^*$ which interferes constructively) and one for $\pi^0\phi$ with a relative contribution to the $K_S K_L \pi^0$ channel of

$$\frac{K^*\overline{K} + K\overline{K}^*}{\pi^0\phi} = 2.04 \pm 0.21.$$
(47)

The final state $K_S K_L \eta$ is much simpler since only $\eta \phi$ contributes (Amsler, 1993d). One obtains by comparing the intensities for $\pi^0 \phi$ and $\eta \phi$

$$\frac{B(\pi^0 \phi)}{B(\eta \phi)} = 8.3 \pm 2.1,\tag{48}$$

taking into account the unobserved decay modes of the η meson.

Events with a K_L interacting in the CsI crystals have been removed by the selection procedure which required exactly six clusters in the barrel. The last two results therefore assume that the interaction probability for K_L in CsI does not vary significantly with K_L momentum. Therefore, this interaction probability needs to be determined to derive absolute branching ratios for $\pi^0 \phi$ and $\eta \phi$. This number cannot be obtained directly by Monte Carlo simulation due to the lack of data for low energy K_L interacting with nuclear matter. With monoenergetic (795 MeV/c) K_L from the channel $\overline{p}p \rightarrow K_S K_L$, Amsler (1995c) finds an interaction probability of (57 ± 3) % in the CsI barrel. This leads to a branching ratio of (9.0 ± 0.6) ×10⁻⁴ for $K_S K_L$, in agreement with bubble chamber data (Table 2).

An average interaction probability of $(54 \pm 4)\%$ was measured with the kinematically well constrained annihilation channel $K_S(\to \pi^+\pi^-)K_L\pi^0$ (Abele, 1997e). However, in Amsler (1995c) a somewhat lower probability was used. Updating their $\pi^0\phi$ branching ratio one finds together with their compatible result from $\pi^0(\phi \to K^+K^-)$:

$$B(\bar{p}p \to \pi^0 \phi) = (6.5 \pm 0.6) \times 10^{-4}.$$
 (49)

From Eq. (48) one then obtains

$$B(\overline{p}p \to \eta\phi) = (7.8 \pm 2.1) \times 10^{-5}.$$
 (50)

Both numbers are slightly higher than from indirect data in gaseous hydrogen which were extrapolated to pure S-wave annihilation (Reifenröther, 1991), see Table 6.

⁵Note that $K^0\overline{K^0}$ recoiling against π^0 appears as $K_SK_S + K_LK_L$ ($J^{PC} = \text{even}^{++}$) from ¹ S_0 and as K_SK_L ($J^{PC} = \text{odd}^{--}$) from ³ S_1 .

Radiative annihilation into ϕ mesons should be suppressed by both the OZI rule and the electromagnetic coupling. Crystal Barrel has studied the channel $\gamma \phi$ with the reactions

$$\overline{p}p \to K_S K_L \gamma \text{ and } K^+ K^- \gamma,$$
(51)

(Amsler, 1995c). In the first reaction K_S decays to $\pi^0 \pi^0$, K_L is not detected and thus the final state consists of five photons. The $K_S K_L \gamma$ final state was selected from 8.7 × 10⁶ 0-prong annihilations by performing a 4C fit, imposing energy and momentum conservation, the masses of the two pions and the K_S mass. The background reaction $\overline{p}p \rightarrow K_S K_L$ with an interacting K_L faking the fifth photon could easily be suppressed since K_L and K_S are emitted back-to-back. The experimental $K_S K_L \gamma$ Dalitz plot is dominated by background from $K_S K_L \pi^0$ with a missing (undetected) low energy γ from π^0 decay and is therefore similar to the one shown in Fig. 16. The background contribution to $\gamma \phi$, mainly from $\pi^0 \phi$ with a missing photon, was estimated by Monte Carlo simulation and by varying the photon detection threshold. This led to $211 \pm 41 \ \gamma \phi$ events corresponding to a branching ratio $B(\gamma \phi) = (2.0 \pm 0.5) \times 10^{-5}$, after correcting for the (updated) K_L interaction probability.

A sample of 1.6×10^6 2-prong annihilations was used to select the second reaction in (51). After a cut on energy and momentum conservation (assuming kaons) the measured ionization loss in the JDC was used to separate kaons from pions. Again, the dominating background to $\gamma\phi$ arose from $\pi^0\phi$ with a missing γ . This background was subtracted by varying the γ detection threshold and by keeping only γ 's with energies around 661 MeV, as required by two-body kinematics. The signal of 29 events led to a branching ratio $B(\gamma\phi) = (1.9 \pm 0.7) \times 10^{-5}$ which is less precise but in good agreement with data from the neutral mode. The average is then

$$B(\overline{p}p \to \phi\gamma) = (2.0 \pm 0.4) \times 10^{-5},\tag{52}$$

which updates the result from Amsler (1995c).

6.2 ϕ/ω ratio

Table 7 and Fig. 17 show the phase space corrected ratios \tilde{R}_X (Eq. (45)). The nearest threshold dominance factors (Eq. (20)) have been used but the measured ratios do not differ significantly from \tilde{R}_X . Phase space factors of the type (28) lead to even larger ratios. For $X = \gamma, \pi^0, \eta$ we used Crystal Barrel data. For $X = \omega$ we used for $\omega\omega$ the branching ratio from Crystal Barrel (multiplied by two for identical particles) and for $\omega\phi$ the branching ratio from Bizzarri (1971) (Table 2). For completeness we also list the result for $X = \rho$ from Reifenröther (1991) and Bizzarri (1969) and the recent Obelix data for R_{π^-} (Ableev, 1995) and R_{π^+} (Ableev, 1994) in $\overline{p}n$ and $\overline{n}p$ annihilation.

Annihilation into $\omega \pi^0 \pi^0$ and $\phi (\to K_L K_S) \pi^0 \pi^0$ can be used to extract the ratio \tilde{R}_{σ} (Spanier, 1997), where σ stands for the low energy $(\pi \pi)$ S-wave up to 900 MeV (section 8.4). Finally, the ratio $R_{\pi^+\pi^-}$ was also measured in $\overline{p}p$ at rest (Bertin, 1996). Table 7 and Fig. 17 show their result for $\pi^+\pi^-$ masses between 300 and 500 MeV.

The production of ϕ mesons is enhanced in all channels except $\eta\phi$ and is especially dramatic in $\gamma\phi$ (from ¹S₀) and $\pi^{0}\phi$ (from ³S₁). Several explanations for this effect have been proposed:

(i) High energy reactions reveal the presence of sea $s\overline{s}$ pairs in the nucleon at high momentum transfers but valence $s\overline{s}$ pairs could enhance the production of ϕ mesons already at small momentum transfers. Figure 18 shows the OZI allowed production of $s\overline{s}$ mesons through the shake-out mechanism (a) and through the OZI allowed rearrangement

process (b) (Ellis, 1995). The fraction of $s\overline{s}$ pairs in the nucleon required to explain the measured $\pi^0 \phi$ rate lies between 1 and 19%. Deep inelastic muon scattering data indicate an $s\overline{s}$ polarization opposite to the spin of the nucleon (Ellis, 1995). For annihilation from the 3S_1 state the wave function of the (3S_1) $s\overline{s}$ would match the wave function of the ϕ in the rearrangement process of Fig. 18(b), leading to an enhanced production of ϕ mesons. The absence of enhancement in $\eta\phi$ could be due to destructive interference between additional graphs arising from the $s\overline{s}$ content of η . However, this model does not explain the large branching ratios for the two-vector channels $\rho^0\phi$, $\omega\phi$ and especially $\gamma\phi$ which proceed from the 1S_0 atomic state.

In the tensor nonet, the mainly $s\overline{s}$ meson is $f'_2(1525)$ and $f_2(1270)$ is the mainly $u\overline{u}+d\overline{d}$. Using annihilation into $K_L K_L \pi^0$ and $3\pi^0$ (section 8) Crystal Barrel has measured the ratio of $f'_2(1525)\pi^0$ to $f_2(1270)\pi^0$ from 1S_0 . After dividing by W (Eq. (20)) one finds with the most recent branching ratio for $f'_2(1525)$ decay to $K\overline{K}$ from Barnett (1996), see Table 13 below:

$$\frac{\tilde{B}(\bar{p}p \to f_2'(1525)\pi^0)}{\tilde{B}(\bar{p}p \to f_2(1270)\pi^0)} = \tan^2(\theta_i - \theta_t) = (2.6 \pm 1.0) \times 10^{-2}.$$
(53)

The mixing angle θ_t in the 2⁺⁺ nonet is found to be $(26.1^{+2.0}_{-1.6})^{\circ}$, in good agreement with the linear (26°) or quadratic (28°) mass formulae (Barnett, 1996). There is therefore no OZI violating $s\overline{s}$ enhancement from $f'_2(1525)\pi^0$ in liquid hydrogen.

(ii) Dover and Fishbane (1989) suggest that the $\pi^0 \phi$ enhancement is due to mixing with a four-quark state $(s\bar{s}q\bar{q})$ with mass below $2m_p$ (Fig. 18(c)). This exotic meson would then have the quantum numbers of the $\bar{p}p$ initial state (${}^3S_1 = 1^{--}$ with I = 1). This would also explain why $\eta \phi$ (I = 0) is not enhanced and why $\pi^0 \phi$ is weak from 1P_1 (Reifenröther, 1991). A 1⁻⁻ state, $C(1480) \to \pi \phi$, has in fact been reported in $\pi^- p \to \pi^0 \phi n$ (Bityukov, 1987). This isovector cannot be $q\bar{q}$ since it would decay mostly to $\pi \omega$, which is not observed. Indeed, Crystal Barrel does not observe any $\pi^0 \omega$ signal in this mass region in $\bar{p}p \to \pi^0 \pi^0 \omega$ at rest (Amsler, 1993a). Also, C(1480) has not been observed in $\bar{p}p$ annihilation at rest into $\pi^+\pi^-\phi$ (Reifenröther, 1991) nor into $\pi^0\pi^0\phi$ (Abele, 1997f). In any case the large $\gamma \phi$ signal with the "wrong" quantum numbers 1S_0 remains unexplained by this model.

(iii) We have seen (Eq. (47)) that the $K\overline{K}\pi$ final state is dominated by $K^*\overline{K}$ production which proceeds dominantly from the I = 1 3S_1 state (see section 8.8). The ϕ enhancement could then be due to $K^*\overline{K}$ and $\rho\rho$ rescattering (Fig.18(d)). In Gortchakov (1996) $K^*\overline{K}$ and $\rho\rho$ interfere constructively to produce a $\pi^0\phi$ branching ratio as high as 4.6×10^{-4} , nearly in agreement with experimental data. In Locher (1994) and Markushin (1997) the large $\gamma\phi$ branching ratio simply arises from VDM: The channels $\rho^0\omega$ and $\omega\omega$ interfere destructively in Eq. (30) (thereby lowering the branching ratio for $\gamma\omega$) while $\rho^0\phi$ and $\omega\phi$ interfere constructively (thus increasing the branching ratio for $\gamma\phi$). This conclusion, however, depends strongly on the phase space correction: Prescription (20) leads to a $\gamma\phi$ branching ratio which exceeds the OZI prediction by a factor of ten (Table 5). Also, as pointed out by Markushin (1997), the large $\rho^0\phi$ and $\omega\phi$ rates remain unexplained but could perhaps be accommodated within a two-step mechanism similar to the one shown in Fig. 18(d).

The origin of the ϕ enhancement is therefore not clear. If I = 1 also dominates $\overline{p}p$ annihilation into $K^*\overline{K}$ from P-states in gaseous hydrogen, then the rescattering model would presumably conflict with the weak $\pi\phi$ production observed from 1P_1 states (Reifenröther, 1991). With strange quarks in the nucleon, the 3S_1 contribution and hence the contribution from $s\overline{s}$ pairs in the nucleon will be diluted by the large number of partial waves at higher \overline{p} momenta. Hence ϕ production should decrease with increasing momentum. Also, the small $\eta\phi$ rate, possibly due to destructive interference, implies that $\eta'\phi$ should

be abnormally large (Ellis, 1995). Finally, since $f'_2(1525)$ is a spin triplet meson one would expect a strong production of $f'_2(1525)\pi^0$ from triplet $\overline{p}p$ states at rest, hence 3P_1 (Ellis, 1995). The analysis of Crystal Barrel data in gaseous hydrogen and in flight will hopefully contribute to a better understanding of the ϕ enhancement in hadronic reactions.

7 Meson Spectroscopy

7.1 Introduction

Mesons made of light quarks u, d, s are classified within the $q\bar{q}$ nonets of SU(3)-flavor. The ground states (angular momentum L = 0) pseudoscalars (0^{-+}) and vectors (1^{--}) are well established. Among the first orbital excitations (L = 1), consisting of the four nonets 0^{++} , 1^{++} , 2^{++} , 1^{+-} , only the tensor (2^{++}) nonet is complete and unambiguous with the well established $a_2(1320)$, $f_2(1270)$, $f'_2(1525)$ and $K^*_2(1430)$ but another tensor, $f_2(1565)$ was discovered at LEAR in the 1500 MeV mass range (May, 1989).

Before Crystal Barrel three scalar (0^{++}) states were already well established: $a_0(980)$, $f_0(980)$ and $K_0^*(1430)$. Further candidates have been reported and we shall discuss the scalars in more details below. In the 1^{++} nonet two states compete for the $s\bar{s}$ assignment, $f_1(1420)$ and $f_1(1510)$. In the 1^{+-} nonet the $s\bar{s}$ meson is not established although a candidate, $h_1(1380)$, has been reported (Aston, 1988a; Abele 1997f). Many of the radial and higher orbital excitations are still missing. Recent experimental reviews on light quark mesons have been written by Blüm (1996) and Landua (1996) and theoretical predictions for the mass spectrum can be found in Godfrey and Isgur (1985).

Only overall color-neutral $q\overline{q}$ configurations are allowed by QCD but additional colorless states are possible, among them multiquark mesons ($\overline{q}^2 q^2$, $\overline{q}^3 q^3$) and mesons made of $q\overline{q}$ pairs bound by an excited gluon g, the hybrid states (Isgur and Paton, 1985; Close and Page, 1995). The 2⁻⁺ state $\eta_2(1870)$ has been reported by Crystal Barrel (Adomeit, 1996) with decay rates to $a_2^0(1320)\pi^0$ and $f_2(1270)\eta$ compatible with predictions for a hybrid state (Close and Page, 1995). Hybrids may have exotic quantum numbers, e.g. 1⁻⁺, which do not couple to $q\overline{q}$. An isovector state, $\hat{\rho}(1405)$, with quantum numbers 1⁻⁺ has been reported (Alde, 1988a; Thompson, 1997). However, lattice QCD predicts the lightest hybrid, a 1⁺⁻, around 2000 MeV (Lacock, 1997).

A striking prediction of QCD is the existence of isoscalar mesons which contain only gluons, the glueballs (for a recent experimental review, see Spanier (1996)). They are a consequence of the non-abelian structure of QCD which requires that gluons couple and hence may bind. The models predict low-mass glueballs with quantum numbers 0^{++} , 2^{++} and 0^{-+} (Szczepaniak, 1996). The ground state glueball, a 0^{++} meson, is expected by lattice gauge theories to lie in the mass range 1500 to 1700 MeV. The mass of the pure gluonium state is calculated at 1550 ± 50 MeV by Bali (1993) while Sexton (1995) predicts a slightly higher mass of 1707 ± 64 MeV. The first excited state, a 2^{++} , is expected around 2300 MeV (Bali, 1993).

Since the mass spectra of $q\overline{q}$ and glueballs overlap, the latter are easily confused with ordinary $q\overline{q}$ states. This is presumably the reason why they have not yet been identified unambiguously. For pure gluonium one expects couplings of similar strengths to $s\overline{s}$ and $u\overline{u} + d\overline{d}$ mesons since gluons are flavor-blind. In contrast, $s\overline{s}$ mesons decay mainly to kaons and $u\overline{u} + d\overline{d}$ mesons mainly to pions. Hence decay rates to $\pi\pi$, $K\overline{K}$, $\eta\eta$ and $\eta\eta'$ can be used to distinguish glueballs from ordinary mesons. However, mixing with nearby $q\overline{q}$ states may modify the decay branching ratios (Amsler and Close, 1996) and obscure the nature of the observed state. Nevertheless, the existence of a scalar gluonium state, whether pure or mixed with $q\bar{q}$, is signalled by a third isoscalar meson in the 0⁺⁺ nonet. It is therefore essential to complete the SU(3) nonets in the 1500 - 2000 MeV region and to identify supernumerary states. The most pressing questions to be addressed are:

- 1. What are the ground state scalar mesons, in particular is $f_0(980)$ the $s\overline{s}$ state and is $a_0(980)$ the isovector or are these states $K\overline{K}$ molecules (Weinstein and Isgur, 1990; Close, 1993) in which case the nonet members still need to be identified? Where are the first radial excitations and is there a supernumerary I = 0 scalar in the 1500 MeV region? Is $f_J(1710)$ scalar or tensor?
- 2. In the 0^{-+} sector, are $\eta(1295)$ and $\eta(1440)$ the two isoscalar radial excitations of η and η' or is $\eta(1440)$ a structure containing several states (Bai, 1990; Bertin, 1995), in particular a non- $q\overline{q}$ state around 1400 MeV?
- 3. Where are the hybrid states? Is $\eta_2(1870)$ a hybrid and does $\hat{\rho}(1405)$ really exist?

Before reviewing the new mesons discovered by Crystal Barrel and providing clues to some of these issues, we shall recall the mathematical tools used to extract the mass, width, spin and parity of intermediate resonances in $\overline{p}p$ annihilation at rest.

7.2 Spin-parity analysis

The Crystal Barrel data have been analyzed using the isobar model in which the $\overline{p}p$ system annihilates into N "stable" particles $(\pi^{\pm}, K^{\pm}, K^0, \pi^0, \eta, \eta')$ through intermediate resonances. The decay chain is assumed to be a succession of two-body decays $a \to bc$ followed by $b \to b_1 b_2$ and $c \to c_1 c_2$, etc. Final state rescattering is ignored. We shall calculate from the N momentum vectors the probability w_D that the final state proceeds through a given cascade of resonances. The final state may be from real data or from phase space distributed Monte Carlo events to be weighted by w_D .

The spins and parities of intermediate resonances are determined using the helicity formalism developed by Jacob and Wick (1959) or the equivalent method of Zemach tensors (Zemach, 1964, 1965). Here we describe briefly the helicity formalism. Suppose that a mother resonance with mass m_0 and spin J decays into two daughters (spins S_1 and S_2) with total spin S and relative angular momentum L. As quantization axis we choose the flight direction of the mother. The decay amplitude is given by the matrix (Amsler and Bizot, 1983)

$$A_{\lambda_1,\lambda_2;M} = D^J_{\lambda M}(\theta,\phi) \langle J\lambda | LS0\lambda \rangle \langle S\lambda | S_1 S_2 \lambda_1, -\lambda_2 \rangle \times BW_L(m),$$
(54)

where the row index $\lambda = \lambda_1 - \lambda_2$ runs over the $(2S_1 + 1)(2S_2 + 1)$ helicity states and the column index M over the 2J + 1 magnetic substates; θ and ϕ refer to the decay angles in the mother rest frame. $BW_L(m)$ is the Breit-Wigner amplitude⁶

$$BW_L(m) = \frac{m_0 \Gamma_0}{m_0^2 - m^2 - im_0 \Gamma(m)} F_L(p) \sqrt{\rho},$$
(55)

where

$$\Gamma(m) = \Gamma_0 \frac{m_0}{m} \frac{p}{p_0} \frac{F_L^2(p)}{F_L^2(p_0)}.$$
(56)

The mass and width of the resonance are m_0 and Γ_0 , p is the two-body decay momentum and p_0 the decay momentum for $m = m_0$. The damping factors $F_L(p)$ are given in Table

⁶ The phase space factor $\sqrt{\rho} = \sqrt{2p/m}$ should be dropped in Eq. (55) when events are drawn by Monte Carlo simulation, already assuming phase space distribution.

4. The matrix D is given by

$$D^{J}_{\lambda M}(\theta,\phi) = e^{iM\phi} d^{J}_{\lambda M}(\theta) \tag{57}$$

where the matrix $d^{J}_{\lambda M}(\theta)$ is the usual representation of a rotation around the *y*-axis, see for example Barnett (1996).

We shall describe the annihilation to the observed final state by a product of matrices A for successive decays in the cascade. Hence we first calculate from the N final state momentum vectors the angles θ and ϕ for all resonances through a series of Lorentz boosts, apply Eq. (54) to each decay and obtain the total amplitude through matrix multiplications, for example

$$A = [A(c \to c_1 c_2) \otimes A(b \to b_1 b_2)] A(\overline{p}p \to bc),$$
(58)

where \otimes denotes a tensor product. The matrix A has as many rows as the total final state spin multiplicity and has 2J + 1 columns, where J is the total spin of the $\overline{p}p$ system. We define the quantization axis as the direction of one of the daughters in the first decay (the annihilating $\overline{p}p$ atom) for which we choose $\theta = 0$, $\phi = 0$ and $BW_L(2m_p) = F_L(p)\sqrt{p}$.

Several decay chains of intermediate resonances may lead to the same observed final state of N stable particles. The transition probability w_D for chains starting from the same atomic state is given by the coherent sum

$$w_D = w \times \epsilon \times \operatorname{Tr} \left[\left(\sum_j \alpha_j A_j \right) \tilde{\rho} \left(\sum_k \alpha_k^* A_k^\dagger \right) \right] = w \times \epsilon \times \operatorname{Tr} \left| \sum_j \alpha_j A_j \right|^2,$$
(59)

where the sums extend over all decay chains labelled by the matrices A_j . We have assumed that the initial spin-density matrix $\tilde{\rho}$ is unity since the $\overline{p}p$ system is unpolarized. The phase space w and the detection probability ϵ will be ignored for Monte Carlo events drawn according to phase space and submitted to the detector simulation, since w = 1 and $\epsilon = 1$ or 0 for every Monte Carlo event. The parameters $\alpha_j = a_j \exp(-i\phi_j)$ are unknown constants to be fitted and one phase, say ϕ_0 , is arbitrary and set to zero. For chains decaying into the same resonances but with different electric charges (e.g. $\rho^+\pi^-, \rho^-\pi^+, \rho^0\pi^0$ $\rightarrow \pi^+\pi^-\pi^0$) these constants are given by isospin relations. The contributions from different atomic states are given by incoherent sums, i.e. by summing weights w_D of the form (59).

As an example, let us derive the weight w_D for the annihilation channel $\overline{p}p \to \rho^0 \rho^0 \to 2\pi^+ 2\pi^-$ from the atomic state ${}^1S_0 \ (J^{PC} = 0^{-+})$. Parity, *C*-parity and total angular momentum conservation require for $\rho^0 \rho^0$ that L = 1 and S = 1 (see section 4.1). The first Clebsch-Gordan coefficient in (54) is, apart from a constant,

$$\langle 0\lambda | 110\lambda \rangle \langle 1\lambda | 11\lambda_1, -\lambda_2 \rangle = \lambda_1 \delta_{\lambda_1 \lambda_2}, \tag{60}$$

and hence the amplitude vanishes unless the ρ 's are emitted with the same helicity $\lambda_1 = \lambda_2 \neq 0$. With J = 0, the matrices (57) are unity and therefore $A(\overline{p}p)$ is a column-vector with 9 rows

$$A(\overline{p}p) = \begin{pmatrix} 1 \\ 0 \\ . \\ . \\ . \\ 0 \\ -1 \end{pmatrix} F_1(p)\sqrt{p}.$$
 (61)

For $\rho \to \pi^+\pi^-$ one finds with S = 0 and J = 1 that L = 1 and the Clebsch-Gordan coefficients are unity. Hence we get with $\lambda = 0$ the 3-dimensional row-vector

$$A(\rho) = [D_{01}^{1}(\theta,\phi), D_{00}^{1}(\theta,\phi), D_{0-1}^{1}(\theta,\phi)]BW_{1}(m).$$
(62)

With Eq. (58) one then obtains

$$A = [A(\rho_1) \otimes A(\rho_2)]A(\overline{p}p)$$

= $[D_{01}^1(\theta_1, \phi_1)D_{01}^1(\theta_2, \phi_2) - D_{0-1}^1(\theta_1, \phi_1)D_{0-1}^1(\theta_2, \phi_2)]$
 $\times BW_1(m_1)BW_1(m_2)F_1(p)\sqrt{p},$
= $i\sin\theta_1\sin\theta_2\sin(\phi_1 + \phi_2)BW_1(m_1)BW_1(m_2)F_1(p)\sqrt{p},$ (63)

and therefore

$$w_D = \sin^2 \theta_1 \sin^2 \theta_2 \sin^2(\phi_1 + \phi_2) |BW_1(m_1)BW_1(m_2)|^2 F_1^2(p)p.$$
(64)

The angles refer to the directions of the pions in the ρ rest frames, with respect to the flight direction of the $\rho's$. Therefore the most probable angle between the planes spanned by the two dipions is 90°. This angular dependence is familiar in parapositronium (0⁻⁺) annihilation or π^0 decay where the γ polarizations are preferably orthogonal ($\phi_1 + \phi_2 = 90^\circ$). However, there are two ways to combine four pions into $\rho^0 \rho^0$ and therefore the final weight is actually given by the coherent sum (59) of two decay chains with $\alpha_1 = \alpha_2$.

As another example of symmetrization let us consider $\overline{p}p$ annihilation into $\pi K\overline{K}$ which will be discussed in detail below. The amplitudes for annihilation through the intermediate K^* are related through isospin Clebsch-Gordan coefficients (see for example Conforto (1967) or Barash (1965)). In general, annihilation may occur from 1S_0 or 3S_1 with isospin I = 0 or 1. For example, $\pi^0 K^+ K^-$ proceeds through $K^{*+} \to \pi^0 K^+$ or $K^{*-} \to \pi^0 K^$ with coefficients α_1 and α_2 equal in absolute magnitude and the two chains interfere. Table 8 gives the relative sign between α_1 and α_2 . Note that for 3S_1 the matrix (57) flips the sign so that the observed interference pattern is the same for 1S_0 or 3S_1 , namely constructive in $\pi^0 K^+ K^-$, $\pi^0 K^0 \overline{K^0}$ and $(I = 0) \pi^{\pm} K^{\mp} K^0$, and destructive in $(I = 1) \pi^{\pm} K^{\mp} K^0$. The signs given in Table 8 also apply to $K\overline{K}$ intermediate states with isospin i = 1 from $I(\overline{p}p) = 0$ and $I(\overline{p}p) = 1$ (the latter only contributing to $\pi^{\pm} K^{\mp} K^0$) and for states with isospin i = 0 from $I(\overline{p}p) = 1$ (to which $\pi^{\pm} K^{\mp} K^0$ does not contribute).

The procedure to analyze data is as follows: Phase space distributed Monte Carlo events are generated, tracked through the detector simulation and submitted to the reconstruction program. As already mentioned, this procedure automatically takes care of the factors ρ , w and ϵ . For $\overline{p}p$ annihilation into three stable particles, there are only two independent kinematic variables. One usually chooses the invariant masses squared m_{12}^2 and m_{13}^2 . The two-dimensional distribution (Dalitz plot) is then uniformly populated for phase space distributed events. The procedure consists in calculating w_D for each Monte Carlo event and to vary the constants α_i , the widths, masses and spin-parity assignments of the resonances until a good fit to the observed Dalitz plot density is achieved. Resonances with spins larger than 2 are too heavy to be produced in $\overline{p}p$ annihilation at rest and are therefore ignored.

For the Dalitz plot fits it is convenient to factorize w_D in terms of the real constants a_j and ϕ_j :

$$w_D = \sum_{i} a_i^2 Q_{ii} + 2 \sum_{i < j} a_i a_j \operatorname{Re}[Q_{ij}] \cos(\phi_i - \phi_j) + 2 \sum_{i < j} a_i a_j \operatorname{Im}[Q_{ij}] \sin(\phi_i - \phi_j), \quad (65)$$

where

$$Q_{ij} = \operatorname{Tr} \left[A_i A_j^{\dagger}\right]. \tag{66}$$

Dalitz plots weighted by Q_{ii} , $\operatorname{Re}[Q_{ij}]$ and $\operatorname{Im}[Q_{ij}]$ are then produced for each pair of chains $i, j \ (i \leq j)$. The Q_{ij} , and correspondingly the weights w_D , are normalized to the total number of real events N_T :

$$Q_{ij} \to Q_{ij} / \sqrt{f_i f_j},$$
 (67)

with

$$f_i = \sum Q_{ii}/N_T,\tag{68}$$

where the sum runs over all Monte Carlo events. One then divides the Dalitz plots into cells, adds them according to Eq. (65) and builds the χ^2

$$\chi^2 = \sum \frac{(n - w_D)^2}{n + w_D^2 / n_{MC}}$$
(69)

where the sum extends over all cells. The number of real events in each cell is denoted by n and the number of Monte Carlo events by n_{MC} .

With limited statistics or for more than two degrees of freedom (final states with more than three stable particles) the χ^2 minimization may be replaced by a likelihood maximization. One minimizes the quantity $S = -2 \ln L$ or

$$S = 2N_T \ln\left(\sum_{i=1}^{M_T} w_i[MC]\right) - 2\sum_{i=1}^{N_T} \ln w_i[DAT],$$
(70)

where $w_i[MC]$ and $w_i[DAT]$ are weights w_D calculated for Monte Carlo and data events, respectively. The sums run over N_T data events and M_T Monte Carlo events.

From the best fit the fractional contributions of the resonances in chain i are given by

$$r_i \equiv \frac{a_i^2}{\sum_i a_i^2},\tag{71}$$

where, obviously, $\sum r_i = 1$. This is a somewhat arbitrary definition which may not agree with the directly visible Dalitz plot densities, because interferences between the chains are neglected in Eq. (71). One may define alternatively

$$r_i \equiv a_i^2, \tag{72}$$

but then $\sum r_i$ may differ significantly from unity in the presence of strong interferences. Hence decay branching fractions for broad interfering resonances are not measurable unambiguously. This is an unavoidable caveat to keep in mind when extracting the internal structure of broad states from their decay branching ratios.

7.3 K-matrix analysis

The Breit-Wigner factors (55) violate unitarity when two resonances with the same quantum numbers overlap and decay into the same final state. Also, they do not describe distortions in the mass spectrum that occur around kinematical thresholds. For example, the $f_0(980) \rightarrow \pi\pi$ appears as a dip rather than a peak in the $\pi\pi$ mass spectrum of elastic $\pi\pi$ scattering, due to the opening of the decay channel $f_0(980) \rightarrow K\overline{K}$ (Au, 1987).

This behaviour can be described with the K-matrix formalism. A detailed description can be found in Chung (1995) and I shall only recall the formulae used in the analysis of Crystal Barrel data. Consider for instance the four scattering reactions

$$\begin{pmatrix}
\pi\pi \to \pi\pi & \pi\pi \to K\overline{K} \\
K\overline{K} \to \pi\pi & K\overline{K} \to K\overline{K}
\end{pmatrix}.$$
(73)

The transition amplitude T for a given partial wave is described by the 2×2 K-matrix

$$T = (1 - iK\rho)^{-1}K (74)$$

with the real and symmetric matrix

$$K_{ij}(m) = \sum_{\alpha} \frac{\gamma_{\alpha_i} \gamma_{\alpha_j} m_{\alpha} \Gamma'_{\alpha}}{m_{\alpha}^2 - m^2} B_{\alpha_i}(m) B_{\alpha_j}(m) + c_{ij}.$$
(75)

The sum runs over all resonances with K-matrix poles m_{α} decaying to $\pi\pi$ and $K\overline{K}$ with (real) coupling constants γ_{α_1} and γ_{α_2} , respectively, where

$$\gamma_{\alpha_1}^2 + \gamma_{\alpha_2}^2 = 1. (76)$$

The factors B_{α_i} are ratios of Blatt-Weisskopf damping factors (Table 4)

$$B_{\alpha_i}(m) = \frac{F_L(p_i)}{F_L(p_{\alpha_i})},\tag{77}$$

where L is the decay angular momentum, p the π or K momenta and p_{α_i} their momenta at the pole mass m_{α} . The optional real constants c_{ij} allow for a background (non-resonating) amplitude⁷. In Eq. (74) the matrix $\rho(m)$ describes the two-body phase space and is diagonal with $\rho_{11} \equiv \rho_1 = 2p_{\pi}/m$ and $\rho_{22} \equiv \rho_2 = 2p_K/m$. For masses far above kinematical threshold $\rho_i \sim 1$ and below $K\overline{K}$ threshold ρ_2 becomes imaginary.

The (K-matrix) partial width of resonance α to decay into channel i is defined as

$$\Gamma_{\alpha_i}(m_\alpha) = \gamma_{\alpha_i}^2 \Gamma'_\alpha \rho_i(m_\alpha), \tag{78}$$

and the (K-matrix) total width as

$$\Gamma_{\alpha} = \sum_{i} \Gamma_{\alpha_{i}}.$$
(79)

For a resonance with mass far above kinematic thresholds one obtains the partial and total widths

$$\Gamma_{\alpha_i} = \gamma_{\alpha_i}^2 \Gamma_{\alpha}', \quad \Gamma_{\alpha} = \Gamma_{\alpha}', \tag{80}$$

respectively. For one resonance and one channel (elastic scattering) the K-matrix reduces to

$$K = \frac{m_0 \Gamma'_0 B^2(m)}{m_0^2 - m^2},\tag{81}$$

and T (Eq. (74)) reduces to the relativistic Breit-Wigner

$$T = \frac{m_0 \Gamma_0 B^2(m) / \rho(m_0)}{m_0^2 - m^2 - im_0 \Gamma(m)},$$
(82)

with

$$\Gamma(m) = \Gamma_0 \frac{\rho(m)}{\rho(m_0)} B^2(m).$$
(83)

For a resonance far above threshold and with $\Gamma_0 \ll m_0$ we get the familiar expression

$$T = \frac{\Gamma_0/2}{m_0 - m - i\Gamma_0/2}.$$
(84)

⁷For the $\pi\pi$ S-wave a factor $(m^2 - 2m_{\pi}^2)/m^2$ is multiplied to the K-matrix to ensure a smooth behaviour near threshold.

Normally, the mass m_R and width Γ_R of a resonance are obtained from the poles of the T-matrix. Extending the mass m to complex values we find from (84) the poles at

$$m_P = m_R - i \frac{\Gamma_R}{2},\tag{85}$$

with $m_R = m_0$ and $\Gamma_R = \Gamma_0$. In general, however, m_R does not coincide with the pole of the K-matrix and Γ_R is different from the K-matrix width. For example, for two nonoverlapping resonances far above threshold, the K-matrix, T-matrix and Breit-Wigner poles coincide. As the resonance tails begin to overlap the two T-matrix poles move towards one another (for an example, see Chung, (1995)).

The $\pi\pi$ S-wave scattering amplitude is related to the $\pi\pi$ phase shift δ and inelasticity η through the relation

$$\rho_1(m)T_{11}(m) = \frac{\eta(m)\exp[2i\delta(m)] - 1}{2i}.$$
(86)

According to Eq. (74) the corresponding K-matrix then reads for pure elastic $\pi\pi$ -scattering ($\eta \equiv 1$)

$$K_{11}(m) = \frac{\tan \delta(m)}{\rho_1(m)}$$
 (87)

and becomes infinite at $m = m_0$, when δ passes through 90°. However, the amplitude T does not, in general, reach a resonance when $\delta = \pi/2$. As an example, consider the $\pi\pi$ S-wave scattering amplitude described by the amplitude (86) in the complex plane (Argand diagram): The intensity $|T|^2$ reaches its maximum value around 850 MeV ($\delta = 90^{\circ}$), loops back and passes rapidly through the $K\overline{K}$ threshold (see Fig. 23 below and Au (1987)). At ~1000 MeV $|T|^2$ reaches its minimum value ($\delta = 180^{\circ}$) and then starts a new (inelastic) loop. The $f_0(980)$ then appears as a hole in the $\pi\pi$ intensity distribution. We shall return to the S-wave Argand diagram when discussing the fits to Crystal Barrel data.

Consider now the production of a resonance α in $\overline{p}p$ annihilation. In the isobar model, the resonance is assumed not to interact with the recoiling system. The coupling strength to $\overline{p}p$ is denoted by the (complex) constant β_{α} while γ_{α_i} describes its decay strength into channel *i* (say $\pi\pi$ for i = 1 and $K\overline{K}$ for i = 2). Following Aitchison (1972) the amplitudes are given by the components of the vector

$$\mathcal{T} = (1 - iK\rho)^{-1}P.$$
(88)

The K-matrix now describes the propagation of the channel *i* through the resonances α while the vector *P* describes their production. *P* and *K* share the common poles m_{α} so that \mathcal{T} remains finite at the poles. The vector *P* is given by

$$P_j(m) = \sum_{\alpha} \frac{\beta_{\alpha} \gamma_{\alpha j} m_{\alpha} \Gamma'_{\alpha} B_{\alpha j}(m)}{m_{\alpha}^2 - m^2},$$
(89)

where the sum runs over all resonances. For a single resonance feeding only one decay channel we again obtain from Eq. (88) a Breit-Wigner distribution of the form (82) with coupling strength β :

$$\mathcal{T} = \frac{\beta m_0 \Gamma_0 B(m) / \rho(m_0)}{m_0^2 - m^2 - i m_0 \Gamma(m)}.$$
(90)

Let us now assume a series of resonances with the same quantum numbers decaying into two final states. The amplitude for the first final state is given by Eq. (88):

$$\mathcal{T}_1 = \frac{(1 - iK_{22}\rho_2)P_1 + iK_{12}\rho_2P_2}{1 - \rho_1\rho_2D - i(\rho_1K_{11} + \rho_2K_{22})},\tag{91}$$

with

$$D \equiv K_{11}K_{22} - K_{12}^2. \tag{92}$$

As an example, consider a single resonance, say $a_0(980)$ decaying to $\eta\pi$ and $K\overline{K}$. In this case $D \equiv 0$ and $B(m) \equiv 1$ (S-wave). We then obtain from Eq. (91) the formula (Flatté, 1976)

$$\mathcal{T}(\eta\pi) = \frac{bg_1}{m_0^2 - m^2 - i(\rho_1 g_1^2 + \rho_2 g_2^2)},\tag{93}$$

with

$$g_i \equiv \gamma_i \sqrt{m_0 \Gamma_0'} \quad \Rightarrow \quad \sum_{i=1}^2 g_i^2 = m_0 \Gamma_0', \tag{94}$$

and

$$b \equiv \beta \sqrt{m_0 \Gamma_0'}.$$
(95)

The phase space factors are

$$\rho_1(m) = \frac{2}{m} p_\eta \text{ and } \rho_2(m) = \frac{2}{m} p_K = \sqrt{1 - \frac{4m_K^2}{m^2}}.$$
(96)

The $\mathcal{T}(K\overline{K})$ amplitude is obtained by interchanging the labels 1 and 2 in Eq. (93). Below $K\overline{K}$ threshold ρ_2 becomes imaginary. Compared to pure $\eta\pi$ decay this leads to a shift of the resonance peak and to a narrower and asymmetric distribution of the observed signal in the $\eta\pi$ channel. This is shown in Fig. 19 for $g_1 = 0.324$ GeV, $g_2 = 0.279$ GeV (hence $\Gamma'_0 = 0.43$ GeV). These parameters have been extracted from the $a_0(980)$ contribution to $\overline{p}p \to \eta\pi^0\pi^0$ and $K\overline{K}\pi$ (section 8.8). A width of 54.12 ± 0.36 MeV was determined directly from the $a_0(980) \to \eta\pi$ signal in the annihilation channel $\omega\eta\pi^0$ (Amsler, 1994c), in good agreement with the observed width in Fig. 19. Also shown in Fig. 19 is the expected distribution for $\Gamma'_0 = 0.43$ GeV, assuming no $K\overline{K}$ decay. The observed width $\Gamma_0 = \Gamma'_0\rho_1(m_0)$ increases to 0.28 GeV.

The standard procedure in the analysis of Crystal Barrel data is to replace the Breit-Wigner function (55) by \mathcal{T} (Eq. (88)) and to fit the parameters g_{α_i} , β_{α} and m_{α} . The resonance parameters m_R and Γ_R are then extracted by searching for the complex poles (Eq. (85)) of the matrix \mathcal{T} . A one-channel resonance appears as a pole in the second Riemann-sheet and a two-channel resonance manifests itself as a pole in the second or third Riemann-sheet (Badalyan, 1982).

Some of the Crystal Barrel Dalitz plots have also been analyzed using the N/D formalism (Chew and Mandelstam, 1960) which takes into account the direct production of three mesons and also the final state interaction. In this formalism the amplitude \mathcal{T} has the same denominator as, e.g., in Eq. (91), but the numerator allows for additional degrees of freedom (Bugg, 1994).

8 Annihilation at Rest into Three Pseudoscalars

Proton-antiproton annihilation at rest into three pseudoscalars is the simplest process to search for scalar resonances $0^+ \rightarrow 0^- 0^-$, the recoiling third pseudoscalar removing the excess energy. The annihilation rates for these processes in liquid hydrogen (¹S₀ atomic state) are reasonably large since no angular momentum barrier is involved. Channels with three pseudoscalars have been studied earlier, but essentially in the 2-prong configuration and with limited statistics, e.g $\pi^+\pi^-\pi^0$ with 3,838 events (Foster, 1968b), $\pi^+\pi^-\eta$ with 459 events (Espigat, 1972) and $\pi^+\pi^-\eta'$ with 104 events (Foster, 1968a). The samples collected by the Asterix collaboration at LEAR (May, 1989; Weidenauer, 1990) are larger but were collected from atomic P-states. The $\pi^+\pi^-\pi^0$ final state revealed the existence of a tensor meson, $f_2(1565)$, produced from P-states (May, 1989, 1990). In the kaonic sector, data were collected in bubble chambers for the final states $\pi^{\pm}K^{\mp}K_S$ (2,851 events) and $\pi^0K_SK_S$ (546 events) in the experiments of Conforto (1967) and Barash (1965). Branching ratios for annihilation into three mesons are listed in Table 9.

Annihilation with charged pions is dominated by $\rho(770)$ production which complicates the spin-parity analysis of underlying scalar resonances in the $\pi\pi$ S-wave. Also, both ${}^{1}S_{0}$ and ${}^{3}S_{1}$ atomic states contribute. All-neutral (0-prong) channels are therefore simpler to analyze but more complex to select due to the large γ -multiplicity. The channel $\pi^{0}\pi^{0}\pi^{0}$ with 2,100 events has been reconstructed earlier with optical spark chambers (Devons, 1973). The existence of a scalar resonance decaying to $\pi\pi$ with mass 1527 and width 101 MeV was suggested in the $3\pi^{0}$ channel and in its $\pi^{-}\pi^{-}\pi^{+}$ counterpart in $\overline{p}n$ annihilation in deuterium (Gray, 1983). This was actually the first sighting of $f_{0}(1500)$ which will be discussed below.

The sizes of the data samples have been vastly increased by Crystal Barrel. We shall first review annihilation into three neutral non-strange mesons. We start from 6γ final states and select the channels $\overline{p}p \to \pi^0 \eta \eta, 3\pi^0, \pi^0 \pi^0 \eta, \pi^0 \eta \eta'$ and $\pi^0 \pi^0 \eta'$ by assuming total energy and total momentum conservation and constraining the 2γ masses to π^0, η and η' decays (7C fits), excluding any other possible configuration: Events are accepted if the kinematic fit satisfies the assumed three-pseudoscalar hypothesis with a confidence level typically larger than 10%. Background from the other 6γ channels is suppressed by rejecting those events that also satisfy any other 6γ final state hypothesis (including the strong $\omega\omega, \omega \to \pi^0 \gamma$) with a confidence level of at least 1%. The absolute branching ratios for the 6γ channels are determined by normalyzing on the branching ratio for $\overline{p}p \to \omega\omega$. These three-pseudoscalar channels have all been analyzed and we now review the salient features in their Dalitz plots. Results on kaonic channels are appended to the next sections.

8.1 $\overline{p}p \rightarrow \pi^0 \eta \eta$

The first evidence for two I = 0 scalars in the 1400 MeV mass region, now called $f_0(1370)$ and $f_0(1500)$, was obtained from a reduced sample of $2.3 \times 10^4 \pi^0 \eta \eta$ events (Amsler, 1992c). The invariant mass distributions are shown in Fig. 20. The two scalars decaying to $\eta \eta$ are also observed when one η decays to $3\pi^0$ (10 γ final state), a channel with entirely different systematics (Fig. 20(b)). The distributions in Fig. 20(a) and (b) are nearly identical.

An amplitude analysis of the Dalitz plot distribution for the 6γ final state was performed with the method outlined in the previous section. However, Breit-Wigner functions of the form (55) were used to describe the resonances. The fit required $J^{PC} = 0^{++}$ for both $\eta\eta$ resonances. The (Breit-Wigner) masses and widths were m = 1430, $\Gamma = 250$ and m = 1560, $\Gamma = 245$ MeV, respectively. Note that the width of the upper state appears smaller in Fig. 20(a,b), due to interference effects. This state may be identical to the scalar meson observed earlier by the GAMS collaboration at 1590 MeV in the $\eta\eta$ and $\eta\eta'$ mass spectrum of high energy πN -interactions (Alde, 1988b; Binon, 1983, 1984).

The final analysis of this channel was performed with a tenfold increase in statistics, namely $3.1 \times 10^4 \pi^0 \eta \eta$ events from 0-prong data and $1.67 \times 10^5 \pi^0 \eta \eta$ events from a triggered data sample requiring online one π^0 and two η mesons (Amsler, 1995e). The Dalitz plot is shown in Fig. 21(a). The horizontal and vertical bands are due to $a_0(980)$ decaying to $\eta \pi^0$. One also observes diagonal bands which correspond to the two states decaying to $\eta \eta$. A residual incoherent flat background of 5%, mainly due to $\pi^0 \pi^0 \omega \to 7\gamma$ with a missing photon, has been subtracted from the Dalitz plot before applying the amplitude analysis, this time with the full *K*-matrix formalism.

Since S-wave dominates in liquid, the channel $\pi^0\eta\eta$ proceeds mainly through the 1S_0 atomic state. The $\eta\pi$ S-wave was parametrized by a 2×2 K-matrix with poles from $a_0(980)$ and $a_0(1450)$. The parameters were taken from the $\pi^0\pi^0\eta$ analysis (section 8.2), leaving the production constants β free. A contribution from $a_2(1320)$ ($\eta\pi$ D-wave) with fixed mass and width was also offered to the fit. The $\eta\eta$ S- and D-waves were described by one-channel K-matrices. Annihilation from atomic P-states was not included in the fit except for tensor mesons (e.g. the expected $f_2(1565)$) decaying to $\eta\eta$. In fact the fit demands a contribution from a tensor meson with mass ~1494 and width ~155 MeV, produced mainly from P-states.

The best fit was obtained with two poles for the $\eta\eta$ S-wave. The resonance parameters (*T*-matrix poles) are:

$$f_0(1370): m = 1360 \pm 35, \ \Gamma = 300 - 600 \ \text{MeV},$$

$$f_0(1500): m = 1505 \pm 15, \ \Gamma = 120 \pm 30 \ \text{MeV}.$$
(97)

The K-matrix mass and width of $f_0(1500)$ are 1569 and 191 MeV, respectively, in accord with the Breit-Wigner parameters of the GAMS resonance (Binon, 1983). This state, previously called $f_0(1590)$, and $f_0(1500)$ are therefore assumed to be identical. The branching ratio for $\pi^0\eta\eta$ is given in Table 9 and the products of resonance production and decay branching ratios are listed in Table 10.

8.2 $\overline{p}p \rightarrow \pi^0 \pi^0 \eta$

This channel is relevant to search for isovector 0^{++} states decaying to $\eta\pi$. The $\pi^0\pi^0\eta$ Dalitz plot (2.8 × 10⁵ events) is shown in Fig. 21(b). Qualitatively, one observes $a_0(980)$ and $a_2(1320)$ decaying to $\eta\pi$ and $f_0(980)$ decaying to $\pi\pi$. The strong interference patterns point to coherent contributions from a single $\overline{p}p$ atomic state (¹S₀).

An amplitude analysis based on the K-matrix formalism (and, alternatively, the N/D formalism) has been performed, assuming pure S-wave annihilation (Amsler, 1994b). The $\pi\pi$ S-wave was described by two poles, one for $f_0(980)$, coupling to $\pi\pi$ and $K\overline{K}$, and one for $f_0(1370)$. Elastic $\pi\pi$ -scattering data (Grayer, 1974; Rosselet, 1977) were included in the fit. The $\pi\pi$ D-wave ($f_2(1270)$) was also introduced but turned out to be negligible. The $\eta\pi$ D-wave was described by one pole for $a_2(1320)$. The $\eta\pi$ S-wave was described by a one-pole 2×2 K-matrix for $a_0(980)$ with couplings g_1 to $\eta\pi$ and g_2 to $K\overline{K}$. Since decay to $K\overline{K}$ was not measured, g_2 was obtained indirectly from the $\eta\pi$ line shape. The fit yielded $g_1 = 0.353$ GeV and

$$\frac{g_2}{g_1} \sim 0.88.$$
 (98)

These amplitudes were, however, not sufficient to describe the data. A satisfactory fit was obtained by adding (i) a second pole to the $\eta\pi$ S-wave, (ii) a second pole to the $\eta\pi$ D-wave and (iii) an $\eta\pi$ P-wave. Branching ratios are given in Table 10. The branching ratio for $\pi^0\pi^0\eta$ (Table 9) is in excellent agreement with the one derived from the channel $\pi^0\pi^0\eta \to \pi^+\pi^-3\pi^0$ (Amsler, 1994d).

The main result was the observation of a new isovector scalar resonance in the $\eta \pi$ S-wave:

$$a_0(1450): m = 1450 \pm 40, \ \Gamma = 270 \pm 40 \text{ MeV}.$$
 (99)

This resonance manifests itself as a depletion in the bottom right (or top left) corner of the Dalitz plot (Fig. 21 (b)). Evidence for the $a_0(1450)$ decaying to $\eta\pi$ is also reported

in an analysis of the channel $\pi^+\pi^-\eta$ which requires, in addition, an amplitude for $\rho\eta$ production from 3S_1 (Abele, 1997a).

The $\eta\pi$ D-wave contribution corresponds to a 2⁺⁺ resonance around 1650 MeV, called $a'_{2}(1650)$ in Table 10, with a width of about 200 MeV. This state could be the radial excitation of $a_{2}(1320)$. The mass and width of the structure in the $\eta\pi$ P-wave (exotic 1⁻⁺) are not well defined. They vary from 1200 to 1600 MeV and from 400 to 1000 MeV, respectively, without significant changes in the χ^{2} . The 1⁻⁺ $\hat{\rho}(1405)$ reported by Alde (1988a) is therefore not confirmed by the present data.

8.3 $\overline{p}p \rightarrow \pi^0 \pi^0 \pi^0$

The first analysis of this channel used a sample of only 5.5×10^4 events and reported an isoscalar 2^{++} meson at 1515 ± 10 MeV with width 120 ± 10 MeV, decaying to $\pi^0 \pi^0$ (Aker, 1991). This state was identified with $f_2(1565)$ that had been observed before in the final state $\pi^+\pi^-\pi^0$ in hydrogen gas (May, 1989, 1990). P-wave annihilation from 3P_1 and 3P_2 was therefore allowed when fitting the $3\pi^0$ channel. Resonances in the $\pi\pi$ S-wave were described by the $\pi\pi$ elastic scattering amplitude, replacing the Breit- Wigner amplitude by

$$BW_0(m) = \frac{m}{p} \left(\frac{\eta(m) \exp[2i\delta(m)] - 1}{2i} \right), \tag{100}$$

according to Eq. (86), where δ and η were taken from the Argand diagram of Au (1987). This is an approximation assuming equal production strengths for all resonances in the $\pi\pi$ S-wave, which is reasonable for the $3\pi^0$ channel, as I will show below.

A statistical sample an order of magnitude larger than revealed a new feature (Amsler, 1994e) which was consolidated by a reanalysis of the early Crystal Barrel data (Anisovich, 1994): the presence in the Dalitz plot of a narrow homogeneously populated band from a scalar resonance, $f_0(1500)$, decaying to $2\pi^0$. The $3\pi^0$ Dalitz plot is shown in Fig. 21(c) and the $2\pi^0$ mass projection in Fig. 22.

Qualitatively, one observes the following features: the population along the $\pi\pi$ mass band marked $f_2(1270)$ increases at the edges of the Dalitz plot indicating that one decay π^0 is preferably emitted along the flight direction of the resonance. This is typical of a spin 2 resonance decaying with the angular distribution $(3\cos^2\theta - 1)^2$ from 1S_0 or $(1 + 3\cos^2\theta)$ from 3P_1 . The blobs labelled $f_2(1565)$ at the corners correspond to an angular distribution $\sin^2\theta$ from another spin 2 resonance produced from 3P_2 , together with constructive interference from the two $\pi\pi$ S-waves. The $f_0(980)$ appears as a narrow dip in the $\pi\pi$ S-wave. The new feature is the homogeneous narrow band marked $f_0(1500)$ which must be due to a spin 0 state.

The analysis of the full data sample was performed with the K-matrix formalism (Amsler, 1995f). A 2 × 2 K-matrix with three poles was sufficient to describe the $\pi\pi$ S-wave. Elastic $\pi\pi$ scattering data up to 1200 MeV from Grayer (1974) and Rosselet (1977) were also included in the fit. The contributing scalar resonances are $f_0(980)$ and

$$f_0(1370): m \simeq 1330, \ \Gamma \sim 760 \ \text{MeV}, f_0(1500): m = 1500 \pm 15, \ \Gamma = 120 \pm 25 \ \text{MeV}.$$
(101)

A 4-pole K-matrix helps to constrain the $f_0(1370)$ parameters, giving

$$f_0(1370): m = 1330 \pm 50, \ \Gamma = 300 \pm 80 \text{ MeV},$$
 (102)

and the 4th pole corresponds to a 600 MeV broad structure around 1100 MeV (called $f_0(400-1200)$ by the Particle Data Group (Barnett, 1996)) and also reported by a recent

reanalysis of $\pi\pi$ S-wave data (Morgan and Pennington, 1993). The data are therefore compatible with 3 or 4 poles and it is not obvious that $f_0(1370)$ and $f_0(400 - 1200)$ are not part of the one and the same object.

A one-dimensional K-matrix describes the $\pi\pi$ D-wave. In addition to $f_2(1270)$ one finds

$$f_2(1565): m \sim 1530, \ \Gamma \sim 135 \text{ MeV}.$$
 (103)

The fractional contribution of P-waves is 46%. Without P-waves the fit deteriorates markedly but the $f_0(1370)$ and $f_0(1500)$ parameters remain stable. We shall return to the $f_2(1565)$ in the discussion below. Branching ratios are given in Table 10.

8.4 Coupled channel analysis

A simultaneous fit was performed to the channels $\pi^0\eta\eta$, $\pi^0\pi^0\eta$ and $3\pi^0$ (Amsler, 1995g) using the full data samples presented in the previous sections with, in addition, the $\pi\pi$ scattering data up to 1200 MeV. However, pure S-wave annihilation was assumed. A 3 × 3 K-matrix with 4 poles was used to describe the $\pi\pi$ S-wave coupling to $\pi\pi$, $\eta\eta$ and the at that time unmeasured $K\overline{K}$ through the resonances $f_0(980)$, $f_0(1370)$, $f_0(1500)$, taking also into account the broad structure around 1100 MeV. Common β_{α} parameters (Eq. (89)) were introduced to describe the production of resonances associated with the same recoiling particle. For example, $f_0(1500)$ recoiling against π^0 is produced with the same strength in $\pi^0\eta\eta$ and $3\pi^0$. The $\eta\pi$ S-wave was described by a 2 × 2 K-matrix for $a_0(980)$ and $a_0(1450)$. The $\pi\pi$, $\eta\eta$ and $\eta\pi$ D-waves were treated with one dimensional K-matrices, the latter including $a_2(1320)$ and $a'_2(1650)$ with pole parameters taken from the $\pi^0\pi^0\eta$ analysis of section 8.2.

The branching ratios are given in Table 10. Note that the $\pi\pi$ S-wave includes contributions from $f_0(400 - 1200)$, $f_0(980)$ and $f_0(1370)$ (but excluding $f_0(1500)$) which cannot be disentangled due to interferences. The fit is in good agreement with the single channel analyses and constrains the resonance parameters. Hence a consistent description of all three annihilation channels was achieved with the following main features:

1. The data demand three scalar resonances in the 1300 - 1600 MeV region:

$$a_0(1450): m = 1470 \pm 25, \ \Gamma = 265 \pm 30 \text{ MeV},$$

 $f_0(1370): m = 1390 \pm 30, \ \Gamma = 380 \pm 80 \text{ MeV},$
 $f_0(1500): m = 1500 \pm 10, \ \Gamma = 154 \pm 30 \text{ MeV}.$ (104)

- 2. The broad scalar structure around 1100 MeV $(f_0(400 1200))$ has very different pole positions in sheets II and III, making a resonance interpretation of this state difficult.
- 3. The production data demand a larger width ($\simeq 100$ MeV) for $f_0(980)$ than the $\pi\pi$ scattering data alone ($\simeq 50$ MeV, according to Morgan and Pennington (1993)).
- 4. A tensor meson is observed in the $\pi\pi$ D-wave with mass 1552 and width 142 MeV, in accord with May (1889, 1990) notwithstanding the absence of atomic P-waves in the present analysis. A structure is also required in this mass range in the $\eta\eta$ D-wave. This state is not compatible with $f'_2(1525)$ which is produced with a much lower rate, as we shall see in section 8.7.

The $\pi\pi$ scattering amplitude T (Eq. (86)) obtained from the fit to the elastic scattering data and the Crystal Barrel data is shown in Fig. 23. Note that Crystal Barrel $K\overline{K}$ data are not yet included and therefore the third K-matrix channel also contains by default all

other unmeasured inelasticities. Figure 24 shows the I = 0 S-wave production intensity $|\mathcal{T}|^2$ (Eq. (88)) for the three annihilation channels. The maxima around 1300 and 1550 MeV correspond to the K-matrix poles for $f_0(1370)$ and $f_0(1500)$. It is instructive to compare the dip around 1000 MeV in the $\pi\pi$ S-wave for the $3\pi^0$ channel to the peak in the $\pi^0\pi^0\eta$ channel, both due to $f_0(980)$. This is produced by interferences between the $\pi\pi$ and the $\eta\pi$ S-waves in $3\pi^0$ which have the opposite sign to the interference between the $\pi\pi$ and the $\eta\pi$ S-waves in $\eta\pi^0\pi^0$. The $\pi\pi$ S-wave in $\pi\pi$ scattering exhibits qualitatively the same behaviour as in $\overline{p}p$ annihilation into $3\pi^0$, namely sharp minima around 1000 and 1450 MeV. The ansatz (100) used in several Crystal Barrel analyses (e.g. in Aker (1991)) for the $\pi\pi$ S-wave is therefore a rough but reasonable approximation.

8.5 $\overline{p}p \rightarrow \pi^0 \eta \eta'$

Another piece of evidence for $f_0(1500)$ stems from $\pi^0\eta\eta'$ (Amsler, 1994f). This channel was also reconstructed from the 6γ final state. Since η' decays to $\gamma\gamma$ with a branching ratio of only 2.1% the data sample is small (977 events). Most of these events were collected with the online trigger requiring one π^0 , one η and one η' . The $\pi^0\eta\eta'$ Dalitz plot shows an accumulation of events at small $\eta\eta'$ masses. Figure 25 shows the $\eta\eta'$ mass projection. The $\eta\eta'$ mass spectrum from the same annihilation channel, but with $\eta' \to \eta\pi^+\pi^-$, has entirely different systematics but is identical (inset in Fig. 25). The enhancement at low masses is due to a scalar resonance since the angular distribution in the $\eta\eta'$ system is isotropic. A maximum likelihood fit was performed to the 6γ channel using a (damped) Breit-Wigner according to Eqs. (55), (56) and a flat incoherent background. The resonance parameters are

$$f_0(1500): m = 1545 \pm 25, \ \Gamma = 100 \pm 40 \text{ MeV}.$$
 (105)

The branching ratio is given in Table 10. The $f_0(1500)$ mass is somewhat larger than for $3\pi^0$ and $\pi^0\eta\eta$. However, Abele (1996a) points out that a constant width in the denominator of the Breit-Wigner function yields a mass around 1500 MeV. This is a more realistic procedure since the total width at the $\eta\eta'$ threshold remains finite due to the channels $\pi\pi$ and $\eta\eta$. However, this does not modify the branching ratio for $f_0(1500) \rightarrow \eta\eta'$. We shall therefore ignore Eq. (105), when averaging below the $f_0(1500)$ mass and width.

8.6 $\overline{p}p \rightarrow \pi^0 \pi^0 \eta'$

With 0-prong data this final state is accessible through $\eta' \to 2\gamma$ or $\eta' \to \eta \pi^0 \pi^0$, leading to 6, respectively 10 photons (Abele, 1997g). The branching ratios from both final state configurations agree (Table 9). A sample of 8,230 10 γ events were kinematically fitted to $4\pi^0\eta$. The $\pi^0\pi^0\eta$ mass distribution (Fig. 26) shows a sharp signal from η' and a shoulder around 1400 MeV due to the *E* meson that will be discussed in section 11.

The $\pi^0 \pi^0 \eta'$ Dalitz plot was obtained by selecting events in the η' peak and subtracting background Dalitz plots from either sides of the peak. It shows a broad accumulation of events in its center which can be described by a dominating $\pi\pi$ S-wave and small contributions from $a_2(1320)$ and $a_0(1450)$ with branching ratios given in Table 10. These resonances are included in the fit with fixed mass and width. The ratios of rates for $a_2(1320)$ and $a_0(1450)$ decays into $\eta\pi$ and $\eta'\pi$ can be predicted from SU(3) and compared with measurements. This will be discussed in section 10.1. The analysis of the 6γ Dalitz plot (3,559 events) leads to similar results. Figure 27 shows that $a_0(1450)$ is required for a satisfactory description of this annihilation channel.

8.7 $\overline{p}p \rightarrow \pi^0 K_L K_L$

The isoscalar $f_0(1500)$ has been observed to decay into $\pi^0 \pi^0$, $\eta \eta$ and $\eta \eta'$. To clarify its internal structure it was essential to also search for its $K\overline{K}$ decay mode. In a previous bubble chamber experiment (Gray, 1983) no $K\overline{K}$ signal had been observed in the 1500 MeV region in $\overline{p}p$ annihilation into $K\overline{K}\pi$, leading to the conclusion that the $f_0(1500)$ coupling to $K\overline{K}$ is suppressed (Amsler and Close, 1996). However, no partial wave analysis was performed due to limited statistics.

Crystal Barrel has therefore searched for $f_0(1500)$ in the annihilation channel $\pi^0 K_L K_L$ (Abele, 1996b; Dombrowski, 1996) which proceeds from the 1S_0 atomic state. Allneutral events were selected with three energy clusters in the barrel and the channel $\overline{p}p \to \pi^0 K_L K_L$ could be reconstructed by measuring the $\pi^0(\to 2\gamma)$ momentum and the direction of one of the K_L which interacts hadronically in the CsI barrel. The main background contribution was due to events with a reconstructed π^0 and one additional γ which happen to fulfil the $\pi^0 K_L K_L$ kinematics but for which one or more γ 's have escaped detection. This background (~ 17%) could be removed by subtracting a Dalitz plot constructed from 2γ pairs with invariant masses just below or above the π^0 mass.

Further background contributions were due to $\overline{p}p \to \omega K_L K_L$ where ω decays to $\pi^0 \gamma$ and both K_L are not detected, and $\overline{p}p \to K_S K_L$ where one photon from $K_S \to \pi^0 \pi^0 \to 4\gamma$ and the K_L are undetected. These events can be removed with appropriate mass cuts. Background from final states like $\omega \eta$, $\omega \pi^0$ and $3\pi^0$ were studied by Monte Carlo simulation. The total residual background contamination was $(3.4 \pm 0.5)\%$.

The background subtracted Dalitz plot is shown in Fig. 21(d). This plot has not been symmetrized with respect to the diagonal axis since one K_L is detected (vertical axis) whilst the other is missing (horizontal axis). The interaction probability as a function of K_L momentum was measured by comparing the intensities along the two K^* bands, $K^* \to K_L \pi^0$. The interaction probability was found to be flat with K_L momentum, but increasing slowly below 300 MeV/c (Dombrowski, 1996). The $\pi^0 K_L K_L$ Dalitz plot shown in Fig. 21(d) is already corrected for detection efficiency and for K_L decay between the production vertex and the crystals. Its symmetry along the diagonal axis is nearly perfect, indicating that acceptance and backgrounds have been taken into account properly.

One observes signals from $K^*(892)$ decaying to $K\pi$ and $a_2(1320)/f_2(1270)$ decaying to $K\overline{K}$. The accumulation of events at the edge for small $K\overline{K}$ masses is due to the tensor $f'_2(1525)$ which is observed for the first time in $\overline{p}p$ annihilation at rest. These resonances and the broad $K^*_0(1430)$ were introduced in a first attempt to fit the Dalitz plot⁸. The K-matrix for the $K\pi$ (I = 1/2) S-wave was written as

$$K = \frac{am}{2 + abp^2} + \frac{m_0 \Gamma_0 / \rho_0}{m_0^2 - m^2},$$
(106)

where the first term describes the low energy $K\pi$ scattering (*a* is the scattering length and *b* the effective range) and the second term describes the $K_0^*(1430)$ resonance. The parameters m_0, Γ_0, a and *b* were determined by fitting the scattering amplitude *T* (Eq. (74)) to the $K\pi$ phase shifts (Aston, 1988b). The fit is shown in Fig. 28. Note that resonance occurs at $\delta \simeq 120^\circ$. The corresponding mass and width (*T*-matrix pole) for $K_0^*(1430)$ are $m = (1423 \pm 10)$ MeV and (277 ± 17) MeV, in close agreement with Aston (1988b) who used a different parametrization and found $m_0 = 1429 \pm 6$ and $\Gamma_0 = 287 \pm 23$ MeV.

⁸The absence of threshold enhancement from $a_0(980)$ or $f_0(980)$ at the upper right border of the Dalitz plot could be due to destructive interference between these states and/or to the loss of acceptance close to the $K\overline{K}$ threshold.

A one-pole K-matrix for a scalar resonance was added for the peak around 1450 MeV in the $K\overline{K}$ mass distribution (Fig. 29). The fit clearly fails to describe the $K\overline{K}$ mass spectrum (dashed line in Fig. 29). The second attempt assumed a K-matrix with two scalar resonances, $f_0(1370)$ and $f_0(1500)$, in the $K\overline{K}$ amplitude. The fit now provided a satisfactory description of the Dalitz plot and the $K\overline{K}$ mass spectrum (full line in Fig. 29). However, the isovector $a_0(1450)$ is also expected to decay to K_LK_L and one cannot distinguish between isovectors and isoscalars from the $\pi^0 K_L K_L$ data alone. Therefore a Breit-Wigner was added for the isovector $a_0(1450)$ with fixed mass and width taken from the coupled channel analysis (section 8.4). The $f_0(1370)$ and $f_0(1500)$ poles are stable, nearly independent of $a_0(1450)$ contribution. One finds

$$f_0(1370): m = 1380 \pm 40, \ \Gamma = 360 \pm 50 \text{ MeV},$$

$$f_0(1500): m = 1515 \pm 20, \ \Gamma = 105 \pm 15 \text{ MeV}, \tag{107}$$

in agreement with the resonance parameters measured in the other decay channels.

Due to uncertainties in the K_L interaction probability the branching ratio for $\pi^0 K_L K_L$ could not be determined accurately. The branching ratios given in Table 11 (Abele, 1996b; Dombrowski, 1996) are therefore normalized to the known branching ratio for $\pi^0 K_S K_S$ (Armenteros, 1965; Barash, 1965)⁹.

The branching ratios for $\overline{p}p \to f_0(1370)$ and $f_0(1500) \to K_L K_L$ also vary with $a_0(1450)$ contribution (Fig. 30). In Table 11 the branching ratios for $f_0(1370)$ and $f_0(1500)$ are therefore derived from Fig. 30 assuming an $a_0(1450)$ contribution r_0 to the $\pi^0 K_L K_L$ final state, derived from its measured contribution $r = (10.8 \pm 2.0)\%$ to $\pi^{\pm} K^{\mp} K_L$ (next section):

$$r_0 = \frac{r}{4} \frac{B(\overline{p}p \to \pi^{\pm} K^{\mp} K_S)}{B(\overline{p}p \to \pi^0 K_S K_S)} = (9.8 \pm 1.9)\%, \tag{108}$$

where we have used the branching ratios from Armenteros (1965) and Barash (1965).

8.8 $\overline{p}p \to \pi^{\pm} K^{\mp} K_L$

This channel selects only isospin 1 resonances decaying to $K\overline{K}$ and therefore permits a direct measurement of the contribution from isovectors to $K\overline{K}\pi$, in particular from $a_0(1450)$. Crystal Barrel has studied the reaction $\overline{p}p \to \pi^{\pm}K^{\mp}K_L$ with a non-interacting K_L (Heinzelmann, 1996; Abele 1997e). This channel is selected from 7.7×10^6 triggered 2-prong data by requiring exactly two clusters in the barrel from π^{\pm} and K^{\mp} . Particle identification is achieved by measuring the ionisation in the drift chamber (Fig. 31) and a (1C) kinematic fit ensures momentum and energy conservation. The background contribution, mainly from $\pi^+\pi^-\pi^0$, is about 2%. The Dalitz plot (Fig. 32) has been corrected for background and acceptance, and for the K_L interaction probability. The latter was determined by reconstructing the channel $\pi^0 K_S(\to \pi^+\pi^-)K_L$ with and without missing K_L . The branching ratio

$$B(\overline{p}p \to \pi^{\pm}K^{\mp}K_L) = (2.91 \pm 0.34) \times 10^{-3}$$
(109)

is in excellent agreement with the one given in Table 11 for $\pi^{\pm} K^{\mp} K_S$ from bubble chamber experiments (Armenteros, 1965; Barash, 1965).

The Dalitz plot shows clear signals from $K^*(892)$, $a_2(1320)$ and $a_0(980)$. The $K^*(892)$ and $a_2(1320)$ were parametrized by Breit-Wigner functions. The $a_0(980)$ was described

⁹The isospin contributions from ${}^{1}S_{0}$ to the $K^{*}\overline{K}$ system cannot be determined in this channel since the K^{*} bands interfere constructively for both I = 0 and I = 1.

by a 2 × 2 K-matrix (Flatté formula (93)). The $K\pi$ S-wave ($K_0^*(1430)$) was treated using the data from Aston (1988b), as described in the previous section. In contrast to $\pi^0 K_L K_L$, both atomic states 1S_0 and 3S_1 contribute. The I = 0 and I = 1 contributions to $K^*(892)\overline{K}$ can be determined from the (destructive) interference pattern around the crossing point of the K^* bands in Fig. 32.

The fit, however, did not provide a satisfactory description of the Dalitz plot and the fitted $a_2(1320)$ mass, 1290 MeV, was significantly lower than the table value, a problem that had been noticed earlier in bubble chamber data (Conforto, 1967). A substantial improvement in the χ^2 (Fig. 33) was obtained when introducing the $a_0(1450)$ as a second pole in the *K*-matrix, together with $a_0(980)$, leading to the resonance parameters (*T*-matrix pole)

$$a_0(1450): m = 1480 \pm 30, \quad \Gamma = 265 \pm 15 \text{ MeV},$$
 (110)

in agreement with the $\eta\pi$ decay mode. The $a_2(1320)$ mass now became compatible with the table value (Barnett, 1996). We shall show below that the contribution to $\pi^{\pm}K^{\mp}K_L$ of (10.8 ± 2.0) % (Fig. 33) is consistent with predictions from the $\pi^0\pi^0\eta$ channel, using SU(3).

An even better fit was achieved by adding a broad structure in the $K\overline{K}$ P-wave, presumably from the radial excitations $\rho(1450)$ and $\rho(1700)$, which could not, however, be disentangled by the fit.

For $a_0(980)$ one finds for the *T*-matrix pole in the second Riemann sheet the mass 987 \pm 3 MeV and the width 86 \pm 7 MeV. Using the $\eta\pi$ decay branching ratio from the $\pi^0\pi^0\eta$ analysis (Table 10) one also obtains the ratio

$$\frac{B(a_0(980) \to K\overline{K})}{B(a_0(980) \to \eta\pi)} = 0.24 \pm 0.06.$$
(111)

With the coupling $g_1 = 0.324$ GeV to $\eta\pi$ (Amsler, 1994b) the coupling g_2 to $K\overline{K}$ can be tuned to satisfy Eq. (111) by integrating the mass distributions over the $a_0(980)$ distribution (Fig. 19). One obtains $g_2 = 0.279$ MeV and the ratio $g_2/g_1 = 0.86$, is in excellent agreement with the estimate from the line shape in the $\pi^0\pi^0\eta$ channel (Eq. (98)).

The branching ratios are given in Table 11. The intermediate $K^*\overline{K}$ is largest in the (I=1) 3S_1 channel, a feature that was noticed before (Barash, 1965; Conforto, 1967) and that we have used in section 6.1 as a possible explanation for the $\pi\phi$ enhancement. The branching ratios are in fair agreement with those from Conforto (1967) and those for $\pi^0 K_L K_L$, except for the much larger $K\pi$ S-wave in $\pi^{\pm} K^{\mp} K_L$.

9 Annihilation at Rest into 5π

Resonances in $\rho^+\rho^-$ have been reported in $\overline{p}n$ annihilation in deuterium: A 2⁺⁺ state was observed in bubble chamber exposures in liquid deuterium (Bridges, 1987). An enhancement was also seen around 1500 MeV by the Asterix collaboration at LEAR in gaseous deuterium but no spin-parity analysis was performed (Weidenauer, 1993). This state was interpreted as $f_2(1565)$ in its $\rho\rho$ decay mode, the slightly lower mass being due to π -rescattering with the recoil proton exciting the Δ resonance (Kolybashov, 1989). The 2⁺⁺ assignment was, however, disputed in favour of 0⁺⁺ by a reanalysis of the bubble chamber data (Gaspero, 1993).

The Crystal Barrel has also searched for scalar mesons decaying to 4π . The $4\pi^0$ decay mode was investigated using $\overline{p}p$ annihilation into $5\pi^0$, leading to 10 detected photons (Abele, 1996c). The branching ratio for annihilation into $5\pi^0$ was found to be $(7.1\pm1.4)\times$ 10^{-3} . After removing the $\eta \to 3\pi^0$ contribution they performed a maximum likelihood analysis of a sample of 25,000 $5\pi^0$ events. The data demand contributions from $\pi(1330) \to 3\pi^0$ and from two scalar resonances decaying to $4\pi^0$. The mass and width of the lower state, presumably $f_0(1370)$, could not be determined precisely.

The upper state has mass ~ 1505 MeV and width ~ 169 MeV and decays into two $\pi\pi$ S-wave pairs and $\pi^0(1300)\pi^0$ with approximately equal rates. The branching ratio for $\overline{p}p \to f_0(1500)\pi^0 \to 5\pi^0$ is $(9.0 \pm 1.4) \times 10^{-4}$. Using the 2π branching ratio from the coupled channel analysis one finds

$$\frac{B(f_0(1500) \to 4\pi)}{B(f_0(1500) \to 2\pi)} = 2.1 \pm 0.6,$$
(112)

$$\frac{B(f_0(1500) \to 4\pi^0)}{B(f_0(1500) \to \eta\eta)} = 1.5 \pm 0.5.$$
(113)

The $4\pi^0$ $(2\pi^0)$ contribution in (112) has been multiplied by 9 (3) to take into account the unobserved charged pions. The ratio (112) is, in principle, a lower limit which does not include $\rho\rho$. However, a reanalysis of the Mark III data on $J/\psi \to \gamma 2\pi^+ 2\pi^-$ finds evidence for $f_0(1500)$ decaying to 4π through two S-wave dipions with negligible $\rho\rho$ contribution (Bugg, 1995). The ratio (113) is in agreement with the result for the former $f_0(1590)$ from Alde (1987) in $\pi^- p \to 4\pi^0 n$: 0.8 ± 0.3 .

A scalar resonance with mass 1374 ± 38 and width 375 ± 61 MeV decaying to $\pi^+\pi^-2\pi^0$ was also reported by Crystal Barrel in the annihilation channel $\pi^+\pi^-3\pi^0$ (Amsler, 1994d). The branching ratio for $\pi^+\pi^-3\pi^0$ was measured to be (9.7 ± 0.6) %. The 4π decay mode of the resonance is five times larger than the 2π , indicating a large inelasticity in the 2π channel. The relative decay ratio to $\rho\rho$ and two $\pi\pi$ S-waves is 1.6 ± 0.2. However, the data do not exclude the admixture of a $f_0(1500)$ contribution.

10 The New Mesons

It is instructive to first check the consistency within Crystal Barrel data and also compare with previous measurements. The squares of the isospin Clebsch-Gordan coefficients determine the total branching ratios, including all charge modes. Note that two neutral isovectors (e.g. $a_2^0(1320)\pi^0$) do not contribute to I = 1. Table 12 gives the corresponding weights to $K\overline{K}$. For $K^*(892), K_0^*(1430), a_2(1320)$ and $a_0(1450)$ contributions to $K\overline{K}\pi$ the $\pi^0 K_L K_L$ ratios in Table 11 must be multiplied by 12 while those for $f_2(1270), f_0(1370),$ $f_0(1500)$ and $f'_2(1525)$ must be multiplied by 4 (since K_S is not observed). For $\pi^{\pm}K^{\mp}K_L$ the resonance contributions in Table 11 have to be multiplied by 3 for $K^*(892), K_0^*(1430),$ by 3 for $a_0(980), a_2(1320), \rho(1450/1700)$ from I = 0 and by 2 for $a_2(1320), \rho(1450/1700)$ from I = 1.

Furthermore, the branching ratios must be corrected for all decay modes of the intermediate resonances to obtain the two-body branching ratios in Table 13. We have used the following decay branching ratios (Barnett, 1996): $(28.2\pm0.6)\%$ for $f_2(1270) \rightarrow \pi^0\pi^0$, $(4.6\pm0.5)\%$ for $f_2(1270) \rightarrow K\overline{K}$, $(14.5\pm1.2)\%$ for $a_2(1320) \rightarrow \eta\pi$, $(4.9\pm0.8)\%$ for $a_2(1320) \rightarrow K\overline{K}$, $(0.57\pm0.11)\%$ for $a_2(1320) \rightarrow \eta'\pi$ and $(88.8\pm3.1)\%$ for $f'_2(1525) \rightarrow K\overline{K}$. There are indications that the $a_2(1320)$ contribution to $\pi\pi\eta$ is somewhat too large. Otherwise the consistency is in general quite good and Crystal Barrel results also agree with previous data. This gives confidence in the following discussion on the new mesons.

10.1 $a_0(1450)$

We begin with the isovector $a_0(1450)$ which has been observed in its $\eta \pi$, $\eta' \pi$ and $K\overline{K}$ decay modes. Averaging mass and width from the coupled channel and the $K\overline{K}$ analyses one finds:

$$a_0(1450): m = 1474 \pm 19, \quad \Gamma = 265 \pm 13 \text{ MeV}.$$
 (114)

The $a_0(1450)$ decay rates are related by SU(3)-flavor which can be tested with Crystal Barrel data. Following Amsler and Close (1996) we shall write for a quarkonium state

$$|q\bar{q}\rangle = \cos\alpha |n\bar{n}\rangle - \sin\alpha |s\bar{s}\rangle, \tag{115}$$

where

$$|n\bar{n}\rangle \equiv (u\bar{u} + d\bar{d})/\sqrt{2}.$$
(116)

The mixing angle α is related to the usual nonet mixing angle θ (Barnett, 1996) by the relation

$$\alpha = 54.7^{\circ} + \theta. \tag{117}$$

Ideal mixing occurs for $\theta = 35.3^{\circ}$ (-54.7°) for which the quarkonium state becomes pure $s\overline{s}$ $(n\overline{n})$.

The flavor content of η and η' are then given by the superposition (see also Eq. (21))

$$\begin{aligned} |\eta\rangle &= \cos\phi |n\bar{n}\rangle - \sin\phi |s\bar{s}\rangle, \\ |\eta'\rangle &= \sin\phi |n\bar{n}\rangle + \cos\phi |s\bar{s}\rangle, \end{aligned} \tag{118}$$

with $\phi = 54.7^{\circ} + \theta_p$, where θ_p is the pseudoscalar mixing angle which we take as $\theta_p = (-17.3 \pm 1.8)^{\circ}$ (Amsler, 1992b).

The partial decay width of a scalar (or tensor) quarkonium into a pair of pseudoscalars M_1 and M_2 is given by

$$\Gamma(M_1, M_2) = \gamma^2(M_1, M_2) f_L(p) p.$$
(119)

The couplings γ can be derived from SU(3)-flavor. The two-body decay momentum is denoted by p and the relative angular momentum by L. The form factor

$$f_L(p) = p^{2L} \exp(-\frac{p^2}{8\beta^2})$$
(120)

provides a good fit to the decay branching ratios of the well known ground state 2^{++} mesons if β is chosen $\geq 0.5 \text{ GeV/c}$ (Amsler and Close, 1996). We choose $\beta = 0.5 \text{ GeV/c}$ although the exponential factor can be ignored ($\beta \to \infty$) without altering the forthcoming conclusions. Replacing $f_L(p)p$ by prescription (28) also leads to a good description of decay branching ratios provided that $p_R > 500 \text{ MeV/c}$, corresponding to an interaction radius of less than 0.4 fm (Abele, 1997g).

The decay of quarkonium into a pair of mesons involves the creation of $q\bar{q}$ pair from the vacuum. We shall assume for the ratio of the matrix elements for the creation of $s\bar{s}$ versus $u\bar{u}$ (or $d\bar{d}$) that

$$\rho \equiv \frac{\langle 0|V|s\bar{s}\rangle}{\langle 0|V|u\bar{u}\rangle} \simeq 1.$$
(121)

This assumption is reasonable since from the measured decay branching ratios of tensor mesons one finds $\rho = 0.96 \pm 0.04$ (Amsler and Close, 1996). Similar conclusions are reached by Peters and Klempt (1995).

Let us now compare the Crystal Barrel branching ratios for $a_2(1320)$ decays to $K\overline{K}$, $\eta\pi$ and $\eta'\pi$ with predictions from SU(3). One predicts for an isovector with the coupling constants γ given in the appendix of Amsler and Close (1996):

$$\frac{\Gamma(a_2^{\pm}(1320) \to K^{\pm}K^0)}{\Gamma(a_2^0(1320) \to \eta\pi^0)} = \frac{1}{2\cos^2\phi} \frac{f_2(p_K)p_K}{f_2(p_\eta)p_\eta} = 0.295 \pm 0.013,$$
(122)

$$\frac{\Gamma(a_2^0(1320) \to \eta' \pi^0)}{\Gamma(a_2^0(1320) \to \eta \pi^0)} = \tan^2 \phi \frac{f_2(p_K)p_K}{f_2(p_\eta)p_\eta} = 0.029 \pm 0.004.$$
(123)

Both ratios are in excellent agreement with world data (Barnett, 1996). The Crystal Barrel numbers to be compared with are taken from Tables 10 and 11 for I = 0. One finds the ratios of branching ratios

$$\frac{B(a_2^{\pm}(1320) \to K^{\pm}K^0)}{B(a_2^0(1320) \to \eta\pi^0)} = 0.21^{+0.04}_{-0.06}, \qquad (124)$$

$$\frac{B(a_2^0(1320) \to \eta' \pi^0)}{B(a_2^0(1320) \to \eta \pi^0)} = 0.034 \pm 0.009,$$
(125)

in fair agreement with SU(3) predictions. We now compare predictions and data for $a_0(1450)$. From SU(3) one expects, using Eq. (122) and (123) with L = 0:

$$\frac{\Gamma(a_0^{\pm}(1450) \to K^{\pm}K^0)}{\Gamma(a_0^0(1450) \to \eta\pi^0)} = 0.72 \pm 0.03,$$
(126)

$$\frac{\Gamma(a_0^0(1450) \to \eta' \pi^0)}{\Gamma(a_0^0(1450) \to \eta \pi^0)} = 0.43 \pm 0.06, \tag{127}$$

in agreement with the experimental results from Tables 10 and 11:

$$\frac{B(a_0^{\pm}(1450) \to K^{\pm}K^0)}{B(a_0^0(1450) \to \eta\pi^0)} = 0.87 \pm 0.23,$$
(128)

$$\frac{B(a_0^0(1450) \to \eta' \pi^0)}{B(a_0^0(1450) \to \eta \pi^0)} = 0.34 \pm 0.15.$$
(129)

This then establishes $a_0(1450)$ as a $q\overline{q}$ isovector in the scalar nonet.

The existence of $a_0(1450)$ adds further evidence for $a_0(980)$ being a non- $q\bar{q}$ state. The $f_0(980)$ and $a_0(980)$ have been assumed to be $K\overline{K}$ molecules (Weinstein, 1990; Close, 1993). This is motivated by their strong couplings to $K\overline{K}$ - in spite of their masses close to the $K\overline{K}$ threshold - and their small $\gamma\gamma$ partial widths. For $f_0(980)$ the 2γ partial width is $\Gamma_{\gamma\gamma} = (0.56 \pm 0.11)$ keV (Barnett, 1996). The relative ratio for $a_0(980)$ decay to $K\overline{K}$ and $\eta\pi$ has been determined by Crystal Barrel (Eq. (111)). Using

$$\Gamma_{\gamma\gamma} B(a_0(980) \to \eta\pi) = 0.24 \pm 0.08 \text{ keV}$$
 (130)

(Barnett, 1996), one then derives the partial width $\Gamma_{\gamma\gamma} = (0.30 \pm 0.10)$ keV. Thus the 2γ partial widths for $f_0(980)$ and $a_0(980)$ appear to be similar, close to predictions for $K\overline{K}$ molecules (0.6 keV) and much smaller than for $q\overline{q}$ states (Barnes, 1985). However, not everybody agrees: In Törnqvist (1995) the $f_0(980)/f_0(1370)$ and the $a_0(980)/a_0(1450)$ are different manifestations of the same uniterized $s\overline{s}$ and $\overline{u}d$ states, while the broad structure around 1100 MeV is the $u\overline{u} + d\overline{d}$ state (Törnqvist and Roos, 1996). This then leaves $f_0(1500)$ as an extra state.

10.2 $f_0(1370)$ and $f_0(1500)$

From the single channel analyses and the $K\overline{K}$ decay mode we find for $f_0(1370)$ and $f_0(1500)$ the average masses and widths:

$$f_0(1370): m = 1360 \pm 23 \text{ MeV}, \ \Gamma = 351 \pm 41 \text{ MeV},$$

$$f_0(1500): m = 1505 \pm 9 \text{ MeV}, \ \Gamma = 111 \pm 12 \text{ MeV}.$$
(131)

The closeness of $a_0(1450)$ and $f_0(1500)$ or even $f_0(1370)$ masses is conspicuous and points to a close to ideally mixed scalar nonet, one of the latter mesons being one of the $q\overline{q}$ isoscalars. However, $f_0(1500)$ with a width of about 100 MeV is much narrower than $a_0(1450)$, $f_0(1370)$ and $K_0^*(1430)$ with widths of typically 300 MeV. Theoretical predictions for the widths of scalar $q\overline{q}$ mesons, based on the 3P_0 model, agree that scalar $q\overline{q}$ mesons have widths of at least 250 MeV (for a discussion and references see Amsler and Close (1996)). We therefore tentatively assign $f_0(1370)$ to the ground state scalar nonet.

If $f_0(980)$ is indeed a molecule then the (mainly) $s\overline{s}$ member of the scalar nonet still needs to be identified. We now show from their decay branching ratios that neither $f_0(1370)$ nor $f_0(1500)$ are likely candidates. To investigate the quark content of $f_0(1500)$ we calculate its relative couplings to $\eta\eta$, $\eta\eta'$ and $K\overline{K}$ and search for a common value of the scalar mixing angle α . The ratios of couplings for a pseudoscalar mixing angle ϕ are (Amsler and Close, 1996):

$$R_{1} \equiv \frac{\gamma^{2}(\eta\eta)}{\gamma^{2}(\pi\pi)} = \frac{(\cos^{2}\phi - \sqrt{2}\tan\alpha\sin^{2}\phi)^{2}}{3},$$

$$R_{2} \equiv \frac{\gamma^{2}(\eta\eta')}{\gamma^{2}(\pi\pi)} = \frac{2(\cos\phi\sin\phi[1+\sqrt{2}\tan\alpha])^{2}}{3},$$

$$R_{3} \equiv \frac{\gamma^{2}(K\overline{K})}{\gamma^{2}(\pi\pi)} = \frac{(1-\sqrt{2}\tan\alpha)^{2}}{3}.$$
(132)

For $\eta\eta$ and $\pi\pi$ we use the branching ratios from the coupled channel analysis (Table 10) and multiply $\pi\pi$ by 3 to take into account the $\pi^+\pi^-$ decay mode. The branching ratio for $K\overline{K}$ is taken from Table 11 and is multiplied by 4. The branching fractions are, including the 4π mode from Eq. (112) and ignoring a possible small $\rho\rho$ contribution to 4π :

$$\begin{aligned}
\pi\pi : & (29.0 \pm 7.5) \% \\
\eta\eta : & (4.6 \pm 1.3) \% \\
\eta\eta' : & (1.2 \pm 0.3) \% \\
K\overline{K} : & (3.5 \pm 0.3) \% \\
4\pi : & (61.7 \pm 9.6) \%.
\end{aligned}$$
(133)

After correcting for phase space and form factor (Eq. (120)) we obtain:

$$R_1 = 0.195 \pm 0.075, \ R_2 = 0.320 \pm 0.114, \ R_3 = 0.138 \pm 0.038.$$
 (134)

Since $f_0(1500)$ lies at the $\eta\eta'$ threshold we have divided the branching ratios by the phase space factor ρ integrated over the resonance and have neglected the form factor when calculating R_2 .

Previously, the upper limit for R_3 was < 0.1 (95% confidence level) from Gray (1983), in which case no value for the mixing angle α could simultaneously fit R_1 , R_2 and R_3 (Amsler and Close, 1996), therefore excluding $f_0(1500)$ as a $q\bar{q}$ state. The (1σ) allowed regions of tan α are shown in Fig. 34 for the ratios (134). The agreement between R_1 and R_3 is not particularly good. Remember, however, that branching ratios are sensitive to interference effects and therefore caution should be exercised in not overinterpreting the apparent discrepancy in Fig. 34. On the basis of the ratios (134), one may conclude that $f_0(1500)$ is not incompatible with a mainly $u\overline{u} + d\overline{d}$ meson ($\alpha = 0$). For a pure $s\overline{s}$ state ($\alpha = 90^\circ$) the ratios (134) would, however, become infinite. Therefore $f_0(1500)$ is not the missing $s\overline{s}$ scalar meson.

Similar conclusions can reached for $f_0(1370)$ which has small decay branching ratios to $\eta\eta$ and $K\overline{K}$. Precise ratios R_i are difficult to obtain in this case since the branching ratio to $\pi\pi$ in Table 10 also includes the low energy $\pi\pi$ S-wave, in particular $f_0(400 - 1200)$.

This analysis shows that both $f_0(1370)$ and $f_0(1500)$ are compatible with isoscalar $u\overline{u} + d\overline{d}$ states, although the latter is much too narrow for the ground state scalar nonet. This then raises the question on whether $f_0(1500)$ could not be the first radial excitation of $f_0(1370)$. This is unlikely because (i) the splitting between ground state and first radial is expected to be around 700 MeV (Godfrey and Isgur, 1985), (ii) the next K_0^* lies at 1950 MeV (Barnett, 1996) and, last but not least, first radials are expected to be quite broad (Barnes, 1997).

The most natural explanation is that $f_0(1500)$ is the ground state glueball predicted in this mass range by lattice gauge theories. However, a pure glueball should decay to $\pi\pi$, $\eta\eta$, $\eta\eta'$ and $K\overline{K}$ with relative ratios 3:1:0:4, in contradiction with our ratios R_i . In the model of Amsler and Close (1996) the finite $\eta\eta'$ and the small $K\overline{K}$ rates can be accommodated by mixing the pure glueball G_0 with the nearby two $n\overline{n}$ and $s\overline{s}$ states. Conversely, the two isoscalars in the $q\overline{q}$ nonet acquire a gluonic admixture. In first order perturbation one finds¹⁰

$$|f_0(1500)\rangle = \frac{|G_0\rangle + \xi(\sqrt{2}|n\overline{n}\rangle + \omega|s\overline{s}\rangle)}{\sqrt{1 + \xi^2(2 + \omega^2)}},\tag{135}$$

where ω is the ratio of mass splittings

$$\omega = \frac{m(G_0) - m(n\overline{n})}{m(G_0) - m(s\overline{s})}.$$
(136)

In the flux tube simulation of lattice QCD the pure gluonium G_0 does not decay to $\pi\pi$ nor to $K\overline{K}$ in first order and hence $f_0(1500)$ decays to $\pi\pi$ and $K\overline{K}$ through its $q\overline{q}$ admixture in the wave function. If G_0 lies between the two $q\overline{q}$ states, ω is negative and the decay to $K\overline{K}$ is hindered by negative interference between the decay amplitudes of the $n\overline{n}$ and $s\overline{s}$ components in Eq. (135). The ratio of couplings to $K\overline{K}$ and $\pi\pi$ is

$$\frac{\gamma^2(K\overline{K})}{\gamma^2(\pi\pi)} = \frac{(1+\omega)^2}{3}.$$
(137)

The cancellation is perfect whenever G_0 lies exactly between $n\overline{n}$ and $s\overline{s}$ ($\omega = -1$). We find with the measured R_3 two solutions, $\omega = -0.36$ or -1.64. Assuming that $f_0(1370)$ is essentially $n\overline{n}$ (with a small gluonic admixture) this leads to an $s\overline{s}$ state around 1900 MeV or 1600 MeV, respectively. Furthermore, the ratio of $\pi\pi$ partial widths for $f_0(1500)$ and $f_0(1370)$, divided by phase-space and form factor, is given by

$$\frac{\tilde{\Gamma}_{2\pi}[f_0(1500)]}{\tilde{\Gamma}_{2\pi}[f_0(1370)]} = \frac{2\xi^2(1+2\xi^2)}{1+\xi^2(2+\omega^2)} \sim 0.5,$$
(138)

using for $f_0(1500)$ the branching ratios from Tables 10 and 11 and the $4\pi/2\pi$ ratio (112). There is, however, a large uncertainty in the ratio (138) due to the branching ratios of

 $^{^{10}}$ We assume here that the quark-gluon coupling is flavor blind, see Amsler and Close (1996) for a generalization.

 $f_0(1370)$ which cannot easily be disentangled from $f_0(400 - 1200)$. This then leads to $|\xi| \sim 0.6$ and according to Eq. (135) to about 30% or about 60% glue in $f_0(1500)$ for an $s\overline{s}$ state at 1600 MeV or 1900 MeV, respectively.

The $f_0(1500)$ has also been observed in $\overline{p}p$ annihilation at higher energies (Armstrong, 1993) and in other reactions, in particular in central production, decaying to $2\pi^+2\pi^-$ (Antinori, 1995). The VES experiment, studying π^-p interactions on nuclei at 36 GeV/c, has reported a resonance, $\pi(1800)$, decaying to $\pi^-\eta\eta'$ (Beladidze, 1992) and $\pi^-\eta\eta$ (Amelin, 1996). The $\pi(1800)$ appears to decay into a resonance with mass 1460 \pm 20 MeV and width 100 \pm 30 MeV - in agreement with $f_0(1500)$ - with a recoiling π . They report an $\eta\eta'/\eta\eta$ ratio of 0.29 \pm 0.07 which is in excellent agreement with the Crystal Barrel ratio for $f_0(1500)$ decays, 0.27 \pm 0.10 (Table 10). Note that if $\pi(1800)$ is indeed a $q\bar{q}g$ (hybrid), as advocated by Close and Page (1995), then decay into gluonium is favoured,.

A reanalysis of J/ψ radiative decay to $2\pi^+2\pi^-$ finds evidence for $f_0(1500)$ decaying to two S-wave dipions with a branching ratio in $J/\psi \to \gamma 4\pi$ of $(5.7 \pm 0.8) \times 10^{-4}$ (Bugg, 1995). This leads to an expected branching ratio of $(2.7\pm0.9)\times10^{-4}$ in $J/\psi \to \gamma 2\pi$, using the Crystal Barrel result (112). It is interesting to compare this prediction with data on $J/\psi \to \gamma \pi^+\pi^-$ from Mark III (Baltrusaitis, 1987) where $f_2(1270)$ is observed together with a small accumulation of events in the 1500 MeV region. Assuming that these are due to $f_0(1500)$, one finds by scaling to $f_2(1270)$ a branching ratio in $J/\psi \to \gamma 2\pi$ of $\simeq 2.9 \times 10^{-4}$, in agreement with the above prediction.

Summarizing, $f_0(1500)$ has been observed in $\overline{p}p$ annihilation in several decay modes, some with very high statististics (~ 150,000 decays into $\pi^0\pi^0$) and also in other processes that are traditionally believed to enhance gluonium production, central production and J/ψ radiative decay. The $K_0^*(1430)$ and $a_0(1450)$ define the mass scale of the $q\overline{q}$ scalar nonet. The $f_0(1500)$ is not the missing $s\overline{s}$ and is anyway too narrow for a scalar $q\overline{q}$ state. The most natural explanation for $f_0(1500)$ is the ground state glueball mixed with nearby scalars. The missing element in this jigsaw puzzle is the $s\overline{s}$ scalar expected between 1600 and 2000 MeV. The analysis of in flight annihilation data will hopefully provide more information in this mass range. The spin of $f_J(1710)$ has not been determined unambiguously. If J = 0 is confirmed then $f_J(1710)$ could be this state or, alternatively, become a challenger for the ground state glueball (Sexton, 1995). A more detailed discussion on $f_0(1500)$ and $f_J(1710)$ can be found in Close (1997).

10.3 $f_2(1565)$

The $f_2(1565)$ with mass 1565 ± 20 and width 170 ± 40 MeV has been observed first by the Asterix collaboration at LEAR in the final state $\pi^+\pi^-\pi^0$ in hydrogen gas (May, 1989, 1990) and then by Aker (1991) in the $3\pi^0$ final state in liquid. The $3\pi^0$ analysis gave 60% P-state contribution to $3\pi^0$ in liquid with roughly equal intensities from $f_2(1565)$ of 9%, each from 1S_0 , 3P_1 and 3P_2 . The full $3\pi^0$ data sample demands 46% P-state annihilation (Amsler, 1995f) and also requires a tensor around 1530 MeV (section 8.3). The $s\overline{s}$ tensor, $f'_2(1525)$, has been observed in its $K\overline{K}$ decay mode (section 8.7). From the observed rate (Table 13) and the known $f'_2(1525)$ decay branching ratios (Barnett, 1996) one finds that $f'_2(1525)$ cannot account for much of the 2^{++} signal in $\pi\pi$ or $\eta\eta$. Hence $f_2(1565)$ is not $f'_2(1525)$.

The large P-state fraction in the $3\pi^0$ channel in liquid is not too surprising: the corresponding channel $\overline{p}p \to \pi^+\pi^-\pi^0$ in liquid proceeds mainly from the (I=0) 3S_1 atomic state while the (I=1) 1S_0 is suppressed by an order of magnitude (Foster, 1968b), as are normally P-waves in liquid. On the other hand, the channel $\overline{p}p \to 3\pi^0$ proceeds only through the (I=1) 1S_0 atomic state while 3S_1 is forbidden. Indeed the branching ratios

for $3\pi^0$ is an order of magnitude smaller than for $\pi^+\pi^-\pi^0$ (Table 9). Hence for $3\pi^0$ Sand P-wave annihilations compete in liquid.

A fraction of 50% P-wave was also required in the Dalitz plot analysis of the I = 1 final state $\pi^{-}\pi^{0}\pi^{0}$ at rest in liquid deuterium (Abele, 1997h) which shows evidence for $f_{0}(1500)$ and $f_{2}(1565)$ production and requires in addition the ρ -meson and two of its excitations, $\rho^{-}(1450)$ and $\rho^{-}(1700)$, decaying to $\pi^{-}\pi^{0}$.

However, the coupled channel analysis described in section 8.4, ignoring P-waves, still requires a tensor at 1552 MeV. Neglecting P-waves increases slightly the contribution from $f_0(1500)$ while decreasing the contribution from $f_2(1565)$, although the rates remain within errors (compare the two $\pi^0\pi^0$ branching ratios in Table 10 for the single and coupled channel analyses).

The alternative N/D analysis also reproduces the features of the $3\pi^0$ Dalitz plot without P-wave contributions, in particular the scalar state around 1500 MeV (Anisovich, 1994). A tensor contribution with mass ~ 1565 and width ~ 165 MeV is, however, still required, but most of the blob structure in Fig. 21(c) is taken into account by interferences in the low energy $\pi\pi$ S-wave.

An N/D analysis of Crystal Barrel data, together with former data from other reactions, also reports a tensor with mass 1534 ± 20 and width 180 ± 60 MeV (Abele, 1996a). They report strong $\rho\rho$ and $\omega\omega$ contributions and therefore assign this signal to $f_2(1640)$ discovered by GAMS in $\pi^- p \to \omega \omega n$ (Alde 1990), also reported to decay into 4π by the Obelix collaboration in $\overline{n}p \to 5\pi$ (Adamo, 1992). It should be emphasized, however, that in Abele (1996a) the inelasticity in the K-matrix is attributed to $\rho\rho$ and $\omega\omega$, although no 4π data are actually included in the fit. Given that mass and width of the tensor agree with $f_2(1565)$, but disagree with $f_2(1640)$, it seems more natural to assign the 2⁺⁺ signal to the former. It is interesting to note that a 2⁺⁺ $\rho\rho$ molecule (Törnqvist, 1991) or a 2⁺⁺ baryonium state (Dover, 1986) decaying strongly to $\rho\rho$ (Dover, 1991) are predicted in this mass range. The $f_2(1565)$ could be one of these states.

In conclusion, there is a certain amount of model dependence when extracting the precise production and decay rates of $f_2(1565)$. However, annihilation data require both a scalar and a tensor around 1500 MeV and the parameters and rates for $f_0(1500)$ are reasonably stable, independent of $f_2(1565)$ contribution. The Crystal Barrel data in gas will hopefully settle the issue of the fraction of P-wave in three-body annihilation.

11 E/ι Decay to $\eta\pi\pi$

The E meson, a 0^{-+} state, was discovered in the sixties in the $K\overline{K}\pi$ mass spectrum of $\overline{p}p$ annihilation at rest into $(K_S K^{\pm} \pi^{\mp}) \pi^+ \pi^-$. Its mass and width were determined to be 1425 ± 7 and 80 ± 10 MeV (Baillon, 1967). Its quantum numbers have remained controversial since other groups have claimed a 0^{-+} state (now called $\eta(1440)$) and a 1^{++} state (now called $f_1(1420)$) in this mass region from various hadronic reactions. A broad structure (previously called ι), has also been observed in radiative J/ψ decay to $K\overline{K}\pi$ (Scharre, 1980). Initially determined to be 0^{-+} , the E/ι structure was then found to split into three states, the first (0^{-+}) at 1416 ± 10 MeV decaying to $a_0(980)\pi$, the second (presumably the 1^{++} $f_1(1420)$) at 1443 ± 8 MeV and the third (0^{-+}) at 1490 ± 16 MeV, both decaying to $K^*\overline{K}$ (Bai, 1990). The widths were not determined accurately. The Obelix collaboration has analyzed the $K\overline{K}\pi$ mass spectrum in $\overline{p}p$ annihilation at rest in liquid and has also reported a splitting of the E meson into two pseudoscalar states at 1416 ± 2 MeV ($\Gamma = 50 \pm 4$ MeV) and 1460 ± 10 MeV ($\Gamma = 105 \pm 15$ MeV) (Bertin, 1995). We shall refer to these pseudoscalars as $\eta(1410)$ and $\eta(1460)$. When using gaseous

hydrogen, one expects the production of 1^{++} mesons from ${}^{3}P_{1}$ recoiling against an Swave dipion: Bertin (1997) indeed observes three states in the $K\overline{K}\pi$ mass spectrum in gas: $\eta(1410)$, $f_{1}(1420)$ and $\eta(1460)$.

In J/ψ radiative decay, ι decays to $K\overline{K}\pi$ through the intermediate $a_0(980)$ and hence a signal was also expected in the $a_0(980)\pi \to \eta\pi\pi$ mass spectrum. This has indeed been observed by Mark III and DM2: Bolton (1992) reports a signal in $a_0^{\pm}\pi^{\mp}$ at 1400 \pm 6 MeV ($\Gamma = 47 \pm 13$ MeV) and Augustin (1990) in $\eta\pi^+\pi^-$ at 1398 \pm 6 MeV ($\Gamma = 53 \pm 11$ MeV). We shall tentatively assign these signals to $\eta(1410)$.

To clarify whether the structures observed in J/ψ radiative decay and in $\overline{p}p$ annihilation are compatible and in particular to confirm the quantum numbers of E (0⁻⁺ and not 1⁺⁺) Crystal Barrel has searched for the $\eta\pi\pi$ decay mode of the E meson in the reaction $\overline{p}p \rightarrow (\eta\pi^+\pi^-)\pi^0\pi^0$ and $(\eta\pi^0\pi^0)\pi^+\pi^-$, leading to two charged particles and 6γ (Amsler, 1995h; Urner, 1995). Since the rate for this reaction was expected to be rather small (~ 10⁻³ of all annihilations), an online trigger required 8 clusters in the barrel and at least two π^0 and one η . A 7C kinematic fit then selected the channel $\pi^+\pi^-2\pi^0\eta$ while suppressing $\pi^+\pi^-2\eta\pi^0$ and $\pi^+\pi^-3\pi^0$. The branching ratio for $\pi^+\pi^-2\pi^0\eta$ was found to be (2.09 ± 0.36) %.

The final state $\pi^+\pi^-2\pi^0\eta$ includes a strong contribution from $\omega\eta\pi^0$ ($\omega \to \pi^+\pi^-\pi^0$), a channel that has been studied in its 7γ decay mode (Amsler, 1994c). Events compatible with $\omega\eta\pi^0$ were removed, leaving a sample of about 127,000 $\pi^+\pi^-2\pi^0\eta$ events. The evidence for $\eta(1410)$ decaying to $\eta\pi\pi$ is shown in the $\pi^0\pi^0\eta$ and $\pi^+\pi^-\eta$ mass distributions (Fig. 35). Some 9,000 $\eta(1410)$ decays into $\eta\pi\pi$ are observed in Fig. 35, an order of magnitude more than for E to $K\overline{K}\pi$ in the seminal work of Baillon (1967).

A partial wave analysis was performed using a maximum likelihood optimization. The signal at 1400 MeV was described by the annihilation channels

$$\overline{p}p \rightarrow \eta(1410)(\rightarrow \eta \sigma^{0})\sigma^{+-},
\rightarrow \eta(1410)(\rightarrow a_{0}^{0}(980)\pi^{0})\sigma^{+-},
\rightarrow \eta(1410)(\rightarrow \eta \sigma^{+-})\sigma^{0},
\rightarrow \eta(1410)(\rightarrow a_{0}^{\pm}(980)\pi^{\mp})\sigma^{0},$$
(139)

where σ^0 and σ^{+-} are shorthands for the $\pi^0\pi^0$ and $\pi^+\pi^-$ S-waves. The latter were described by prescriptions of the form (100) which is reasonable since the $\pi\pi$ masses lie below 900 MeV. Background contributions, e.g. from $\eta\rho^0\sigma^0$ and $\eta'\rho^0$, were also included in the fit. Figure 36 shows for example the $a_0^{\pm}(980)$ angular distribution in the $\eta(1410)$ rest frame together with the best fit for a 0^{-+} state. The data exclude 1^{++} , hence $\eta(1410)$ is definitively pseudoscalar and is produced from the 1S_0 atomic state. It has mass and width

$$\eta(1410): m = 1409 \pm 3 \text{ MeV}, \ \Gamma = 86 \pm 10 \text{ MeV}.$$
 (140)

The width is somewhat larger than for $\eta \pi \pi$ in J/ψ decay (Bolton, 1992; Augustin, 1990) and for $K\overline{K}\pi$ in $\overline{p}p$ annihilation at rest (Bertin, 1995).

The branching ratio to $K\overline{K}\pi$ has been measured earlier (Baillon, 1967):

$$B(\overline{p}p \to E\pi\pi, E \to K\overline{K}\pi) = (2.0 \pm 0.2) \times 10^{-3}, \tag{141}$$

while Crystal Barrel finds for the $\eta\pi\pi$ mode

$$B(\overline{p}p \to \eta(1410)\pi\pi, \eta(1410) \to \eta\pi\pi) = (3.3 \pm 1.0) \times 10^{-3}.$$
 (142)

The fit yields $\eta\sigma$ and $a_0(980)(\rightarrow \eta\pi)\pi$ decay contributions with a relative rate of 0.78 \pm 0.16. Assuming that 50% of the $K\overline{K}\pi$ mode proceeds through $\eta(1410)$ decaying to

 $a_0(980)\pi$ (Baillon, 1967) one can estimate from these branching ratios

$$\frac{B(a_0(980) \to K\overline{K})}{B(a_0(980) \to \eta\pi)} \sim 0.54 \pm 0.18,$$
(143)

somewhat larger but not in violent disagreement with the result (111).

The observation of the $\eta \pi^0 \pi^0$ decay mode also lifts the earlier isospin ambiguity for the *E* meson and clearly establishes that this state is isoscalar (*C* = +1). Note that the Crystal Barrel data do not exclude the presence of the other *I* = 0 pseudoscalar, $\eta(1460)$, since the latter was observed in $K^*\overline{K}$ and not in $\eta\pi\pi$.

The first radial excitation of the η could be $\eta(1295)$ decaying to $\eta\pi\pi$ (Barnett, 1996). Hence one of two pseudoscalars in the ι structure could be the radial excitation of the η' . The near equality of the $\eta(1295)$ and $\pi(1300)$ masses suggests an ideally mixed nonet of 0^{-+} radials. This implies that the second isoscalar in the nonet should be mainly $s\overline{s}$ and hence decays to $K^*\overline{K}$, in accord with observations for $\eta(1460)$. This scheme then favours an exotic interpretation for $\eta(1410)$, perhaps gluonium mixed with $q\overline{q}$ (Close, 1997) or a bound state of gluinos (Farrar, 1996). The gluonium interpretation is, however, not favoured by lattice gauge theories, which predict the 0^{-+} state above 2 GeV (see Szczpaniak (1996)).

12 Summary and Outlook

Crystal Barrel has collected $10^8 \ \overline{p}p$ annihilation at rest in liquid hydrogen, three orders of magnitudes more than previous bubble chamber experiments. The results reviewed in this report were achieved thanks to the availability of pure, cooled and intensive low energy antiproton beams which allow a good spatial definition of the annihilation source and thanks to the refinement of the analysis tools warranted by the huge statistical samples. The data processed so far concentrate on annihilations at rest into 0-prong that had not been investigated before. The data collected with the 0-prong trigger correspond to 6.3×10^8 annihilations.

The measurement of the branching ratio for annihilation into $\pi^0 \pi^0$ leads, together with a cascade calculation of the antiprotonic atom, to a fraction of (13 ± 4) % P- wave in liquid hydrogen. Therefore S-wave dominance has been, in general, assumed to analyze the data.

The branching ratios for annihilation into two neutral light mesons $(\pi^0\eta, \pi^0\eta', \eta\eta, \eta\eta', \omega\eta, \omega\eta', \eta\rho^0, \eta'\rho^0)$ reveal the interplay of constituent quarks in hadrons. The non-planar quark rearrangement graph must play an important role in the annihilation process. Using the OZI rule the pseudoscalar mixing angle was determined to be $(-17.3 \pm 1.8)^{\circ}$.

However, the production of ϕ mesons is enhanced in nearly all channels compared to predictions by the OZI rule. The most significant deviation is found in the annihilation channel $\pi^0 \phi$. After phase space correction, the $\pi^0 \phi / \pi^0 \omega$ ratio is (10.6 ± 1.2) % while OZI predicts 0.42 %. Whether this enhancement can be explained by final state corrections or by $s\overline{s}$ pairs in the nucleon is not clear yet. The analysis of data in P-state annihilations, in gas or at higher momenta, will be helpful in settling the nature of this phenomenon.

In electromagnetic processes, the radiative annihilations $\pi^0\gamma$, $\eta\gamma$ and $\omega\gamma$ have been observed with rates consistent with predictions from VDM, but $\phi\gamma$ may be enhanced. The branching ratio for $\omega \to \eta\gamma$, $(6.6 \pm 1.7) \times 10^{-4}$, was measured independently of $\rho - \omega$ interference. This results solves the ambiguity in e^+e^- formation experiments, selecting the constructive $\rho - \omega$ interference solution. The $\eta \to 3\pi^0$ Dalitz plot is not homogeneous but shows a negative slope of $\alpha = 0.052 \pm 0.020$. Crystal Barrel data also confirms the evidence for the direct decay $\eta' \to \pi^+ \pi^- \gamma$, in addition to $\eta' \to \rho \gamma$.

A decisive progress has been achieved in understanding scalar mesons by studying annihilation into three pseudoscalars. An isovector state, $a_0(1450)$, with mass and width $(m,\Gamma) = (1474 \pm 19, 265 \pm 13)$ MeV has been observed to decay into $\eta\pi$, $\eta'\pi$ and $K\overline{K}$ with rates compatible with SU(3) flavor. The existence of $a_0(1450)$ adds evidence for $a_0(980)$ not being $q\overline{q}$, but perhaps a $K\overline{K}$ molecule. The ratio of $a_0(980)$ decay rates to $K\overline{K}$ and $\eta\pi$ was measured to be 0.24 ± 0.06 .

An isoscalar state, $f_0(1370)$, with mass and width $(m, \Gamma) = (1360 \pm 23, 351 \pm 41)$ MeV has been observed to decay into $\pi\pi$, $\eta\eta$, $K\overline{K}$ and 4π . Obtaining accurate branching ratios for $f_0(1370)$ is difficult due to interferences with the broad structure $f_0(400 - 1200)$. The nature of this structure (meson or slowly moving background phase) is unclear. Whether $f_0(400 - 1200)$ is really distinct from $f_0(1370)$ is not entirely clear. Both questions will probably remain with us for some time. The states $a_0(1450)$, $f_0(1370)$ and $K_0^*(1430)$ are broad, consistent with expectations for $q\overline{q}$ scalar mesons. The small coupling of $f_0(1370)$ to $K\overline{K}$ makes it an unlikely candidate for the $s\overline{s}$ meson, which is therefore still missing. More information on this state will hopefully emerge in the mass range above 1600 MeV from Crystal Barrel data in flight.

An additional isoscalar state, $f_0(1500)$, with mass and width $(m, \Gamma) = (1505 \pm 9, 111 \pm 12)$ MeV has been observed to decay into $\pi\pi$, $\eta\eta$, $\eta\eta'$, $K\overline{K}$ and 4π . The decay branching ratios are 29, 5, 1, 3 and 62 %, respectively. These rates exclude this state to be the missing $s\overline{s}$. Hence $f_0(1500)$ is supernumerary and anyway too narrow to be easily accommodated in the scalar nonet. The likely explanation is that $f_0(1500)$ is the ground state glueball predicted by QCD, mixed with the two nearby $q\overline{q}$ isoscalars, $f_0(1370)$ and the higher lying $s\overline{s}$ state.

The tensor $f_2(1565)$ is dominantly produced from P-states. It is, however, still required to fit the data when assuming pure S-wave annihilation: Its mass and width are $\simeq 1552$ and $\simeq 142$ MeV. The systematic inclusion of P-wave annihilation at rest in all analyses is, however, prevented by the large number of fit parameters. Data from Crystal Barrel and Obelix in liquid and gaseous hydrogen might alleviate this problem, perhaps also modifying slightly some of the branching ratios obtained from liquid only.

A 0⁻⁺ state, $\eta(1410)$, with mass and width $(m, \Gamma) = (1409 \pm 3, 80 \pm 10)$ MeV has been observed to decay into $\eta \pi^0 \pi^0$ and $\eta \pi^+ \pi^-$ with approximately equal rates through $a_0(980)\pi$ and $(\pi\pi)_S\eta$. The neutral decay mode establishes this state as an isoscalar and, together with other experiments, strengthens the evidence for two I = 0 pseudoscalars in the 1400 - 1500 MeV region.

Crystal Barrel data also show evidence for the two excitations of the ρ meson, $\rho(1450)$ and $\rho(1700)$ and for the radial excitation $a'_2(1650)$. The analysis of in-flight data will hopefully reveal further radial excitations, hybrid mesons and higher mass glueballs. For glueballs, a more definitive progress will probably be achieved in radiative J/ψ decay at a high luminosity e^+e^- factory or in central collisions at the forthcoming Compass experiment at CERN.

13 Acknowledgements

The results presented in this review have been obtained through the efforts of many physicists and technicians from the Crystal Barrel collaboration¹¹ and from the supporting

¹¹Universities of California (Berkeley and Los Angeles), Bochum, Bonn, Hamburg, Karlsruhe, Mainz, Munich, Paris VI, Zurich, Carnegie Mellon University, Academy of Science (Budapest), Rutherford Appleton Laboratory,

institutions. The author also wishes to thank C. Batty, F. Close, H. Genz, P. Giarritta, F. Heinsius, M. Heinzelmann, M. Locher, V. Markushin, L. Montanet, R. Ouared, S. Spanier, U. Wiedner and Č. Zupančič for reading the manuscript and for helpful discussions.

References

Abele, A., et al., 1996a, Nucl. Phys. A 609, 562.

Abele, A., et al., 1996b, Observation of $f_0(1500)$ decay into $K_L K_L$, Phys. Lett. **B** 385, 425.

Abele, A., et al., 1996c, A study of $f_0(1500)$ decays into $4\pi^0$ in $\overline{p}p \to 5\pi^0$ at rest, Phys. Lett. **B** 380, 453.

Abele, A., et al., 1997a, $\rho - \omega$ interference in $\overline{p}p$ annihilation at rest into $\pi^+\pi^-\eta$, submitted to Phys. Lett. **B**.

Abele, A., et al., 1997b, Momentum Dependence of the Decay $\eta \to \pi^+ \pi^- \pi^0$, submitted to Phys. Lett. **B**.

Abele, A., et al., 1997c, Decay dynamics of the process $\eta \to 3\pi^0$, submitted to Phys. Lett. **B**.

Abele, A., et al., 1997d, Measurement of the $\omega \to \eta \gamma$ decay branching ratio, submitted to Phys. Lett. **B**.

Abele, A., et al., 1997e, $\overline{p}p$ annihilation at rest into $K_L K^{\pm} \pi^{\mp}$, submitted to Phys. Lett. **B**.

Abele, A., et al., 1997f, Antiproton-proton annihilation at rest into $K_L K_S \pi^0 \pi^0$, submitted to Phys. Lett. **B**.

Abele, A., et al., 1997g, Study of the $\pi^0 \pi^0 \eta'$ final state in $\overline{p}p$ annihilation at rest, Phys. Lett. **B** 404, 179.

Abele, A., et al., 1997h, High-mass ρ meson states from $\overline{p}d$ annihilation at rest into $\pi^{-}\pi^{0}\pi^{0}\pi^{0}p_{spectator}$, Phys. Lett. **B 391**, 191.

Abele, A., et al., 1997i, Measurement of the decay distribution of $\eta' \to \pi^+\pi^-\gamma$ and evidence for the box anomaly, Phys. Lett. **B** 402, 195.

Ableev, V.G., et al., 1994, Phys. Lett. B 334, 237.

Ableev, V.G., et al., 1995, Nucl. Phys. A 585, 577.

Achasov, N.N., and G.N. Shestakov, 1978, Sov. J. Part. Nucl. 9, 19.

Adamo, A., et al., 1992, Phys. Lett. B 287, 368.

Adiels, L., et al., 1987, Z. Phys. C 35, 15.

Adiels, L., et al., 1989, Z. Phys. C 42, 49.

Adomeit, J., et al., 1996, Evidence for two isospin zero $J^{PC} = 2^{-+}$ mesons at 1645 and 1875 MeV, Z. Phys. C 71, 227.

Ahmad, S., et al., 1985, Phys. Lett. 157 B, 333.

Aitchison, I.J.R., 1972, Nucl. Phys. A 189, 417.

Aker, E., et al., 1991, Observation of a 2^{++} resonance at 1515 MeV in proton-antiproton annihilations into $3\pi^0$, Phys. Lett. **B 260**, 249.

Aker, E., et al., 1992, The Crystal Barrel spectrometer at LEAR, Nucl. Instrum.

Methods A 321, 69.

Alde, D., et al., 1984, Z. Phys. C 25, 225.

Alde, D., et al., 1987, Phys. Lett. B 198, 286.

Alde, D., et al., 1988a, Phys. Lett. B 205, 397.

Alde, D., et al., 1988b, Phys. Lett. B 201, 160.

Alde, D., et al., 1990, Phys. Lett. B 241, 600.

CERN, Queen Mary and Westfield College, Centre de Recherches Nucléaires (Strasbourg).

Alde, D., et al., 1994, Z. Phys. C 61, 35.

Amelin, D.V., et al., 1996, Phys. At. Nucl. 59, 976.

Amsler, C., and J.C. Bizot, 1983, Comp. Phys. Comm. 30, 21.

Amsler, C., 1987, in *Advances in Nuclear Physics*, edited by J.W. Negele and E. Vogt (Plenum, New York), Vol. 18, p. 183.

Amsler, C., and F. Myhrer, 1991, Ann. Rev. Nucl. Part. Sci. 41, 219.

Amsler, C., et al., 1992a, P- versus S-wave $\overline{p}p$ annihilation at rest in LH₂, Phys. Lett. **B 297**, 214.

Amsler, C., et al., 1992b, The pseudoscalar mixing angle Θ_{PS} from η and η' production in $\overline{p}p$ annihilation at rest, Phys. Lett. **B 294**, 451.

Amsler, C., et al., 1992c, Proton-antiproton annihilation into $\eta\eta\pi$ - observation of a scalar resonance decaying into $\eta\eta$, Phys. Lett. **B** 291, 347.

Amsler, C., et al., 1993a, Antiproton-proton annihilation at rest into $\omega \pi^0 \pi^0$, Phys. Lett. **B 311**, 362.

Amsler, C., et al., 1993b, Antiproton-proton annihilation at rest into two-body final states, Z. Phys. C 58, 175.

Amsler, C., et al., 1993c, Radiative protonium annihilation into $\gamma\gamma, \gamma\pi^0, \gamma\eta, \gamma\omega$ and $\gamma\eta'$, Phys. Lett. **B 311**, 371.

Amsler, C., et al., 1993d, Protonium annihilation into $K_L^0 K_S^0 \pi^0$ and $K_L^0 K_S^0 \eta$, Phys. Lett. **B** 319, 373.

Amsler, C., et al., 1994a, Search for a new light gauge boson in decays of π^0 and η , Phys. Lett. **B** 333, 271.

Amsler, C., et al., 1994b, Observation of a new $I^G(J^{PC}) = 1^-(0^{++})$ resonance at 1450 MeV, Phys. Lett. **B 333**, 277.

Amsler, C., et al., 1994c, Study of $\overline{p}p$ annihilation at rest into $\omega\eta\pi^0$, Phys. Lett. **B 327**, 425.

Amsler, C., et al., 1994d, Observation of a scalar resonance decaying to $\pi^+\pi^-\pi^0\pi^0$ in $\overline{p}p$ annihilation at rest, Phys. Lett. **B 322**, 431.

Amsler, C., et al., 1994e, in Hadron '93, Proceedings of the Hadron 93 Conf., edited by T. Bressani et al., Nuovo Cimento **107 A**, 1815.

Amsler, C., et al., 1994f, $\eta\eta'$ threshold enhancement in $\overline{p}p$ annihilation into $\pi^0\eta\eta'$ at rest, Phys. Lett. **B 340**, 259.

Amsler, C., et al., 1995a, First observations of Pontecorvo reactions with a recoiling neutron, Z. Phys. A 351, 325.

Amsler, C., et al., 1995b, First observation of the production of nucleon resonances in antiproton annihilation in liquid deuterium, Phys. Lett. **B** 352, 187.

Amsler, C., et al., 1995c, Observation of radiative $\overline{p}p$ annihilation into a ϕ meson, Phys. Lett. **B 346**, 363.

Amsler, C., et al., 1995d, η decays into three pions, Phys. Lett. **B 346**, 203.

Amsler, C., et al., 1995e, High statistics study of $f_0(1500)$ decay into $\eta\eta$, Phys. Lett. **B** 353, 571.

Amsler, C., et al., 1995f, High-statistics study of $f_0(1500)$ decay into $\pi^0\pi^0$, Phys. Lett. **B 342**, 433.

Amsler, C., et al., 1995g, Coupled channel analysis of $\overline{p}p$ annihilation into $\pi^0\pi^0\pi^0$, $\pi^0\eta\eta$ and $\pi^0\pi^0\eta$, Phys. Lett. **B 355**, 425.

Amsler, C., et al., 1995h, E decays to $\eta\pi\pi$ in $\overline{p}p$ annihilation at rest, Phys. Lett. **B** 358, 389.

Amsler, C., et al., 1996a, Search for a new light gauge boson in π^0 , η and η' decays, Z. Phys. C 70, 219.

Amsler C., and F.E. Close, 1996, Phys. Rev. D 53, 295; see also Amsler C., and F.E.

- Close, 1995, Phys. Lett. **B** 353, 385.
- Andrews, D.E., et al., 1977, Phys. Rev. Lett. 38, 198.
- Anisovich, V.V., et al., 1994, Observation of two $J^{PC} = 0^{++}$ isoscalar resonances at
- 1365 and 1520 MeV, Phys. Lett. B 323, 233.
- Antinori, F., et al., 1995, Phys. Lett. B 353, 589.
- Armenteros, R., et al., 1965, Phys. Lett. 17, 170.
- Armenteros R., and B. French, 1969, in \overline{NN} Interactions in High Energy Physics, edited
- by E.H.S. Burhop (Academic, New York), Vol. 4, p. 237.
- Armstrong, T., et al., 1993, Phys. Lett. B 307, 394, 399.
- Aston, D., el al., 1988a, Phys. Lett. B 201, 573.
- Aston, D., *el al.*, 1988b, Nucl. Phys. **B 296**, 493.
- Atiya, M.S., et al., 1992, Phys. Rev. Lett. 69, 733.
- Au, K.L., D. Morgan, and M.R. Pennington, 1987, Phys. Rev. D 35, 1633.
- Augustin, J.-E., et al., 1990, Phys. Rev. D 42, 10.
- Badalayan, A.M., L.P. Kok, M.I. Policarpov, and Yu. A. Simonov, 1982, Phys. Rep. 82, 31.
- Bai, Z., et al., 1990, Phys. Rev. Lett. 65, 2507.
- Baillon, P., et al., 1967, Nuovo Cimento 50 A, 393.
- Baker, C.A., et al., 1988, Nucl. Phys. A 483, 631.
- Bali, G.S., et al., 1993, Phys. Lett. B 309, 378.
- Baltay, C., et al., 1966, Phys. Rev. B 145, 1103. Baltrusaitis, R.M., et al., 1987, Phys. Rev. D 35, 2077.
- Barash, N., et al., 1965, Phys. Rev. B 139, 1659.
- Barnes, T., 1985, Phys. Lett. 165 B, 434.
- Barnes, T., F.E. Close, P.R. Page, and E.S. Swanson, 1997, Phys. Rev. D 55, 4157.
- Barnett, R.M. et al. (Particle Data Group), 1996, Phys. Rev. D 54, 1.
- Bassompierre, G., et al., 1976, Phys. Lett. B 64, 475.
- Batty, C.J., 1989, Rep. Prog. Phys. 52, 1165.
- Batty, C.J., 1996, Nucl. Phys. A 601, 425.
- Beladidze, G.M., et al., 1992, Sov. J. Nucl. Phys. 55, 1535.
- Benayoun, M., et al., 1993, Z. Phys. 58, 31.
- Bertin, A., et al., 1995, Phys. Lett. B 361, 187.
- Bertin, A., et al., 1996, Phys. Lett. B 388, 450.
- Bertin, A., et al., 1997, Phys. Lett. B 400, 226.
- Binon, F., et al., 1983, Nuovo Cimento 78 A, 313.
- Binon, F., et al., 1984, Nuovo Cimento 80 A, 363.
- Bityukov, S.I., et al., 1987, Phys. Lett. B 188, 383.
- Bityukov, S.I., et al., 1991, Z. Phys. C 50, 451.
- Bizzarri, R., et al., 1969, Nucl. Phys. B 14, 169.
- Bizzarri, R., et al., 1971, Nucl. Phys. B 27, 140.
- Blüm, P., 1996, Int. J. Mod. Phys. A 11, 3003.
- Bolton, T., et al., 1992, Phys. Rev. Lett. 69, 1328.
- Bridges, D., I. Daftari, and T.E. Kalogeropoulos, 1987, Phys. Rev. Lett. 57, 1534.
- Bugg, D.V., V.V. Anisovich, A. Sarantsev, and B.S. Zou, 1994, Phys. Rev. D 50, 4412.
- Bugg, D.V., et al., 1995, Phys. Lett. B 353, 378.
- Bugg, D.V., A.V. Sarantsev, and B.S. Zou, 1996, Nucl. Phys. B 471, 59.
- Carbonell, J., G. Ihle, and J.M. Richard, 1989, Z. Phys. A 334, 329.
- Chamberlain, O., E. Segrè, C.E. Wiegand, and T. Ypsilantis, 1955, Phys. Rev. 100, 947.
- Chew, F. G., and S. Mandelstam, 1960, Phys. Rev. 119, 467.
- Chiba, M., et al., 1987, in Physics at LEAR with Low Energy Antiprotons, Nuclear

Science Research Conf. Series, Vol. 14, edited by C. Amsler *et al.*, (Harwood, Chur), p. 401.

- Chiba, M., *et al.*, 1988, Phys. Rev. **D** 38, 2021, see also Chiba, M., *et al.*, 1989, Phys. Rev. **D** 39, 3227.
- Chung, S.U., et al., 1995, Ann. Phys. 4, 404.
- Close, F.E., G.R. Farrar, and Z. Li, 1997, Phys Rev D 55, 5749.
- Close, F.E., N. Isgur, and S. Kumano, 1993, Nucl. Phys. B 389, 513.
- Close, F.E., and P.R. Page, 1995, Nucl. Phys. B 443, 233.
- Conforto, B., et al., 1967, Nucl. Phys. B 3, 469.
- Cooper, A. M., et al., 1978, Nucl. Phys. B 146, 1.
- Day, T.B., G.A. Snow, and T. Sucher, 1960, Phys. Rev. 118, 864.
- Delcourt, B., J. Layssac, and E. Pelaquier, 1984, in Physics at LEAR with Low Energy
- Antiprotons, edited by U. Gastaldi and R. Klapisch, (Plenum, New York), p. 305.
- Devons, S., et al., 1971, Phys. Rev. Lett. 27, 1614.
- Devons, S., et al., 1973, Phys. Lett. 47 B, 271.
- Dobroliubov, M.I., and A. Yu. Ignatiev, 1988, Nucl. Phys. B 309, 655.
- Dobroliubov, M.I., 1990, Sov. J. Nucl. Phys. 52, 352.
- Dolinsky, S.I. et al., 1989, Z. Phys. C 42, 511.
- Dombrowski, S. v., 1996, Ph.D. thesis (University of Zurich).
- Donoghue, J.F., B.R. Holstein, and D. Wyler, 1992, Phys. Rev. Lett. 69, 3444.
- Doser, M., et al., 1988, Nucl. Phys. A 486, 493.
- Dover, C.B., 1986, Phys. Rev. Lett. 57, 1207.
- Dover, C.B., and P. M. Fishbane, 1989, Phys. Rev. Lett. 62, 2917.
- Dover, C.B., T. Gutsche, and A. Faessler, 1991, Phys. Rev. C 43, 379.
- Dover, C.B., and J.M. Richard, 1980, Phys. Rev. C 21, 1466.
- Ellis, J. , M. Karliner, D.E. Kharzeev, and M.G. Sapozhnikov, 1995, Phys. Lett. **B 353**, 319.
- Espigat, P., C. Guesquière, E. Lillestol, and L. Montanet, 1972, Nucl. Phys. B 36, 93.
- Farrar, G.R., 1996, Phys. Rev. Lett. 76, 4111.
- Flatté, S.M., 1976, Phys. Lett. 63 B, 224.
- Foster, M., et al., 1968a, Nucl. Phys. B 8, 174.
- Foster, M., et al., 1968b, Nucl. Phys. B 6, 107.
- Gaspero, M., 1993, Nucl. Phys. A 562, 407.
- Gasser, J., and H. Leutwyler, 1985, Nucl. Phys. B 250, 539.
- Genz, H., 1983, Phys. Rev. D 28, 1094.
- Genz, H., 1985, Phys. Rev. D 31, 1136.
- Genz., H., M. Martinis, and S. Tatur, 1990, Z. Phys. A 335, 87.
- Gilman, F.G., and R. Kauffman, 1987, Phys. Rev. D 36, 2761.
- Godfrey, S., and N. Isgur, 1985, Phys. Rev. D 32, 189.
- Goldhaber, A.S., G.C. Fox, and C. Quigg, 1969, Phys. Lett. 30 B, 249.
- Gortchakov, O., M.P. Locher, V.E. Markushin, and S. von Rotz, 1996, Z. Phys. A 353, 447.
- Gray, L., et al., 1983, Phys. Rev. D 27, 307.
- Grayer, G., et al., 1974, Nucl. Phys. B 75, 189.
- Guesquière, C., 1974, in Antinucleon-Nucleon Interactions, Proceedings of the Liblice
- Symposium, CERN Yellow Report 74-18, p. 436.
- Hartmann, U., E. Klempt, and J. Körner, 1988, Z. Phys. A 331, 217.
- Heinzelmann, M., 1996, Diploma thesis (University of Zurich).
- Hippel, F.v., and C. Quigg, 1972, Phys. Rev. **D** 5, 624; see also Blatt, J.M., and V.F. Weisskopf, 1952, in *Theoretical Nuclear Physics*, (Wiley, New York), p. 361.

- Isgur, N., and J. Paton, 1985, Phys. Rev. D 31, 2910.
- Jacob, M., and G.C. Wick, 1959, Ann. Phys. (NY) 7, 404.
- Jaenicke, J., B. Kerbikov, and H.-J. Pirner, 1991, Z. Phys. A 339, 297.
- Kambor, J., C. Wiesendanger and D. Wyler, 1996, Nucl. Phys. B 465, 215.
- Klempt, E., 1990, Phys. Lett. B 244, 122.
- Kolybashov, V.M., I.S. Shapiro, and Yu.N. Sokolskikh, 1989, Phys. Lett. B 222, 135.
- Lacock, P., C. Michael, P. Boyle, and P. Rowland, 1997, Phys. Lett. B 401, 308.
- Landua, R., 1996, Ann. Rev. Nucl. Part. Sci. 46, 351.
- Layter, J.G., et al., 1973, Phys. Rev. D 7, 2565.
- Locher, M.P., Y. Lu, and B.S. Zou, 1994, Z. Phys. A 347, 281.
- Markushin, V.E., 1997, Nucl. Phys. B (Proc. Suppl.) 56 A, 303.
- May, B., et al., 1989, Phys. Lett. 225 B, 450.
- May, B., et al., 1990, Z. Phys. C 46, 191, 203.
- Meijer Drees, R., et al., 1992, Phys. Rev. Lett. 68, 3845.
- Morgan, D., and M.R. Pennington, 1993, Phys. Rev. D 48, 1185.
- O'Connell, H.B., et al., 1995, Phys. Lett. B 354, 14.
- O'Donnell, P.J., 1981, Rev. Mod. Phys. 53, 673.
- Okubo, S., 1963, Phys. Lett. 5, 165.
- Ore, A., and J.L. Powell, 1949, Phys. Rev. 75, 1696.
- Orfanidis, S.J., and V. Rittenberg, 1973, Nucl. Phys. B59, 570.
- Pais, A., 1960, Ann. Phys. (NY), 9, 548.
- Peters, K., and E. Klempt, 1995, Phys. Lett. 352, 467.
- Pietra, C., 1996, Diploma thesis (University of Zurich).
- Prokoshkin, Yu. D., and V.D. Samoilenko, 1995, Sov. Phys. Dokl. 342, 273.
- Regenfus, C., 1997, Nucl. Instrum. Methods A 386, 60.
- Reifenröther, J., et al., 1991, Phys. Lett. B 267, 299.
- Rosselet, L., et al., 1977, Phys. Rev. D 15, 574.
- Scharre, D.L., et al., 1980, Phys. Lett. B 97, 329.
- Schmid, B., 1991, Ph.D. thesis (University of Zurich).
- Sedlák, J., and V. Šimák, 1988, Sov. J. Part. Nucl. 19, 191.
- Sexton, J., A. Vaccarino, and D. Weingarten, 1995, Phys. Rev. Lett. 75, 4563.
- Spanier, S., 1994, Ph.D. thesis (University of Mainz).
- Spanier, S., 1996, Yad. Fiz. 59, 1352.
- Spanier, S., 1997, Workshop on The Strange Structure of the Nucleon, CERN.
- Szczepaniak, A., E.S. Swanson, C.R. Ji, and S.R. Cotanch, 1996, Phys. Rev. Lett. 76, 2011.
- Thompson, D.R., et al., 1997, Phys. Rev. Lett. (in print)
- Törnqvist, N.A., 1991, Phys. Rev. Lett. 67, 556.
- Törnqvist, N.A., 1995, Z. Phys. C 68, 647.
- Törnqvist, N.A., and M. Roos, 1996, Phys. Rev. Lett. 76, 1575.
- Urner, D., 1995, Ph.D. thesis (University of Zurich).
- Vandermeulen, J., 1988, Z. Phys. C 37, 563.
- Weidenauer, P., et al., 1990, Z. Phys. C 47, 353.
- Weidenauer, P., et al., 1993, Z. Phys. C 59, 387.
- Weinstein, J., and N. Isgur, 1990, Phys. Rev. D 41, 2236.
- Zemach, Ch., 1964, Phys. Rev. B 133, 1201.
- Zemach, Ch., 1965, Phys. Rev. B 140, 97, 109.

Table 1: Summary of data (in millions of events) with a minimum bias trigger (MB), for 0-, 2-, 4-prong and with more specialized triggers at rest (first three rows) and in liquid hydrogen at high \overline{p} momenta (in MeV/c).

LH₂: liquid hydrogen; LD₂: liquid deuterium; GH₂: gaseous hydrogen. ^{*a*} $K_S(\rightarrow \pi^+\pi^-)X$, ^{*b*} $\pi^+\pi^-\pi^0\pi^0\eta$, ^{*c*} $\pi^0\eta\eta$, ^{*d*} 1-prong, ^{*e*} 3-prong, ^{*f*} $\pi^+\pi^-\pi^0\eta$, ^{*g*} $\pi^+\pi^-\eta$

	MB	0	2	4	r	Frigger	s	
LH_2	16.8	24.7	19.3	10.4	16.9^{a}	8.5^{b}	4.0^{c}	0.4^{g}
LD_2	3.2	6.0	0.5	0.5	11.9^{a}	8.1^d	11.7^{e}	
GH_2	8.6	18.0	14.3	8.2	6.4^{a}			
600	1.3	5.9	2.2		1.2^{a}			
900		20.0	19.4					
1050	0.3	7.2						
1200	1.6	10.4	6.0		2.0^{f}			
1350	1.0	11.5						
1525	20.6	10.2	4.5					
1642	0.1	11.1	12.5					
1800		6.8	3.6					
1900	13.6	14.5	15.7					

Table 2: Branching ratios B for $\overline{p}p$ annihilation at rest in liquid. See Amsler and Myhrer (1991) for annihilation in gaseous hydrogen. Further branching ratios from Dalitz plot analyses are listed in Table 13 below.

^{*a*} From $\omega \to \pi^0 \gamma$ ^{*b*} From $\omega \to \pi^+ \pi^- \pi^0$

 c average between Baltay (1966), Espigat (1972) and Foster (1968a)

‡ Crystal Barrel experiment

Channel			В		Reference
e^+e^-	3.2	\pm	0.9	10^{-7}	Bassompierre (1976)
$\pi^0\pi^0$	6.93	\pm	0.43	10^{-4}	Amsler $(1992a)$ ‡
	4.8	\pm	1.0	10^{-4}	Devons (1971)
$\pi^+\pi^-$	3.33	\pm	0.17	10^{-3}	Armenteros and French (1969)
$\pi^+\pi^-$	3.07	\pm	0.13	10^{-3}	Amsler $(1993b)$ ‡
$\pi^0\eta$	2.12	\pm	0.12	10^{-4}	Amsler $(1993b)$ ‡
$\pi^0\eta^\prime$	1.23	\pm	0.13	10^{-4}	Amsler $(1993b)$ ‡
$\pi^0 ho^0$	1.72	\pm	0.27	10^{-2}	Armenteros and French (1969)
$\pi^{\pm}\rho^{\mp}$	3.44	\pm	0.54	10^{-2}	Armenteros and French (1969)
$\eta\eta$	1.64	\pm	0.10	10^{-4}	Amsler $(1993b)$ ‡
$\eta\eta^\prime$	2.16	\pm	0.25	10^{-4}	Amsler $(1993b)$ ‡
$\omega \pi^0$	5.73	\pm	0.47	10^{-3}	Amsler $(1993b)^a \ddagger$
	6.16	\pm	0.44	10^{-3}	Schmid $(1991)^{b}$ ‡
$\omega\eta$	1.51	\pm	0.12	10^{-2}	Amsler $(1993b)^a \ddagger$
	1.63	\pm	0.12	10^{-2}	Schmid $(1991)^{b}$ ‡
$\omega\eta'$	0.78	\pm	0.08	10^{-2}	Amsler $(1993b)$ ‡
$\omega\omega$	3.32	\pm	0.34	10^{-2}	Amsler $(1993b)$ ‡
ηho^0	4.81	\pm	0.85	10^{-3}	c
	3.87	\pm	0.29	10^{-3}	Abele (1997a)‡
$\eta' ho^0$	1.29	\pm	0.81	10^{-3}	Foster (1968a)
	1.46	\pm	0.42	10^{-3}	Urner (1995)‡
$ ho^0 ho^0$	1.2	\pm	1.2	10^{-3}	Armenteros and French (1969)
$ ho^0 \omega$	2.26	\pm	0.23	10^{-2}	Bizzarri (1969)
K^+K^-	1.01	\pm	0.05	10^{-3}	Armenteros and French (1969)
K^+K^-	0.99	\pm	0.05	10^{-3}	Amsler $(1993b)$ ‡
$K_S K_L$	7.6	\pm	0.4	10^{-4}	Armenteros and French (1969)
$K_S K_L$	9.0	±	0.6	10^{-4}	Amsler $(1995c)$ ‡

Table 3: Pseudoscalar mixing angle θ_p derived from the measured ratios of two-body branching ratios ($\theta_i = 35.3^{\circ}$). The first four rows assume only the QLR in the annihilation process. The last six rows assume in addition the dominance of the annihilation graph A.

_

Ratio	Prediction	$ heta_p$	[°]	
$\frac{\tilde{B}(\pi^0\eta)}{\tilde{B}(\pi^0\eta')}$	$\tan^2(\theta_i-\theta_p)$	-18.1	\pm	1.6
$\frac{\tilde{B}(\eta\eta)}{\tilde{B}(\eta\eta')}$	$\frac{1}{2}\tan^2(\theta_i - \theta_p)$	-17.7	\pm	1.9
$\frac{\tilde{B}(\omega\eta)}{\tilde{B}(\omega\eta')}$	$\tan^2(\theta_i-\theta_p)$	-21.1	\pm	1.5
$\frac{\tilde{B}(\eta\rho^0)}{\tilde{B}(\eta'\rho^0)}$	$\tan^2(\theta_i-\theta_p)$	-25.4	+	$5.0 \\ 2.9$
$\frac{\tilde{B}(\eta\rho^0)}{\tilde{B}(\omega\pi^0)}$	$\sin^2(\theta_i - \theta_p)$	-11.9	±	3.2
$\frac{\tilde{B}(\eta'\rho^0)}{\tilde{B}(\omega\pi^0)}$	$\cos^2(\theta_i - \theta_p)$	-30.5	\pm	3.5
$\frac{\hat{B}(\eta\eta)}{\tilde{B}(\pi^0\pi^0)}$	$\sin^4(\theta_i - \theta_p)$	-6.2	+ -	$\begin{array}{c} 0.6 \\ 1.1 \end{array}$
$\frac{\tilde{B}(\eta\eta')}{\tilde{B}(\pi^0\pi^0)}$	$2\sin^2(\theta_i - \theta_p)$	14.6	\pm	1.8
. ,	$\times \cos^2(\theta_i - \theta_p)$	or -34.0	\pm	1.8
$\frac{\tilde{B}(\omega\eta)}{\tilde{B}(\pi^0\rho^0)}$	$\sin^2(\theta_i - \theta_p)$	-23.7	+	$\begin{array}{c} 7.6 \\ 8.9 \end{array}$
$\frac{\tilde{B}(\omega\eta')}{\tilde{B}(\pi^0\rho^0)}$	$\cos^2(\theta_i - \theta_p)$	-20.1	±	3.7

Table 4: Damping factors $F_L(p)$ where z stands for $(p/p_R)^2$ and p_R is usually taken as 197 MeV/c (after Hippel and Quigg (1972)).

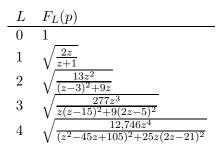


Table 5: Branching ratios B for radiative $\overline{p}p$ annihilation at rest in liquid from Crystal Barrel (Amsler, 1993c, 1995c). The lower and upper limits L and U, calculated from VDM, are given in the third and fourth column, respectively. † 95% confidence upper limit.

Channel			В		L	U
$\pi^0\gamma$	4.4	±	0.4	$\times 10^{-5}$	3.1×10^{-5}	6.8×10^{-5}
$\eta\gamma$	9.3	\pm	1.4	$\times 10^{-6}$	1.0×10^{-6}	2.5×10^{-5}
$\omega\gamma$	6.8	\pm	1.8	$\times 10^{-5}$	8.5×10^{-6}	1.1×10^{-4}
$\eta'\gamma$	< 1.2			$\times 10^{-5}$ †	$2.7 imes 10^{-7}$	10^{-5}
$\gamma\gamma$	< 6.3			$\times 10^{-7}$ †		
$\phi\gamma$	2.0	\pm	0.4	$\times 10^{-5}$	2.1×10^{-7}	1.5×10^{-6}

Table 6: Branching ratios for ϕ production at rest in liquid.

- ^a updates Amsler (1995c)
 ^b annihilation in gas extrapolated to pure S-wave annihilation
 ^d using Chiba (1988) in liquid
 ^d using Bizzarri (1971) in liquid

- ‡ Crystal Barrel experiment

Channel			B		Reference
$\pi^0 \phi$	6.5	\pm	0.6	10^{-4}	a_{\ddagger}
$\pi^0 \phi$	3.0	\pm	1.5	10^{-4}	Chiba (1988)
$\pi^0 \phi$	4.0	\pm	0.8	10^{-4}	Reifenröther $(1991)^{bc}$
$\eta\phi$	7.8	\pm	2.1	10^{-5}	Amsler $(1995c)$ ‡
$\eta\phi$	3.0	\pm	3.9	10^{-5}	Reifenröther $(1991)^b$
$\omega\phi$	6.3	\pm	2.3	10^{-4}	Bizzarri (1971)
$\omega\phi$	5.3	\pm	2.2	10^{-4}	Reifenröther $(1991)^{bd}$
$ ho^0 \phi$	3.4	\pm	1.0	10^{-4}	Reifenröther $(1991)^b$
$\gamma\phi$	2.0	±	0.4	10^{-5}	

Table 7: Ratio of ϕ to ω production in low energy annihilation in liquid.

X	\tilde{R}_X	[10	$^{-2}]$
γ	29.4	±	9.7
π^0	10.6	\pm	1.2
η	0.46	\pm	0.13
ω	1.02	\pm	0.39
$ ho^0$	1.57	\pm	0.49
π^{-}	13.0	\pm	2.5
π^+	10.8	\pm	1.5
σ	1.75	\pm	0.25
$\pi^+\pi^-$	1.65	\pm	0.35

Table 8: Relative sign of α_1 and α_2 for $\overline{p}p$ annihilation into $\pi K\overline{K}$ (see text).

Channel	${}^{1}S_{0}(\overline{p}p)$		${}^{3}S_{1}(\overline{p}p)$	
	I = 0	I = 1	I = 0	I = 1
$\pi^{\pm}K^{\mp}K^0$	+	_	_	+
$\pi^0 K^+ K^-$	+	+	_	_
$\pi^0 K^0 \overline{K^0}$	+	+	_	_

Table 9: Branching ratios for $\overline{p}p$ annihilation at rest into three narrow mesons. Mesons in parentheses were not detected. ^a using $B(\pi^0 \phi)$ from Table 6 and Eq. (47) ^b average between Armenteros (1965) and Barash (1965)

‡ Crystal Barrel experiment

Channel	Final state			В		Reference
$\pi^0\pi^0\pi^0$	6γ	6.2	\pm	1.0	10^{-3}	Amsler $(1995f)$ ‡
$\pi^+\pi^-\pi^0$	$\pi^+\pi^-(\pi^0)$	6.9	\pm	0.4	10^{-2}	Foster $(1968b)$
$\pi^0\eta\eta$	6γ	2.0	\pm	0.4	10^{-3}	Amsler $(1995e)$ ‡
$\pi^0\pi^0\omega$	7γ	2.00	\pm	0.21	10^{-2}	Amsler $(1993a)$ ‡
	$\pi^+\pi^-6\gamma$	2.57	\pm	0.17	10^{-2}	Amsler $(1994d)$ ‡
$\pi^+\pi^-\omega$	$2\pi^+ 2\pi^-(\pi^0)$	6.6	\pm	0.6	10^{-2}	Bizzarri (1969)
$\omega\eta\pi^0$	7γ	6.8	\pm	0.5	10^{-3}	Amsler $(1994c)$ ‡
$\pi^0\pi^0\eta$	6γ	6.7	\pm	1.2	10^{-3}	Amsler $(1994b)$ ‡
	$\pi^+\pi^-6\gamma$	6.50	\pm	0.72	10^{-3}	Amsler $(1994d)$ ‡
$\pi^+\pi^-\eta$	$\pi^+\pi^-2\gamma$	1.63	\pm	0.12	10^{-2}	Abele (1997a)‡
	$\pi^+\pi^-6\gamma$	1.33	\pm	0.16	10^{-2}	Amsler $(1994d)$ ‡
	$2\pi^+ 2\pi^-(\pi^0)$	1.38	\pm	0.17	10^{-2}	Espigat (1972)
	$2\pi^+ 2\pi^-(\pi^0)$	1.51	+	$\begin{array}{c} 0.17 \\ 0.21 \end{array}$	10^{-2}	Foster (1968a)
$\pi^0\pi^0\eta^\prime$	10γ	3.2	\pm	0.5	10^{-3}	Abele $(1997g)$ ‡
	6γ	3.7	\pm	0.8	10^{-3}	Abele $(1997g)$ ‡
$\pi^+\pi^-\eta'$	$\pi^+\pi^-6\gamma$	7.5	\pm	2.0	10^{-3}	Urner (1995)‡
	$3\pi^+3\pi^-(\pi^0)$	2.8	\pm	0.9	10^{-3}	Foster (1968a)
$\pi^0\eta\eta^\prime$	6γ	2.3	\pm	0.5	10^{-4}	Amsler $(1994f)$ ‡
$\pi^0\pi^0\phi$	$8\gamma(K_L)$	9.7	\pm	2.6	10^{-5}	Abele (1997f)‡
$\pi^+\pi^-\phi$	$2\pi^+ 2\pi^- (K_L)$	4.6	\pm	0.9	10^{-4}	Bizzarri (1969)
$\pi^0 K_S K_L$	$3\pi^0(K_L)$	6.7	\pm	0.7	10^{-4}	Amsler $(1993d)^a$ ‡
$\pi^0 K_S K_S$	$2\pi^+ 2\pi^-(\pi^0)$	7.5	\pm	0.3	10^{-4}	b
$\pi^{\pm}K^{\mp}K_S$	$\pi^+\pi^-\pi^\pm K^\mp$	2.73	\pm	0.10	10^{-3}	b
$\pi^{\pm}K^{\mp}K_L$	$\pi^{\pm}K^{\mp}(K_L)$	2.91	\pm	0.34	10^{-3}	Abele $(1997e)$ ‡
$\omega K_S K_S$	$3\pi^+3\pi^-(\pi^0)$	1.17	\pm	0.07	10^{-3}	Bizzarri (1971)
$\omega K^+ K^-$	$K^+K^-\pi^+\pi^-(\pi^0)$	2.30	±	0.13	10^{-3}	Bizzarri (1971)

Table 10: Branching ratios for $\overline{p}p$ annihilation at rest in liquid determined from Dalitz plot analyses. The branching ratios include all decay modes of the final state stable particles (e.g. π^0 , η , η') but only the decay mode of the intermediate resonance leading to the observed final state.

Channel	Contributing resonances
Subchannel	Branching ratio
$\pi^0\eta\eta$	$a_0(980), f_0(1370), f_0(1500), a_2(1320), X_2(1494)$
$f_0(1370)\pi^0$	$\sim 3.5 \times 10^{-4}$
$f_0(1500)\pi^0$	$(5.5 \pm 1.3) \times 10^{-4}$
$a_2(1320)\eta$	$\sim 5.6 imes 10^{-5}$
$X_2(1494)\pi^0$	$\sim 4.0 \times 10^{-4}$ (dominantly P-wave annihilation)
$\pi^0\pi^0\eta$	$a_0(980), a_0(1450), a_2(1320), a'_2(1650), (\eta\pi)_P$
	$(\pi\pi)_S \equiv f_0(400 - 1200) + f_0(980) + f_0(1370)$
$a_0(980)\pi^0$	$(8.7 \pm 1.6) \times 10^{-4}$
$a_0(1450)\pi^0$	$(3.4 \pm 0.6) \times 10^{-4}$
$(\pi\pi)_S \ \eta$	$(3.4 \pm 0.6) \times 10^{-3}$
$(\eta\pi)_P \pi$	$\sim 1.0 \times 10^{-4}$
$a_2(1320)\pi^0$	$(1.9 \pm 0.3) \times 10^{-3}$
$a_2'(1650)\pi^0$	$\sim 1.3 \times 10^{-4}$
$\pi^0\pi^0\pi^0$	$(\pi\pi)_S + f_0(1500), f_2(1270), f_2(1565)$
$(\pi\pi)_S \pi^0$	$\sim 2.6 \times 10^{-3}$
$f_0(1500)\pi^0$	$(8.1 \pm 2.8) \times 10^{-4}$
$f_2(1270)\pi^0$	$\sim 1.8 \times 10^{-3}$
$f_2(1565)\pi^0$	$\sim 1.1 \times 10^{-3}$
$\pi^0\eta\eta,\pi^0\pi^0\eta,3\pi^0$	Coupled channels (S-wave annihilation only)
	$(\eta\eta)_S \equiv f_0(400 - 1200) + f_0(1370)$
$(\pi\pi)_S \pi^0$	$(3.48 \pm 0.89) \times 10^{-3}$
$(\pi\pi)_S \eta$	$(3.33 \pm 0.65) imes 10^{-3}$
$(\eta\eta)_S \pi^0$	$(1.03 \pm 0.29) \times 10^{-3}$
$f_0(1500) (\to \pi^0 \pi^0) \pi^0$	$(1.27 \pm 0.33) \times 10^{-3}$
$f_0(1500) (\to \eta \eta) \pi^0$	$(0.60 \pm 0.17) \times 10^{-3}$
$f_2(1270)(\to \pi^0\pi^0)\pi^0$	$(0.86 \pm 0.30) imes 10^{-3}$
$f_2(1565)(\to \pi^0\pi^0)\pi^0$	$(0.60 \pm 0.20) imes 10^{-3}$
$f_2(1565)(\rightarrow \eta\eta)\pi^0$	$(8.60 \pm 3.60) \times 10^{-5}$ (may be more than one object)
$a_0(980)(\to \pi^0 \eta)\pi^0$	$(0.81 \pm 0.20) \times 10^{-3}$
$a_0(980)(\rightarrow \pi^0 \eta)\eta$	$(0.19 \pm 0.06) imes 10^{-3}$
$a_0(1450)(\to \pi^0\eta)\pi^0$	$(0.29 \pm 0.11) \times 10^{-3}$
$a_2(1320)(\to \pi^0 \eta)\pi^0$	$(2.05 \pm 0.40) \times 10^{-3}$ (including $a'_2(1650)$)
$\pi^0\eta\eta^\prime$	$f_0(1500)$
$f_0(1500)\pi^0$	$(1.6 \pm 0.4) \times 10^{-4}$
$\pi^0\pi^0\eta'$	$(\pi\pi)_S, a_2(1320), a_0(1450)$
$(\pi\pi)_S \eta'$	$(3.1 \pm 0.4) \times 10^{-3}$
$a_2(1320)\pi^0$	$(6.4 \pm 1.3) \times 10^{-5}$
$a_0(1450)\pi^0$	$(1.16 \pm 0.47) imes 10^{-4}$

Table 11: Branching ratios for $\overline{p}p$ annihilation at rest in liquid into kaonic channels. The branching ratios include only the decay mode of the intermediate resonance leading to the observed final state.

^a from the corresponding K_S channels (Armenteros, 1965; Barash, 1965) ^b includes low energy $K\pi$ scattering ^c fixed by $\pi^{\pm}K^{\mp}K_L$ data

Channel	$\overline{p}p(I)$	Contributing resonances
Subchannel		Branching ratio
$\pi^0 K_L K_L$		$K^*(892), K^*_0(1430), a_2(1320), f_2(1270), f'_2(1525)$
		$f_0(1370), f_0(1500), a_0(1450)$
Total^a		$(7.5 \pm 0.3) \times 10^{-4}$
$K^*(892)\overline{K}$	${}^{1}S_{0}(0,1)$	$(8.71 \pm 0.68) \times 10^{-5}$
$K_0^*(1430)\overline{K}$		$(4.59 \pm 0.46) \times 10^{-5} b$
$a_2(1320)\pi^0$	${}^{1}S_{0}(0)$	$(6.35 \pm 0.74) \times 10^{-5}$
$a_0(1450)\pi^0$	_	$(7.35 \pm 1.42) \times 10^{-5} c$
$f_2(1270)\pi^0$	${}^{1}S_{0}(1)$	$(4.25 \pm 0.59) \times 10^{-5}$
$f_2'(1525)\pi^0$		$(1.67 \pm 0.26) \times 10^{-5}$
$f_0(1370)\pi^0$		$(2.20 \pm 0.33) \times 10^{-4}$
$\frac{f_0(1500)\pi^0}{\pi^{\pm}K^{\mp}K_L}$		$(1.13 \pm 0.09) \times 10^{-4}$
$\pi^{\pm}K^{\mp}K_L$		$K^*(892), K^*_0(1430), a_2(1320)$
		$a_0(980), a_0(1450), \ \rho(1450/1700)$
Total^a		$(2.73 \pm 0.10) \times 10^{-3}$
$K^*(892)\overline{K}$	${}^{1}S_{0}(0)$	$(2.05 \pm 0.28) \times 10^{-4}$
$K_0^*(1430)\overline{K}$		$(8.27 \pm 1.93) \times 10^{-4} \ ^{b}$
$a_0(980)\pi$		$(1.97 \ ^+ \ ^0.15 \ ^- \ ^0.34) \times 10^{-4}$
$a_2(1320)\pi$		$(3.99 + 0.31)_{-0.83} \times 10^{-4}$
$a_0(1450)\pi$		$(2.95 \pm 0.56) \times 10^{-4}$
$K^*(892)\overline{K}$	${}^{1}S_{0}(1)$	$(3.00 \pm 1.10) \times 10^{-5}$
$K_0^*(1430)\overline{K}$		$(1.28 \pm 0.55) \times 10^{-4} \ ^{b}$
$\rho(1450/1700)\pi$		$(8.73 \ ^{+1.40}_{-2.75}) \times 10^{-5}$
$K^*(892)\overline{K}$	${}^{3}S_{1}(0)$	$(1.50 \pm 0.41) \times 10^{-4}$
$ ho(1450/1700)\pi$	_	$(8.73 \pm 2.75) \times 10^{-5}$
$K^*(892)\overline{K}$	${}^{3}S_{1}(1)$	$(5.52 \pm 0.84) \times 10^{-4}$
$a_2(1320)\pi$		$(1.42 \pm 0.44) \times 10^{-4}$

Table 12: Weights of the channels contributing to $\overline{p}p \to \pi K\overline{K}$. I refers to the $\overline{p}p$ isospin and i to the $K\overline{K}$ isospin.

Channel	i = 1/2	i = 1	i = 0	i = 1
	I = 0, 1	I = 1	I = 1	I = 0
$\pi^{\pm}K^{\mp}K^{0}$	4	2	0	4
$\pi^0 K^+ K^-$	1	0	1	1
$\pi^0 K^0 \overline{K^0}$	1	0	1	1

Table 13: Branching ratios B for two-body $\overline{p}p$ annihilation at rest in liquid hydrogen (including all decay modes), calculated from the final states given in the last column.

^{*a*} assumes 100% b_1 decay to $\pi\omega$ ^{*b*} using $B(\pi^0\phi)$ from Table 6 and Eq. (47)

$\begin{array}{cccccccccc} f_2(1270)\pi^0 & 3.1 \pm 1.1 & 10^{-3} & \pi^0\pi^0\pi^0 \\ f_2(1270)\pi^0 & 3.7 \pm 0.7 & 10^{-3} & \pi^0K_LK_L \\ & 4.3 \pm 1.2 & 10^{-3} & \text{Foster} & (1968) \\ f_2(1270)\omega & 3.26 \pm 0.33 & 10^{-2} & \text{Bizzarri} & (1966) \\ f_2(1270)\omega & 2.01 \pm 0.25 & 10^{-2} & \text{Amsler} & (1995) \\ f_0(1500)\pi^0 & 1.29 \pm 0.11 & 10^{-2} & \pi^0K_LK_L \\ f_2'(1525)\pi^0 & 7.52 \pm 1.20 & 10^{-5} & \pi^0K_LK_L \end{array}$	5 9)
$\begin{array}{rrrrrrrrrrrrrrrrrrrrrrrrrrrrrrrrrrrr$	5 9)
$\begin{array}{rcl} f_2(1270)\omega & 3.26 \pm 0.33 & 10^{-2} & \text{Bizzarri} & (196)\\ f_2(1270)\omega & 2.01 \pm 0.25 & 10^{-2} & \text{Amsler} & (1993)\\ f_0(1500)\pi^0 & 1.29 \pm 0.11 & 10^{-2} & \pi^0 K_L K_L \end{array}$	5 9)
$ \begin{array}{rcl} f_2(1270)\omega & 2.01 \pm 0.25 & 10^{-2} & \text{Amsler (1993)} \\ f_0(1500)\pi^0 & 1.29 \pm 0.11 & 10^{-2} & \pi^0 K_L K_L \end{array} $	/
$f_0(1500)\pi^0$ 1.29 ± 0.11 10^{-2} $\pi^0 K_L K_L$	Ba)
$f_2'(1525)\pi^0$ 7.52 ± 1.20 10^{-5} $\pi^0 K_L K_L$	
$a_2(1320)\pi$ 3.93 ± 0.70 10^{-2} $\pi^0\pi^0\eta$	
$({}^{1}S_{0})$ 3.36 ± 0.94 10^{-2} $\pi^{0}\pi^{0}\eta'$	
$1.55 \pm 0.31 \ 10^{-2} \ \pi^0 K_L K_L$	
$2.44 \stackrel{+}{_{-}} \stackrel{0.44}{_{-}} 10^{-2} \pi^{\pm} K^{\mp} K_L$	
$1.32 \pm 0.37 \ 10^{-2} \ \text{Conforto} (19)$	67)
$a_2^{\pm}(1320)\pi^{\mp}$ 5.79 \pm 2.02 10^{-3} $\pi^{\pm}K^{\mp}K_L$	
$({}^{3}S_{1})$ 4.49 ± 1.83 10 ⁻³ Conforto (19	67)
$b_1^{\pm}(1235)\pi^{\mp}$ 7.9 ± 1.1 10 ⁻³ Bizzarri (196	$(59)^{a}$
$b_1^{\bar{0}}(1235)\pi^0$ 9.2 ± 1.1 10 ⁻³ Amsler (1993)	$Ba)^a$
$a_2^0(1320)\omega$ 1.70 ± 0.15 10 ⁻² Amsler (1994)	4c)
$K^*(892)\overline{K}$ 7.05 ± 0.90 10^{-4} $\pi^{\pm}K^{\mp}K_L$	
$({}^{1}S_{0})$ 1.05 ± 0.08 10^{-3} $\pi^{0}K_{L}K_{L}$	
$1.5 \pm 0.3 \ 10^{-3}$ Conforto (19)	(67)
$K^*(892)\overline{K}$ 2.11 ± 0.28 10^{-3} $\pi^{\pm}K^{\mp}K_L$	
$({}^{3}S_{1})$ 2.70 ± 0.37 10 ⁻³ $\pi^{0}K_{S}K_{L}$ ^b	
$\geq 2.51 \pm 0.22 \ 10^{-3}$ Conforto (19)	(67)

Figure 1: Pion multiplicity distribution for $\overline{p}p$ annihilation at rest in liquid hydrogen. Open squares: statistical distribution; full circles: data; open circles: estimates from Guesquière (1974). The curve is a Gauss fit assuming $\langle N \rangle = 5$.

Figure 2: Fraction f_P of P-wave annihilation as a function of hydrogen density (curve). The dots with error bars give the results from one particular optical model (Dover and Richard, 1980) using two-body branching ratios (adapted from Batty (1996)).

Figure 3: The Crystal Barrel detector. 1,2 - yoke, 3 - coil, 4 - CsI(Tl) barrel, 5 - JDC, 6 - PWC's, 7 - LH₂ target.

Figure 4: The silicon vertex detector. 1 - microstrip detectors, 2 - hybrids, 3 - readout electronics, 4 - cooling ring (from Regenfus (1997)).

Figure 5: 2γ invariant mass distribution for a sample of 4γ events (6 entries/event).

Figure 6: $\pi^0 \gamma$ momentum distribution in $\overline{p}p \to 4\pi^0 \gamma$ (4 entries/event). The peak is due to $\overline{p}p \to \omega \eta$. The inset shows the ω -region and a fit (Gaussian and polynomial background).

Figure 7: $\pi^+\pi^-\pi^0$ invariant mass distribution for $\pi^+\pi^-\pi^0\eta$ events. The peak is due to $\overline{p}p \to \omega\eta$. The inset shows the background subtracted angular distribution in the ω -rest frame (see text).

Figure 8: γ angular distribution in the ω rest frame for $\omega \eta(\omega \to \pi^0 \gamma)$ (see text).

Figure 9: Annihilation graph A and rearrangement graph R for $\overline{p}p$ annihilation into two mesons.

Figure 10: Following VDM, radiative annihilation can be described by a superposition of two isospin amplitudes with unknown relative phase β . X stands for any neutral meson.

Figure 11: Energy deposits in the barrel versus polar angle Θ and azimuthal angle Φ for a $\pi^0 \gamma$ event. The two γ 's from π^0 decay cluster near the minimum opening angle (16.5°).

Figure 12: Energy distribution (24,503 events) of the single γ in the missing π^0 rest frame for events satisfying the kinematics $\overline{p}p \rightarrow 2\pi^0$ and a missing π^0 . The full line is a fit. The dotted curve shows the expected signal for a branching ratio of 5×10^{-4} .

Figure 13: 90 % confidence level upper limits for radiative pseudoscalar decays as a function of missing mass.

Figure 14: Squared matrix element for $\eta \to 3\pi^0$. The straight line shows the fit according to Eq. (37).

Figure 15: (a) $\omega \to 3\gamma$ Dalitz plot for $\pi^0 \omega$ events (62,853 events, 6 entries/event); (b) $\omega \to 3\gamma$ Dalitz plot for $\eta \omega$ events (54,865 events, 6 entries/event).

Figure 16: Dalitz plot of the final state $K_S K_L \pi^0$ (2,834 events).

Figure 17: Ratio of ϕ to ω production in low energy annihilation. The measured branching ratios have been divided by the factor W (Eq. (20)). The expectation from the OZI rule using the quadratic mass formula (4.2×10^{-3}) is shown by the horizontal line.

Figure 18: (a,b): OZI allowed ϕ production with $s\overline{s}$ pairs in the nucleon. In (c) an intermediate four-quark state is excited below threshold. The production of ϕ mesons can also be enhanced by final state rescattering, $K^*\overline{K} \to \pi\phi$ or $\rho\rho \to \pi\phi$ (d).

Figure 19: $\eta\pi$ and $K\overline{K}$ mass distributions for the $a_0(980)$ resonance in $\overline{p}p \to \eta\pi X$ and $K\overline{K}X$ (in arbitrary units and assuming that no other resonance is produced in these channels). The dashed line shows the $\eta\pi$ mass distribution for the same width Γ'_0 in the absence of $K\overline{K}$ coupling $(g_2 = 0)$.

Figure 20: Invariant mass distributions for $\pi^0\eta\eta$; (a) $\eta\eta$ mass distribution for 6γ events showing the two new scalar mesons; (b) $\eta\eta$ mass distribution for one η decaying to $3\pi^0$ (10 γ final state, not corrected for acceptance); (c) $\pi^0\eta$ mass distribution for 6γ events (2 entries/event) showing the $a_0(980)$. The solid lines in (a) and (c) represent the best fit described in Amsler (1992c).

Figure 21: Dalitz plots of 3-pseudoscalar channels. Red and blue regions correspond to high, respectively low, event densities; (a) $\pi^0\eta\eta$ (198,000 events). The Dalitz plot is symmetrized across the main diagonal; (b) $\pi^0\pi^0\eta$ (symmetrized, 280'000 events); (c): $3\pi^0$ (712,000 events). Each event is entered six times for symmetry reasons; (d) $\pi^0K_LK_L$ (37,358 events).

Figure 22: $\pi^0 \pi^0$ mass projection in $\overline{p}p \to 3\pi^0$ (3 entries/ event) with the fit (solid line) described in the text.

Figure 23: Argand diagram of the $\pi\pi$ scattering amplitude T obtained from a common fit to production and scattering data (from Spanier, 1994).

Figure 24: Isoscalar S-wave production intensities $|\mathcal{T}|^2$ in $3\pi^0$ (full curve), $2\pi^0\eta$ (dashed curve) and $2\eta\pi^0$ (dotted curve) before multiplying by the phase space factor ρ . The vertical scale is arbitrary (from Spanier, 1994).

Figure 25: $\eta \eta'$ mass projection in $\pi^0 \eta \eta'$. The full curve is the fit to the 6γ data with a scalar resonance close to threshold and the dashed curve shows the expected phase space distribution. The inset shows the $\eta \eta'$ mass distribution from $\pi^0 \eta (\to 2\gamma) \eta' (\to \eta \pi^+ \pi^-)$.

Figure 26: $2\pi^0\eta$ mass distribution recoiling against $\pi^0\pi^0$ for events with 10 reconstructed photons (6 entries/event).

Figure 27: $\eta' \pi^0$ mass projection in $\pi^0 \pi^0 \eta' \to 6\gamma$ for data (dots) and fits (histograms); (a) $(\pi \pi)$ S-wave and $a_2(1320)$; (b) including $a_0(1450)$ (best fit). Figure 28: The phase shift δ in elastic $K\pi$ scattering from Aston (1988b). The curve shows the fit using prescription (106).

Figure 29: $K\overline{K}$ mass projection in $\pi^0 K_L K_L$. The dashed line shows the fit with one scalar resonance, the full line the fit with two scalar resonances. The peak on the left is due to $f_2(1270)$ and $a_2(1320)$ and the peak on the right to $K^*(892)$ reflections. The central peak is due to interference from various amplitudes.

Figure 30: Branching ratio for $f_0(1370)$ and $f_0(1500)$ decay into $K\overline{K}$ as a function of $a_0(1450)$ contribution to $\pi^0 K_L K_L$ (from Dombrowski (1996)).

Figure 31: dE/dx distribution in the jet drift chamber for 2-prong events with a missing K_L . The curve shows the expected (Bethe-Bloch) dependence.

Figure 32: $\pi^{\pm}K^{\mp}K_L$ Dalitz plot (11,373 events).

Figure 33: χ^2 dependence on the fractional contribution from $a_0(1450)$ to $\pi^{\pm}K^{\mp}K_L$.

Figure 34: Tangent of the nonet mixing angle α as a function of R_1 (solid), R_2 (dotted) and R_3 (dashed curve). The shaded areas show the experimentally allowed regions for $f_0(1500)$, assuming that this state is $q\bar{q}$.

Figure 35: $\pi^0 \pi^0 \eta$ (a) and $\pi^+ \pi^- \eta$ (b) mass distributions in $\overline{p}p$ annihilation at rest into $\pi^+ \pi^- \pi^0 \pi^0 \eta$, showing the η' and $\eta(1410)$ signals. The dashed line shows the result of the fit.

Figure 36: Angular distribution of $a_0(980)^{\pm}$ in the $\eta(1410)$ rest frame. The data are shown with error bars. The full curve shows the fit for a 0^{-+} state and the dashed curve the prediction for a 1^{++} state produced with the same intensity.

This figure "fig1-1.png" is available in "png" format from:

This figure "fig1-2.png" is available in "png" format from:

This figure "fig1-3.png" is available in "png" format from:

This figure "fig1-4.png" is available in "png" format from:

This figure "fig1-5.png" is available in "png" format from:

This figure "fig1-6.png" is available in "png" format from:

This figure "fig1-7.png" is available in "png" format from:

This figure "fig1-8.png" is available in "png" format from:

This figure "fig1-9.png" is available in "png" format from:

This figure "fig1-10.png" is available in "png" format from:

This figure "fig1-11.png" is available in "png" format from:

This figure "fig1-12.png" is available in "png" format from:

This figure "fig1-13.png" is available in "png" format from:

This figure "fig1-14.png" is available in "png" format from:

This figure "fig1-15.png" is available in "png" format from:

This figure "fig1-16.png" is available in "png" format from:

This figure "fig1-17.png" is available in "png" format from:

This figure "fig1-18.png" is available in "png" format from:

This figure "fig1-19.png" is available in "png" format from:

This figure "fig1-20.png" is available in "png" format from:

This figure "fig1-21.png" is available in "png" format from:

This figure "fig1-22.png" is available in "png" format from:

This figure "fig1-23.png" is available in "png" format from:

This figure "fig1-24.png" is available in "png" format from:

This figure "fig1-25.png" is available in "png" format from:

This figure "fig1-26.png" is available in "png" format from:

This figure "fig1-27.png" is available in "png" format from:

This figure "fig1-28.png" is available in "png" format from:

This figure "fig1-29.png" is available in "png" format from:

This figure "fig1-30.png" is available in "png" format from: